This is to certify that the
dissertation entitled

PYRUVATE FORMATE LYASE AND PYRUVATE FORMATE LYASE ACTIVATING ENZYME: SPECTROSCOPIC CHARACTERISTICS, INTERACTION AND MECHANISM

presented by

YI PENG

has been accepted towards fulfillment
of the requirements for the

Ph.D. degree in Chemistry

Major Professor's Signature

March 26, 2008

Date

PYRUVATE FORMATE LYASE AND PYRUVATE FORMATE LYASE ACTIVATING ENZYME: SPECTROSCOPIC CHARACTERISTICS, INTERACTION AND MECHANISM

By

Yi Peng

A DISSERTATION

Submitted to
Michigan State University
In partial fulfillment of the requirements
for the degree of

DOCTOR OF PHILOSOPHY

Department of Chemistry

2008

ABSTRACT

PYRUVATE FORMATE LYASE AND PYRUVATE FORMATE LYASE ACTIVATING ENZYME: SPECTROSCOPIC CHARACTERISTICS, INTERACTION AND MECHANISM

By

Yi Peng

Pyruvate formate-lyase (PFL) reversibly converts pyruvate and coenzyme A (CoA) into formate and acetyl-CoA, a key step in anaerobic metabolism for facultative anaerobes. A glycyl radical on Gly-734 in PFL, generated by the pyruvate formate-lyase activating enzyme (PFL-AE), initiates the reaction. PFL-AE utilizes S-adenosylmthionine (AdoMet or SAM), which binds to a unique site in the Fe_4S_4 cluster of PFL-AE, to produce a putative deoxyadenosyl radical intermediate. It is this intermediate that abstracts the hydrogen from PFL Gly-734 to generate the glycyl radical. Sulfur K-edge X-ray absorption spectroscopy (XAS) has been used to probe the interaction between AdoMet and the cluster. The spectra show a sulfur K-edge absorption at 2472.5 eV and a pre-edge feature at 2470.3 eV. Upon AdoMet binding, the intensity of the pre-edge absorption increases, indicating change in Fe-S bond covalency. DFT calculations illustrate a 37% increase in covalency of the Fe-S bonds, in which 12% is attributed to Fe-$\mu_3S_{sulfide}$ and 25% to Fe-$^tS_{thiolate}$. The optimized model shows that the AdoMet 5'-C-S σ^* bond has backbonding interactions with filled Fe-S bonds, which shifts the charge density from the cluster to AdoMet. The effect causes enhancement of overall cluster covalency, and induces the S 1s to 5'-C-S transition in the pre-edge feature.

To investigate the possible exogenous ligand binding to the unique Fe in the absence of AdoMet, nuclear resonance vibrational spectroscopy (NRVS) was used. The spectra exhibit cubane cluster twist bands below 100 cm^{-1}, S-Fe-S' bending modes around 160 cm^{-1}, and Fe-S stretching modes above 200 cm^{-1}. In the presence of AdoMet, the intensity of the Fe-ligand + Fe-^{t}S stretching mode at 432 cm^{-1} increases, which might provide clues as to the identity of the exogenous ligand.

PFL-AE has no direct access to Gly-734, which is buried in the core of PFL, however direct interaction between them is necessary to generate the glycyl radical. We have obtained evidence from EPR spin quantification, H/D exchange of Gly-734 and PFL activity assays that Gly-734 is more exposed and unstable in the presence of PFL-AE, supporting the notion that the PFL/PFL-AE interaction involves significant rearrangement of the glycine loop. Circular dichroism (CD) spectra of activated PFL show that PFL-AE causes a conformational change in PFL. All evidence supports the proposal that the glycine loop undergoes conformational change to allow Gly-734 to bind at the PFL-AE active site during activation. Investigation of the PFL structure suggests that the C-terminal region, residues 710 – 759, might be the structure interacting with PFL-AE and pulling Gly-734 out.

It has been proposed that a thiyl radical on Cys-418 or Cys-419 might initiate PFL catalysis. EPR spectra show that activated C418A-PFL in D_2O has H/D exchange on the glycyl radical, indicating Cys-419 is not acetylated by pyruvate. The result implies that Cys-419 does not attack pyruvate directly, and that Cys-418 might be the residue to initiate the reaction.

I dedicate this work to my lovely and pretty wife Haolan Dong for her thorough support in my life no matter what it is, and putting up during all the hard time. I could never have made it this far without you and expect much more in the rest of our life.

ACKNOWLEDGEMENTS

I would like to express sincere appreciation to my advisor Dr. Joan Broderick, who has provided me with academic guidance through my whole graduate program, and encouraged me to pursue research goals. Thank you for everything and wish you the best in your academic and personal lives.

I would also like to thank my graduate committee members, Dr. David Weliky, Dr. Jack Watson and Dr. Gary Blanchard who helped me set up the laser for the Raman spectrometer and gave me the suggestion in resonance Raman spectroscopy. I thank Dr. Gavin Reid who did the mass spectrometry for the product of PFL.

I would like to thank Dr. Mbako Nnyepi for teaching me how to conduct PFL activity assay. I wish I could see you again sometime in Botswana. I also appreciate Dr. Jian Yang showing me how to use the EPR machine. My thanks go to Dr. Danilo Ortillo and Dr. Jeff Buis for their help in using the lab equipments. I acknowledge Dr. Will Broderick from whom I learned how to purify PFL-AE.

I appreciate our collaborators, Prof. Ed Solomon and Dr. Abhishek Dey for their work in the XAS project, Dr. Tim Sage and Weiqiao Zeng for their work in the NRVS project, and Prof. Vincent Huynh and Dr. Ricardo Garcia for his help of the Mössbauer spectra of the NRVS samples.

I would also like to thank my lab mates, Dr. Meng Li for her friendship; Dr.Susan Veneziano for explaining to me so many American slangs; Dr. Tilak Chandra's incredible Indian foods; and all other members in our lab, Magdalena Makowska-Gryska, Ziyang Su, Efthalia Kalliri, Kaitlin Duschene, Sunshine Silver, Rachel Undelhoven and Eric Sheperd. It has been always a lot of fun working with you.

TABLE OF CONTENTS

LIST OF TABLES

LIST OF SCHEMES

LIST OF FIGURES

LIST OF ABREVIATIONS

AdoMet.....S-adenosyl-L-methionine

aRNR.....anaerobic ribonucleotide reductase

ATP.....adenosine triphosphate

BioB.....biotin synthase

β-ME.....β–mercaptoethanol

BSA.....bovine serum albumin

CD.....circular dichroism

CoA.....coenzyme A

DFT.....density function theory

DTT.....dithiothreitol

EDTA.....ethylenedinitriolotetra-acetic acid disodium salt

ENDOR.....electron nuclear double resonance

EPR.....electron paramagnetic resonance

EXFAS.....extended X-ray absorption fine structure

FPLC.....fast protein liquid chromatography

HemN.....oxygen independent coprophyringogen-III-oxidase

E. coli.....*Escherichia coli*

IPTG.....isopropyl-β-D-thioglactopyranoside

LAM.....lysine 2,3-aminomutase

LB.....Luria Bertani

MOPS.....3-(N-morphlino)propanesulfonic acid

LMCT.....ligand to metal charge transfer

NAD^+.....nicotinamide adenine dinucleotide (oxidized form)

NADH.....nicotinamide adenine dinucleotide (reduced form)

NMR.....nuclear magnetic resonance

NRVS.....nuclear resonance vibrational spectroscopy

PFL.....pyruvate formate-lyase

PFL-AE.....pyruvate formate-lyase activating enzyme

PMSF.....phenylmethyl sulfonyl fluoride

RNA.....ribonucleic acid

SAM.....S-adenosyl-L-methionine

SDS-PAGE.....sodium dodecyl sulfate-polyacrylamide gel electrophoresis

SPL.....spore photoproduct lyase

XAS.....X-ray absorption spectroscopy

CHAPTER I

INTRODUCTION

I.1 PFL is a key enzyme in anaerobic metabolism for facultative anaerobes

Glycolysis, a series of reactions converting glucose into pyruvate, is an almost universal route for organisms to generate metabolic energy. Under aerobic conditions, glycolysis is followed by the citric acid cycle, in which pyruvate is completely oxidized to CO_2 and H_2O, and reducing equivalents that feed into the electron transport chain are generated. Most of the ATPs required in the metabolism are generated during the process. To enter the citric acid cycle, pyruvate and coenzyme A (CoA) are irreversibly converted into acetyl CoA and CO_2, catalyzed by pyruvate dehydrogenase complex. Facultative anaerobes such as *E. coli*, have an alternative reaction under anaerobic conditions in which pyruvate formate-lyase (PFL) reversibly converts pyruvate and CoA into formate and acetyl-CoA; this represents the first and key step in anaerobic metabolism. [1] PFL exhibits two-step ping-pong kinetics with an acetylated enzyme intermediate (Scheme I.1).

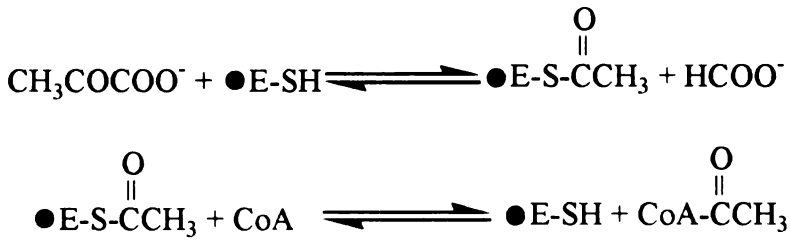

Scheme I.1 Schematic representation of ping-pong mechanism of PFL catalysis.

I.2 PFL is a free radical enzyme

It has been demonstrated that PFL can exist in either inactive or active forms; [1,2] the later is generated under anaerobic conditions and contain a stable protein-centered free radical. [3] Electron paramagnetic resonance (EPR) spectra revealed a hyperfine coupling between the electronic spin and the nuclear spin on ^{13}C in partially ^{13}C-labeled PFL; together with the lack of coupling to ^{33}S and other nuclei, this indicated the radical was carbon centered. [4] In 1992, Knappe and coworkers determined that the radical was on a glycine residue based on the hyperfine interaction between the unpaired electron and ^{13}C-labeled glycine. [5] The radical form of PFL is extremely sensitive to O_2. [3] In the presence of O_2, activated PFL is cleaved into two fragments, a larger fragment (82 kDa) and a smaller one (3 kDa). [5] Sequencing of the smaller fragment illustrated that the enzyme was cleaved at position Gly-734, which was, thus, assigned as the radical site. [5]

Incubation of PFL with 2-^{14}C-pyruvate results in labeling of the protein to generation of the acetyl-enzyme intermediate. [6] To identify the position of the ^{14}C label, the acetyl-PFL was cleaved by CNBr to generate several fragments. Sequencing of the peptide with radioactive label revealed that the ^{14}C-acetyl moiety was located on Cys-419. [6] When the ^{14}C-acetylated PFL was treated with hypophosphite (a formate analogue known as an inactivator of PFL [3]) to mimic the reverse reaction, the ^{14}C label was found on Cys-418. [6] The structure of the hypophosphite treated intermediate was determined as 1-hydroxyethylphosphonate with a thioester linkage to Cys-418, using ^{31}P-NMR spectroscopy and chemical characterization (Scheme I.2). [6] These results suggested that both Cys-418 and Cys-419 were involved in PFL radical mechanism. [6] To further investigate this proposal, two PFL mutants, C419S and C418S, were made by Knappe

and coworkers. [7] Although EPR spectra showed that both mutants could be activated to contain the glycyl radical as with wild-type PFL, both mutants had no activity, suggesting that these two cysteines are critical for PFL catalysis. [7]

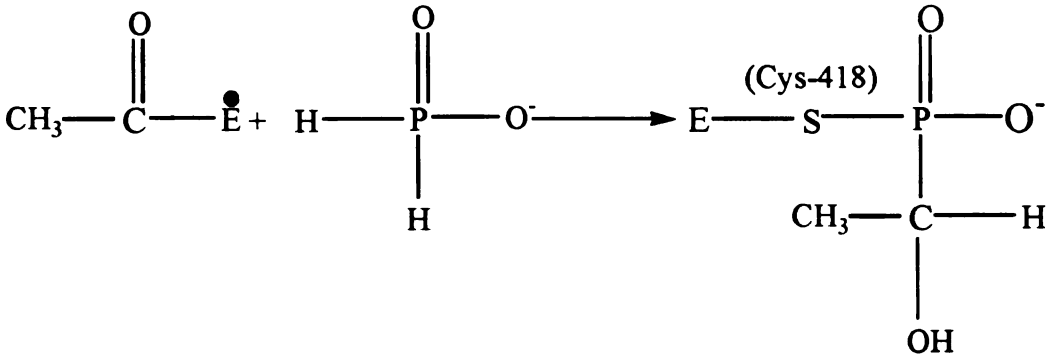

Scheme I.2: Schematic representation of acetylated PFL radical reacting with hypophosphite.

The glycyl radical gives rise to a doublet EPR signal (g = 2.0037, A = 1.5 mT). The coupling is due to the interaction between the unpaired electron and the nuclear spin of the ^1H on the α-carbon of the glycyl residue. The doublet signal changes to a singlet when PFL is mixed with D_2O, [3, 4] suggesting that the α-hydrogen on Gly-734 exchanges with deuterium from the solvent. Kozarich and coworkers showed that C419S-PFL retained its doublet EPR signal in D_2O, [8] indicating that Cys-419 was critical for the exchange. Together, the results suggested that the glycyl radical abstracts a hydrogen atom from Cys-419, thereby transferring the radical to Cys-419 to form a thiyl radical; in D_2O the thiol of Cys-419 would be deuterated, and so the glycyl radical would abstract deuterium from Cys-419. Multiple H/D atom abstraction between Gly-734 and Cys-419 would result in essentially full deuteration. Activated C418S-PFL, on the other hand,

undergoes the doublet to singlet EPR signal change, indicating that Cys-418 is not required for the solvent hydrogen exchange on the glycyl radical. [8]

The results just described led to a proposal in which an intermediate thiyl radical on either Cys-419 or Cys-418 attacks pyruvate as a key step in PFL catalysis. [9-11] A thiyl radical is also known to participate in the mechanism of *E. coli* ribonucleotide reductase (RNR) catalysis. [12] Abstraction of a 3'-hydrogen from the nucleotide by a cyeteine thiyl radical is believed to initiate the reduction of the ribonucleotide. Although the thiyl radical has yet to be observed in PFL, a thiyl radical coupled to cob(II)alamin in ribonucleoside triphosphate reductase (RTN) from *Lactobacills leichmannii* was trapped by rapid freeze quench techniques and detected by EPR. [13] The detection of a thiyl radical in PFL would provide strong evidence for the proposed radical mechanism.

I.3 Structure of PFL

PFL is a 170 kDa homodimer, containing 759 amino-acid residues in each subunit with no metals or bound cofactors. [14, 15] The crystal structure of the non-radical form of PFL and its complex with the substrate analog oxamate were firstly reported by Knappe and coworkers. [11] The overall structure of the monomer is a 10-stranded β/α barrel. Gly-734 and Cys-419/Cys-418 are located on two short loops, pointing toward each other and approximately 4Å apart. The structure of PFL in complex with both substrates (pyruvate and CoA) bound was solved by Becker and Kabsh. [16] In this structure, pyruvate was clearly located in the active site, whereas the adenine moiety of CoA was bound at a distance of 15 Å from the active site with its thiol moiety not far away from the pyruvate

binding pocket. This is consistent with the ping-pong mechanism in which CoA binds to the active site only after pyruvate is cleaved.

I.4 Generation of the glycyl radical in PFL requires an activating enzyme

PFL purified aerobically is in an inactive form. [1, 2, 13] To convert PFL to an active form containing the glycyl radical, the pyruvate formate-lyase activating enzyme (PFL-AE) is required. [17, 18] During PFL activation, S-adenosylmethionine (AdoMet or SAM) is stoichiometrically converted to methionine and 5'-deoxyadenosine. When ^{2}H-glycine labeled PFL was activated with PFL-AE and AdoMet, a ^{2}H was observed in the product 5'-deoxyadenosine via mass spectrometry and NMR. [19] It was proposed that PFL-AE reductively cleaves AdoMet to form the deoxyadenosyl radical, which abstracts the hydrogen from Gly-734 to activate PFL. [19] To further investigate this proposal, an octapeptide mimic of the short loop containing Gly-734, was used to trigger the AdoMet cleavage in PFL-AE. [20] A dehydroalanyl residue (ΔAla) took the place of Gly-734 in this peptide. After the reaction, it was discovered by MS and 2D NMR that the deoxyadenosyl moiety was connected to the C=C double bond of ΔAla (Scheme I.3). [20] The mechanism of this reaction was proposed to involve the deoxyadenosyl radical attacking the C=C double bond.

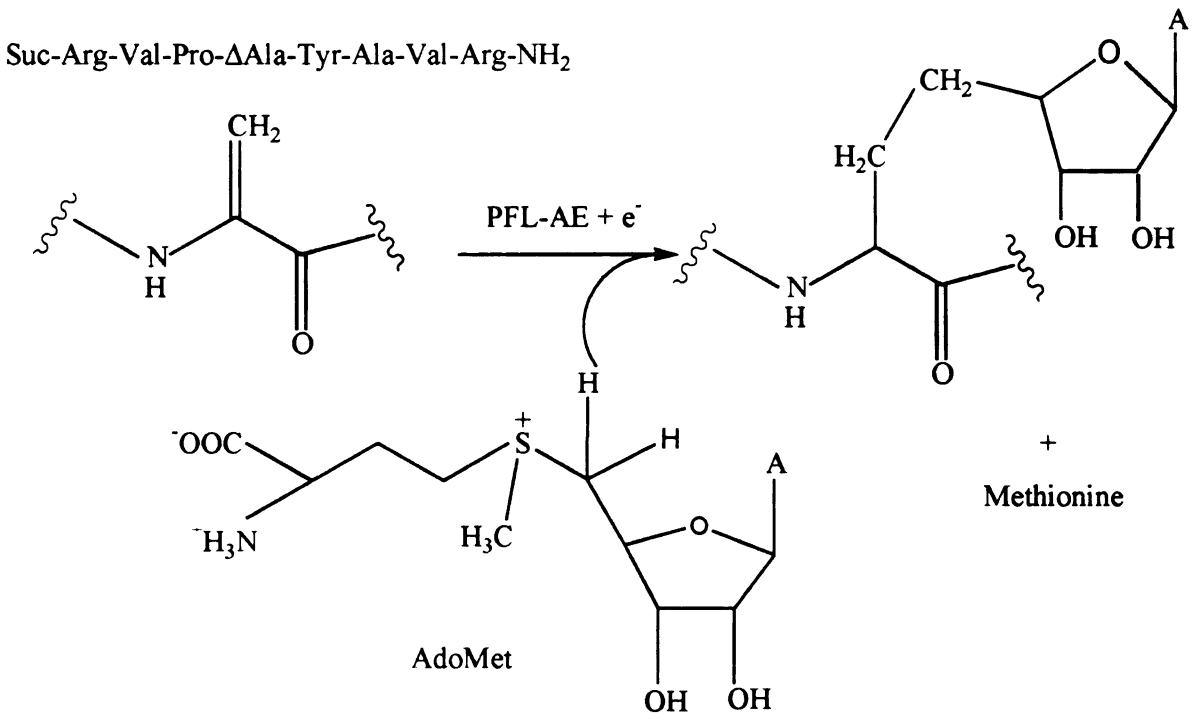

Scheme I.3: Schematic representation of the addition of deoxyadenosyl to the ΔAla as a result of AdoMet cleavage. [20]

DNA sequencing showed that the *E. coli* PFL-AE was a 28 kDa enzyme containing 245 amino-acid residues. [14] The PFL and PFL-AE genes are located adjacent to each other on the *E. coli* chromosomal map. Overexpression of PFL-AE was initially conducted by Kozarich and coworkers. [21] The aerobically purified enzyme was barely soluble in H_2O, and thus was purified after denaturation. The protein, reconstituted with Fe^{2+} and DTT after it was refolded, contained one mole Fe per mole enzyme. Broderick and coworkers subsequently demonstrated that overexpressed and anaerobically purified PFL-AE contained an iron-sulfur cluster. [22] The average number of Fe in one mole of PFL-AE was 1.5, and the enzyme also had much higher activity than the form characterized by Kozarich and coworkers. [21, 22] UV-Vis, EPR and resonance Raman (RR) spectroscopies showed that the enzyme contained $[2Fe\text{-}2S]^{2+}$ and $[4Fe\text{-}4S]^{2+}$ clusters. [22]

Hence, PFL-AE was identified as an iron-sulfur cluster protein, and a Fe_4S_4 cluster was proposed to be required for activity. Anaerobically reconstituted protein also showed Fe_4S_4 cluster signals in UV-Vis and EPR. [23]

A direct measurement of the generation of the PFL glycyl radical by the [4Fe-4S]$^{1+}$ cluster of PFL-AE was carried out by EPR spin quantification of the cluster and the radical. [24] PFL-AE was photoreduced by 5-deazariboflavin, and AdoMet was added after photoreduction. The quantity of the [4Fe-4S]$^{1+}$ increased with illumination time up to 30 minutes. PFL was then added to each sample, and EPR showed the presence of glycyl radicals in amounts directly corresponding to the amount of [4Fe-4S]$^{1+}$ originally present. There was no [4Fe-4S]$^{1+}$ cluster signal in PFL-AE after the glycyl radicals were generated, suggesting a stoichiometric turnover of PFL by PFL-AE in a controlled reducing environment.

I.5 PFL-AE is a radical SAM superfamily enzyme

AdoMet, a widely used substrate in biological systems, is involved in many important biochemical reactions. [25] In various types of organisms, AdoMet is considered as the major methyl donor in methylation reaction, [26] including the insertion of methyl groups into DNA, hormones, neurotransmitters, phospholipids and the cobalamin cofactors. AdoMet is also a methylene source for cyclopropane fatty acid formation in eubacteria and some eukaryotic organisms, [27] as well as for the post transcriptional modification of tRNAs. [28] Moreover, this compound can donate its amino group. [29, 30]

The discovery that AdoMet was essential for the activity of three different enzymes, lysine 2,3-aminomutase (LAM), PFL-AE and anaerobic ribonucleotide reductase (aRNR), all of which had free radical mechanisms, led to the idea that AdoMet could also be a radical initiator. [31-34] It is now believed that these enzymes uses reductive cleavage of AdoMet to produce a 5'-deoxyadenosyl radical as a key intermediate. Enzymes that utilize AdoMet (also called SAM) to generate the 5'-dAdo radical intermediate (Scheme I.4) comprise the radical SAM superfamily. [35] Although there has not yet been any direct observation of this extremely reactive radical intermediate, a radical on an allylic analog, S-3',4'-anhydroadenosyl-methionine, has been detected by EPR at 77 K in the enzymatic reaction of LAM. [36]

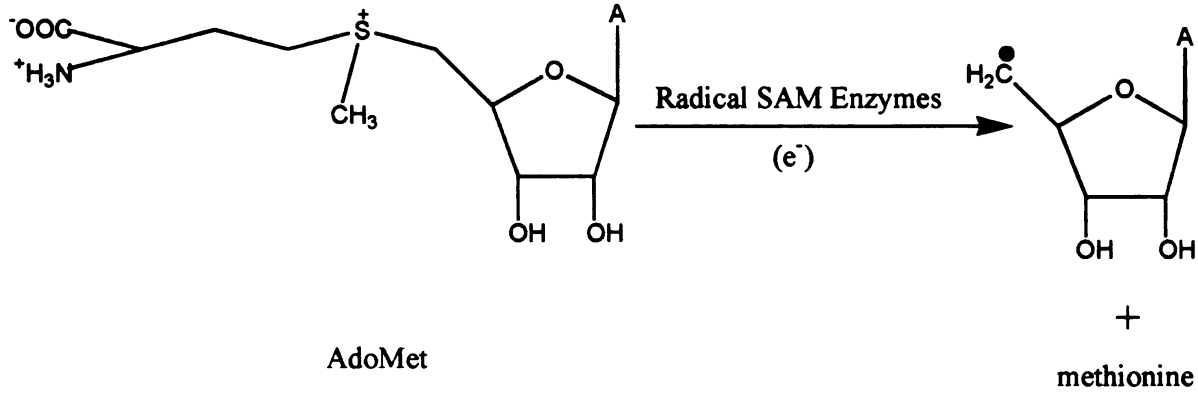

Scheme I.4: AdoMet is cleaved by radical SAM superfamily enzymes to generate a deoxyadenosyl radical and a methionine.

The radical SAM superfamily is thought to be composed of more than 600 different enzymes with different functionalities. Some well-studied samples include the sulfur insertion enzymes biotin synthase (BioB) [37, 38] and lipoate synthase (LipA); [39] the mutase lysine 2,3-aminomutase (LAM); [40] the radical activation enzymes pyruvate formate-lyase activating enzyme (PFL-AE), [32] anaerobic ribonucleotide reductase activating enzyme (aRNR-AE) [41] and benzylsuccinate synthase activating enzyme; [42] the DNA repair enzyme spore photoproduct lyase (SPL); [43] and the biological cofactor biosynthesis enzymes oxygen-independent coproporphyrinogen-III oxidase (HemN) [44] and MoaA [45] (BioB and LipA are also considered in this category).

Early work on these enzymes suggested the involvement of Fe-S clusters were observed under different conditions, however the exact form was unclear since numerous different cluster types ($[2Fe\text{-}2S]^{2+}$, $[3Fe\text{-}4S]^{1+}$ and $[4Fe\text{-}4S]^{2+}$) were observed under different conditions. [22, 46-49] Only LAM was unequivocally identified as an Fe_4S_4 cluster enzyme. [50, 51] Iron-sulfur clusters, in synthesized complexes or in proteins, have long been known to be remarkably versatile. [52] Distinct forms are interchangeable under different conditions (Scheme I.5). In the radical SAM proteins PFL-AE and BioB, EPR, RR, UV and Mössbauer spectroscopic techniques demonstrated that the $[2Fe\text{-}2S]^{2+}$ and $[3Fe\text{-}4S]^{1+}$ can be converted to $[4Fe\text{-}4S]^{2+}$ under reducing conditions. [49, 53, 54] In earlier PFL-AE preparations, 66% of total irons were in the $[3Fe\text{-}4S]^{1+}$ state, 12% were in the $[2Fe\text{-}2S]^{2+}$ state, 8% were in the $[4Fe\text{-}4S]^{2+}$ state and 10% in the linear $[3Fe\text{-}4S]^{1+}$ state. [53] Upon dithionite reduction, 88% of total iron was in Fe_4S_4 clusters. [53] Further reduction could convert $[4Fe\text{-}4S]^{2+}$ into $[4Fe\text{-}4S]^{1+}$, the active form to cleave AdoMet (Scheme I.6). [24, 55] Because the cluster interconversions occurred without added iron, these studies also

suggested the conversions were a result of "cannibalization", which meant the extra irons and sulfurs needed to assemble the [4Fe-4S] cluster were taken from other clusters with lower numbers of iron. More strictly anaerobic purification of PFL-AE in the presence of 1 mM DTT now results in almost exclusively $[4Fe\text{-}4S]^{2+}$ clusters. [56]

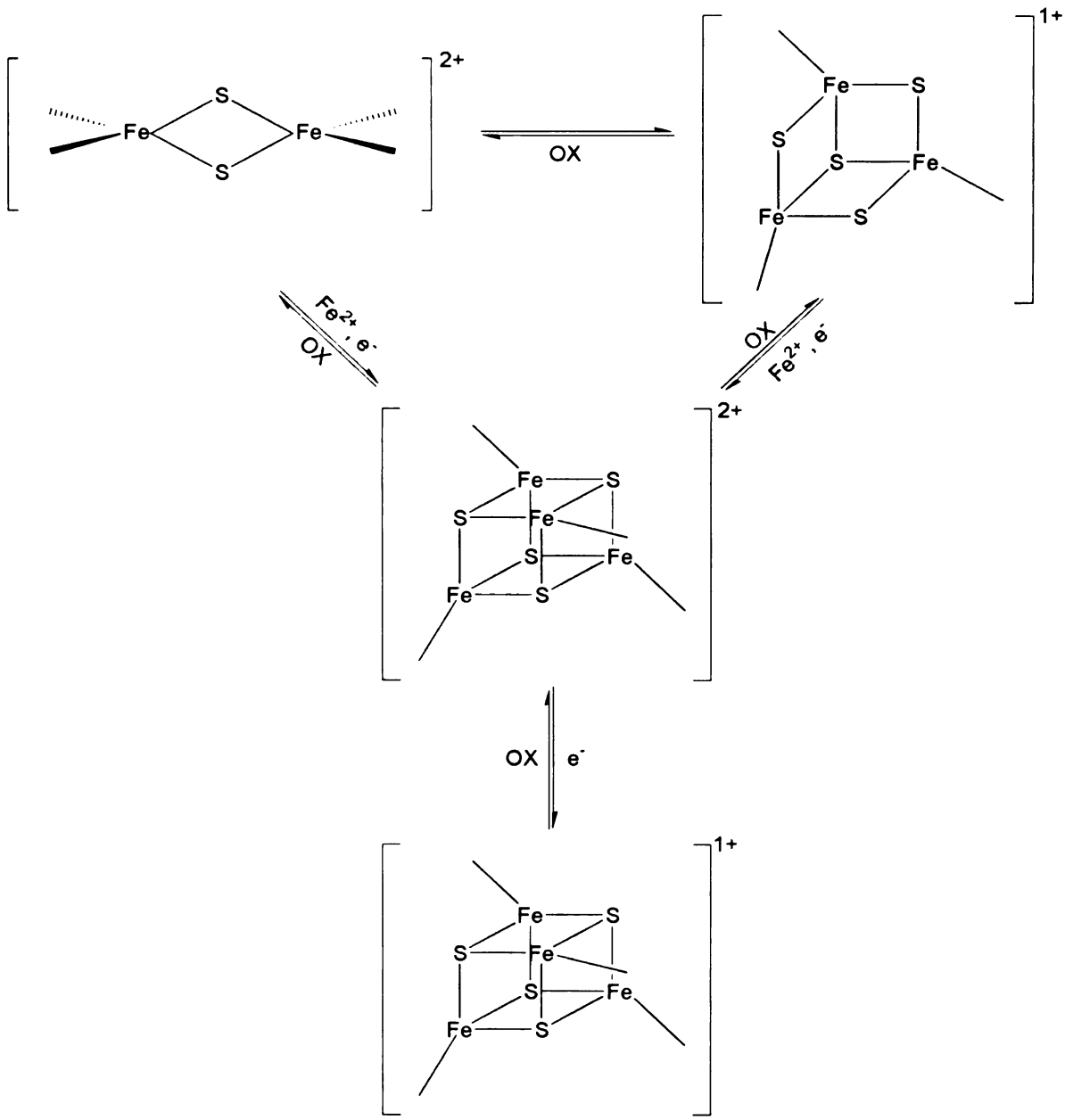

Scheme I.5: Schematic representation of the conversions among different Fe-S clusters.

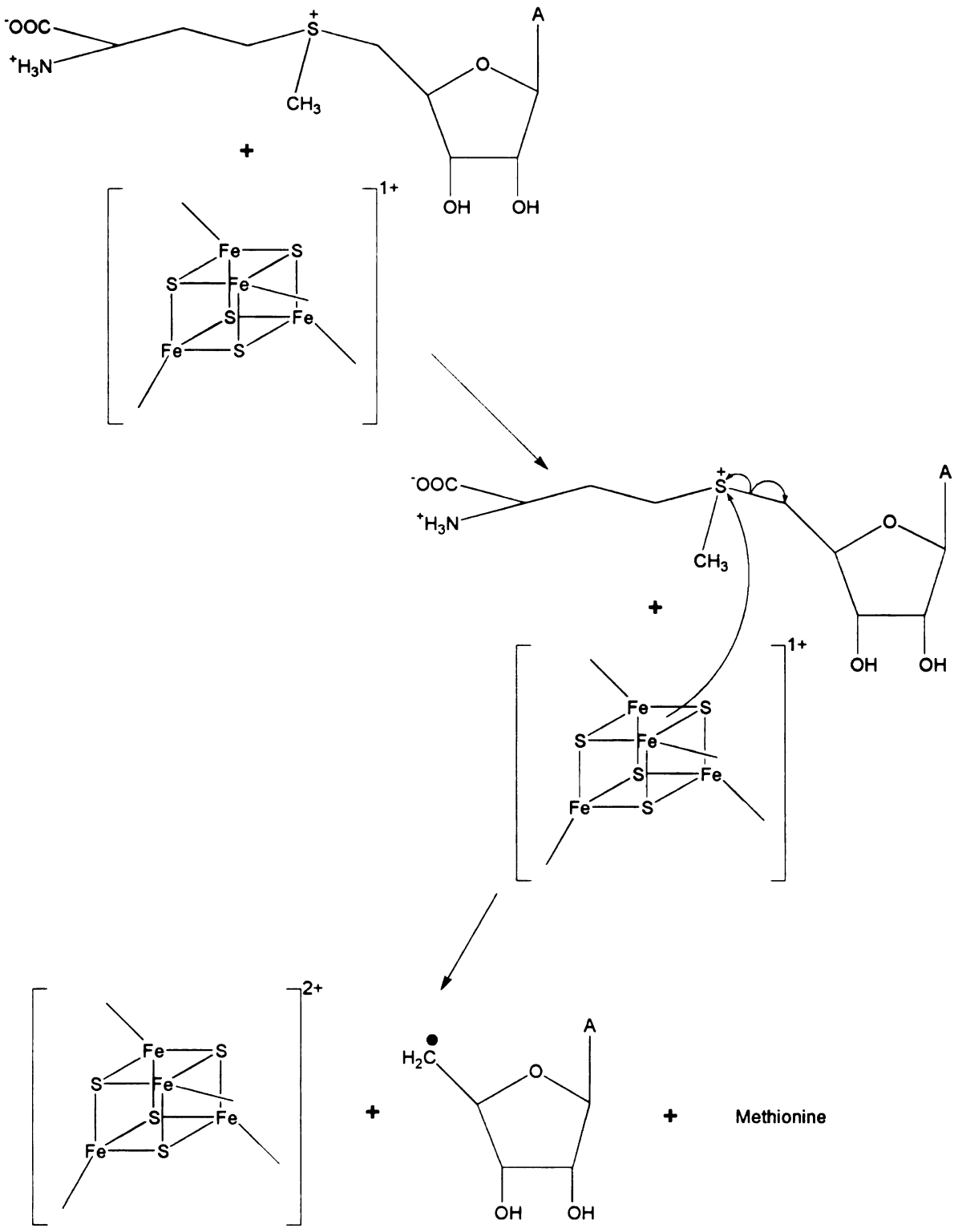

Scheme I.6: Schematic representation of AdoMet cleavage by $[4Fe\text{-}4S]^{1+}$.

The conversions among iron-sulfur clusters in the radical SAM superfamily, especially the one between the $[3Fe\text{-}4S]^{1+}$ and $[4Fe\text{-}4S]^{2+}$, suggested that there was at least one labile Fe in the 4Fe cluster. The proposed labile site was consistent with the conserved three cysteines motif (Fig. I.1) shown to be required for activity. [23] In PFL-AE, Cys-29, Cys-33 and Cys-36 were proposed to bind 3 of the 4 irons in the $[4Fe\text{-}4S]^{2+}$ cluster, which left one Fe not coordinated and thus more labile. The special CX_3CX_2C motif is highly conserved in radical SAM superfamily enzymes (Fig I.1), and thought to be crucial for the catalytic mechanism of the cluster. [31, 33, 35]

PFL-AE	24	I	T	F	F	Q	G	C	L	M	R	C	L	Y	C	H	N	R	D
SPL	86	I	P	F	A	T	G	C	M	G	H	C	H	Y	C	Y	L	Q	T
aRNR-AE	20	V	L	F	V	T	G	C	L	H	K	C	E	G	C	Y	N	R	S
BioB	47	S	I	K	T	G	A	C	P	Q	D	C	K	Y	C	P	Q	T	S
LipA	48	M	I	L	G	A	I	C	T	R	R	C	P	F	C	D	V	A	H
LAM	132	L	L	I	T	D	M	C	S	M	Y	C	R	H	C	T	R	R	R
HemN	53	Y	F	H	I	P	F	C	Q	S	M	C	L	Y	C	G	C	S	I
MoaA	15	I	A	V	T	P	E	C	N	L	D	C	F	F	C	H	M	E	F

Figure I.1: Conserved Fe-S cluster binding motif in radical SAM superfamily

I.6 AdoMet binds to the [4Fe-4S] cluster through the unique Fe site

The implication of the three-cysteine binding motif is that the unbound Fe could be the coordination site of AdoMet as seen in the substrate binding site in aconitase. [57] Aconitase is a Fe_4S_4 cluster enzyme, although not a radical SAM superfamily member, catalyzing the reversible conversion of citrate to isocitrate. [58] Three cysteines Cys-358, Cys-421 and Cys-424 provide the ligation of the cluster to the enzyme [59]. Spectroscopic studies and the crystal structure of aconitase show that isocitrate, the substrate, binds to the cluster by coordination to the unique Fe site (Fig I.2). [58 - 60]

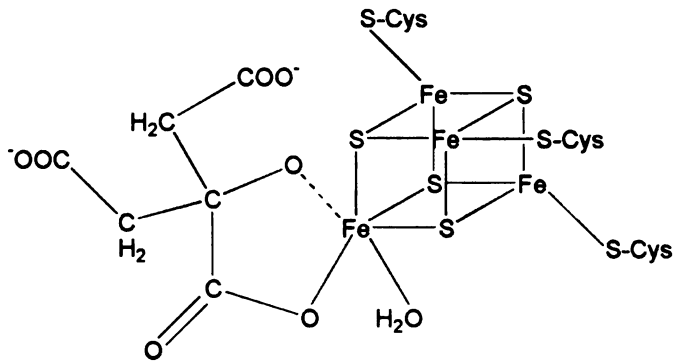

Figure I.2: Isocitrate binds to the unique Fe of the [4Fe-4S] cluster in aconitase.

To investigate the possibility of AdoMet coordination to the cluster, ^{57}Fe reconstituted PFL-AE was studied by Mössbauer spectroscopy. [61] The ^{57}Fe was incorporated into the unique site by adding 1 equivalent of ^{57}Fe to PFL-AE containing $[3Fe\text{-}4S]^{1+}$ under reducing conditions. In the presence of AdoMet, a significant change of the spectral parameters of the unique site was observed, suggesting an increase in coordination number of the unique Fe; this in turn suggested that AdoMet binds to the cluster. Further studies of PFL-AE were carried out by electron nuclear double resonance

(ENDOR) spectroscopy. [56, 62, 63] The carboxylate group in AdoMet was labeled with ^{17}O and ^{13}C, and the α-amino group was labeled with ^{15}N. The cluster in PFL-AE was photoreduced to $[4Fe\text{-}4S]^{1+}$, and the interaction between the cluster and AdoMet was monitored. The hyperfine couplings of ^{17}O and ^{13}C to the cluster were almost the same as that observed for the carboxylate group of isocitrate coordinating to the unique Fe in aconitase. [56] The hyperfine interaction of N to the Fe was comparable to the interaction between the histidine N and the ferrous Fe in Rieske protein with a [2Fe-2S] cluster. [64] These results suggested that AdoMet was binding to the unique Fe via the carboxylate and amino groups (Fig I.3).

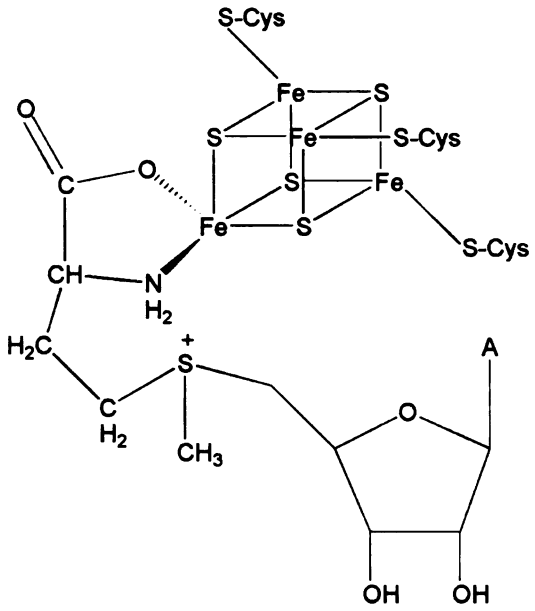

Figure I.3: AdoMet binds to the [4Fe-4S] cluster through the unique Fe.

Similar ENDOR results were observed in AdoMet binding to LAM. [65] RR, EPR and Mössbauer spectroscopies were used to investigate the coordination between AdoMet

and the cluster in reconstituted BioB. [66] In the presence of AdoMet, the symmetric stretching mode of the $[4Fe\text{-}4S]^{2+}$ cluster shifted from 338 to 342 cm^{-1}, which was out of the range (333 – 339 cm^{-1}) for a Fe_4S_4 cluster coordinated by 4 exogenous cysteinyl ligands. The Mössbauer data also indicated an increase of coordination number and/or a noncysteinyl ligand binding to a unique Fe. The theoretical simulation of an AdoMet interaction, similar to that in PFL-AE and LAM, fit well with the experimental data. [66] The results from different proteins suggested the binding mode between AdoMet and the unique Fe site of the Fe_4S_4 cluster is common in radical SAM superfamily members.

Recently published crystal structures of BioB (3.4 Å), LAM (2.1 Å), HemN (2.1 Å), and MoaA (2.2 Å) confirmed this type of AdoMet coordination in the superfamily. [45, 67-69] All the enzymes have (β/α) barrel or TIM barrel structures, with a $(\beta/\alpha)_8$ barrel for BioB, and a ¾ TIM barrel or $(\beta/\alpha)_6$ barrel for the other three proteins. This type of structure has been proposed as a common feature in the radical SAM enzymes. [70] The distances from the AdoMet carboxylate O to the unique Fe are 2.0, 2.3 and 2.5 Å in HemN, BioB and MoaA respectively. The distances between the amino N and the unique Fe are 2.3, 2.4 and 2.6 Å in the three enzymes. The distance between the Se and the unique Fe is 3.2 Å in the LAM structure crystallized with Se-AdoMet. Our crystal structure study of PFL-AE (manuscript in preparation) shows distances from the carboxylate O, the amino N, and the sulfonium S to the unique Fe similar to the published structures. The noncysteine bound Fe might be the position to lock AdoMet binding and donate one electron from the cluster to the substrate to catalyze the deoxyadenosyl radical generation.

References

1. Knappe, J.; Blaschkowski, H. P.; Groebner, P.; Schmitt, T., *European Journal of Biochemistry* **1974,** 50, (1), 253-63.

2. Knappe, J.; Schacht, J.; Moeckel, W.; Hoepner, T.; Vetter, H., Jr.; Edenharder, R., *European Journal of Biochemistry* **1969,** 11, (2), 316-27.

3. Knappe, J.; Neugebauer, F. A.; Blaschkowski, H. P.; Gaenzler, M., *Proceedings of the National Academy of Sciences of the United States of America* **1984,** 81, (5), 1332-5.

4. Unkrig, V.; Neugebauer, F. A.; Knappe, J., *European Journal of Biochemistry* **1989,** 184, (3), 723-8.

5. Wagner, A. F. V.; Frey, M.; Neugebauer, F. A.; Schaefer, W.; Knappe, J., *Proceedings of the National Academy of Sciences of the United States of America* **1992,** 89, (3), 996-1000.

6. Plaga, W.; Frank, R.; Knappe, J., *European Journal of Biochemistry* **1988,** 178, (2), 445-50.

7. Knappe, J.; Elbert, S.; Frey, M.; Wagner, A. F. V., *Biochemical Society Transactions* **1993,** 21, (3), 731-4.

8. Parast, C. V.; Wong, K. K.; Lewisch, S. A.; Kozarich, J. W.; Peisach, J.; Magliozzo, R. S., *Biochemistry* **1995,** 34, (8), 2393-9.

9. Ulissi-DeMario, L.; Brush, E. J.; Kozarich, J. W., *Journal of the American Chemical Society* **1991,** 113, (11), 4341-2.

10. Brush, E. J.; Kozarich, J. W., *Enzymes (3rd Ed.)* **1992,** 20, 317-403.

11. Becker, A.; Fritz-Wolf, K.; Kabsch, W.; Knappe, J.; Schultz, S.; Wagner, A. F. V., *Nature Structural Biology* **1999,** 6, (10), 969-975.

12. Mao, S. S.; Yu, G. X.; Chalfoun, D.; Stubbe, J., *Biochemistry* **1992,** 31, (40), 9752-9.

13. Licht, S.; Gerfen, G. J.; Stubbe, J., *Science* **1996,** 271, (5248), 477-81.

14. Roedel, W.; Plaga, W.; Frank, R.; Knappe, J., *European Journal of Biochemistry* **1988,** 177, (1), 153-8.

15. Conradt, H.; Hohmann-Berger, M.; Hohmann, H. P.; Blaschkowski, H. P.; Knappe, J., *Archives of Biochemistry and Biophysics* **1984,** 228, (1), 133-42.

16. Becker, A.; Kabsch, W., *Journal of Biological Chemistry* **2002,** 277, (42), 40036-40042.

17. Knappe, J.; Schmitt, T., *Biochemical and Biophysical Research Communications* **1976,** 71, (4), 1110-17.

18. Blaschkowski, H. P.; Neuer, G.; Ludwig-Festl, M.; Knappe, J., *European Journal of Biochemistry* **1982,** 123, (3), 563-9.

19. Frey, M.; Rothe, M.; Wagner, A. F. V.; Knappe, J., *Journal of Biological Chemistry* **1994,** 269, (17), 12432-7.

20. Wagner, A. F. V.; Demand, J.; Schilling, G.; Pils, T.; Knappe, J., *Biochemical and Biophysical Research Communications* **1999,** 254, (2), 306-310.

21. Wong, K. K.; Murray, B. W.; Lewisch, S. A.; Baxter, M. K.; Ridky, T. W.; Ulissi-DeMario, L.; Kozarich, J. W., *Biochemistry* **1993,** 32, (51), 14102-10.

22. Broderick, J. B.; Duderstadt, R. E.; Fernandez, D. C.; Wojtuszewski, K.; Henshaw, T. F.; Johnson, M. K., *Journal of the American Chemical Society* **1997,** 119, (31), 7396-7397.

23. Kulzer, R.; Pils, T.; Kappl, R.; Huttermann, J.; Knappe, J., *Journal of Biological Chemistry* **1998,** 273, (9), 4897-4903.

24. Henshaw, T. F.; Cheek, J.; Broderick, J. B., *Journal of the American Chemical Society* **2000,** 122, (34), 8331-8332.

25. Cantoni, G. L., *Annu Rev Biochem* **1975,** 44, 435-51.

26. Chiang, P. K.; Gordon, R. K.; Tal, J.; Zeng, G. C.; Doctor, B. P.; Pardhasaradhi, K.; McCann, P. P., *Faseb J* **1996,** 10, (4), 471-80.

27. Grogan, D. W.; Cronan, J. E., Jr., *Microbiol Mol Biol Rev* **1997,** 61, (4), 429-41.

28. Bjork, G. R.; Ericson, J. U.; Gustafsson, C. E.; Hagervall, T. G.; Jonsson, Y. H.; Wikstrom, P. M., *Annu Rev Biochem* **1987,** 56, 263-87.

29. Stoner, G. L.; Eisenberg, M. A., *J Biol Chem* **1975,** 250, (11), 4037-43.

30. Stoner, G. L.; Eisenberg, M. A., *J Biol Chem* **1975,** 250, (11), 4029-36.

31. Frey, P. A.; Magnusson, O. T., *Chemical Reviews (Washington, DC, United States)* **2003,** 103, (6), 2129-2148.

32. Jarrett, J. T., *Current Opinion in Chemical Biology* **2003,** 7, (2), 174-182.

33. Cheek, J.; Broderick, J. B., *Journal of biological inorganic chemistry : JBIC : a publication of the Society of Biological Inorganic Chemistry* **2001,** 6, (3), 209-26.

34. Fontecave, M.; Mulliez, E.; Ollagnier-de-Choudens, S., *Current Opinion in Chemical Biology* **2001,** 5, (5), 506-512.

35. Sofia, H. J.; Chen, G.; Hetzler, B. G.; Reyes-Spindola, J. F.; Miller, N. E., *Nucleic Acids Research* **2001,** 29, (5), 1097-1106.

36. Magnusson, O. T.; Reed, G. H.; Frey, P. A., *Biochemistry* **2001,** 40, (26), 7773-82.

37. Lotierzo, M.; Bui, B. T. S.; Florentin, D.; Escalettes, F.; Marquet, A., *Biochemical Society Transactions* **2005,** 33, (4), 820-823.

38. Jarrett, J. T., *Arch Biochem Biophys* **2005,** 433, (1), 312-21.

39. Ollagnier-de Choudens, S.; Fontecave, M., *FEBS Lett* **1999,** 453, (1-2), 25-8.

40. Frey, P. A., *Book of Abstracts, 216th ACS National Meeting, Boston, August 23-27* **1998**, BIOL-007.

41. Tamarit, J.; Gerez, C.; Meier, C.; Mulliez, E.; Trautwein, A.; Fontecave, M., *Journal of Biological Chemistry* **2000,** 275, (21), 15669-15675.

42. Leuthner, B.; Leutwein, C.; Schulz, H.; Horth, P.; Haehnel, W.; Schiltz, E.; Schagger, H.; Heider, J., *Mol Microbiol* **1998,** 28, (3), 615-28.

43. Cheek, J.; Broderick, J. B., *J Am Chem Soc* **2002,** 124, (12), 2860-1.

44. Layer, G.; Verfurth, K.; Mahlitz, E.; Jahn, D., *Journal of Biological Chemistry* **2002,** 277, (37), 34136-34142.

45. Haenzelmann, P.; Schindelin, H., *Proceedings of the National Academy of Sciences of the United States of America* **2004,** 101, (35), 12870-12875.

46. Broderick, J. B.; Henshaw, T. F.; Cheek, J.; Wojtuszewski, K.; Smith, S. R.; Trojan, M. R.; McGhan, R. M.; Kopf, A.; Kibbey, M.; Broderick, W. E., *Biochemical and Biophysical Research Communications* **2000,** 269, (2), 451-456.

47. Ollagnier, S.; Mulliez, E.; Gaillard, J.; Eliasson, R.; Fontecave, M.; Reichard, P., *J Biol Chem* **1996,** 271, (16), 9410-6.

48. Miller, J. R.; Busby, R. W.; Jordan, S. W.; Cheek, J.; Henshaw, T. F.; Ashley, G. W.; Broderick, J. B.; Cronan, J. E., Jr.; Marletta, M. A., *Biochemistry* **2000,** 39, (49), 15166-78.

49. Sanyal, I.; Cohen, G.; Flint, D. H., *Biochemistry* **1994,** 33, (12), 3625-31.

50. Song, K. B.; Frey, P. A., *J Biol Chem* **1991,** 266, (12), 7651-5.

51. Petrovich, R. M.; Ruzicka, F. J.; Reed, G. H.; Frey, P. A., *J Biol Chem* **1991,** 266, (12), 7656-60.

52. Beinert, H.; Holm, R. H.; Munck, E., *Science (Washington, D. C.)* **1997,** 277, (5326), 653-659.

53. Krebs, C.; Henshaw, T. F.; Cheek, J.; Huynh, B. H.; Broderick, J. B., *Journal of the American Chemical Society* **2000,** 122, (50), 12497-12506.

54. Duin, E. C.; Lafferty, M. E.; Crouse, B. R.; Allen, R. M.; Sanyal, I.; Flint, D. H.; Johnson, M. K., *Biochemistry* **1997,** 36, (39), 11811-11820.

55. Wu, W.; Booker, S.; Lieder, K. W.; Bandarian, V.; Reed, G. H.; Frey, P. A., *Biochemistry* **2000,** 39, (31), 9561-70.

56. Walsby, C. J.; Hong, W.; Broderick, W. E.; Cheek, J.; Ortillo, D.; Broderick, J. B.; Hoffman, B. M., *Journal of the American Chemical Society* **2002,** 124, (12), 3143-3151.

57. Werst, M. M.; Kennedy, M. C.; Houseman, A. L.; Beinert, H.; Hoffman, B. M., *Biochemistry* **1990,** 29, (46), 10533-40.

58. Beinert, H.; Kennedy, M. C.; Stout, C. D., *Chemical Reviews (Washington, D. C.)* **1996,** 96, (7), 2335-2373.

59. Robbins, A. H.; Stout, C. D., *Proc Natl Acad Sci U S A* **1989,** 86, (10), 3639-43.

60. Werst, M. M.; Kennedy, M. C.; Beinert, H.; Hoffman, B. M., *Biochemistry* **1990,** 29, (46), 10526-32.

61. Krebs, C.; Broderick, W. E.; Henshaw, T. F.; Broderick, J. B.; Huynh, B. H., *Journal of the American Chemical Society* **2002,** 124, (6), 912-913.

62. Walsby, C. J.; Ortillo, D.; Broderick, W. E.; Broderick, J. B.; Hoffman, B. M., *Journal of the American Chemical Society* **2002,** 124, (38), 11270-11271.

63. Walsby, C. J.; Ortillo, D.; Yang, J.; Nnyepi, M. R.; Broderick, W. E.; Hoffman, B. M.; Broderick, J. B., *Inorganic Chemistry* **2005,** 44, (4), 727-741.

64. Gurbiel, R. J.; Doan, P. E.; Gassner, G. T.; Macke, T. J.; Case, D. A.; Ohnishi, T.; Fee, J. A.; Ballou, D. P.; Hoffman, B. M., *Biochemistry* **1996,** 35, (24), 7834-45.

65. Chen, D.; Walsby, C.; Hoffman, B. M.; Frey, P. A., *Journal of the American Chemical Society* **2003,** 125, (39), 11788-11789.

66. Cosper, M. M.; Jameson, G. N. L.; Davydov, R.; Eidsness, M. K.; Hoffman, B. M.; Huynh, B. H.; Johnson, M. K., *Journal of the American Chemical Society* **2002,** 124, (47), 14006-14007.

67. Berkovitch, F.; Nicolet, Y.; Wan, J. T.; Jarrett, J. T.; Drennan, C. L., *Science (Washington, DC, United States)* **2004,** 303, (5654), 76-80.

68. Lepore, B. W.; Ruzicka, F. J.; Frey, P. A.; Ringe, D., *Proceedings of the National Academy of Sciences of the United States of America* **2005,** 102, (39), 13819-13824.

69. Layer, G.; Moser, J.; Heinz, D. W.; Jahn, D.; Schubert, W.-D., *EMBO Journal* **2003,** 22, (23), 6214-6224.

70. Nicolet, Y.; Drennan, C. L., *Nucleic Acids Res* **2004,** 32, (13), 4015-25.

CHAPTER II

OVEREXPRESSION AND PURIFICATION OF PYRUVATE FORMATE-LYASE AND PYRUVATE FORMATE-LYASE ACTIVATING ENZYME

II.1 Introduction

Purifying proteins from organisms or tissues was once a very difficult and time-consuming process. It took large quantities of cells or tissues to obtain a relatively small amount of protein, since the protein of interest usually comprised less than 1% of the total protein content in the raw material. [1] Numerous steps were required to get enough purified protein for research. During the process, much of the target protein was lost or degraded. It was extremely difficult to study human proteins as sufficient quantity of human tissues or organs was always a big problem.

In the 1950's and 1960's, protein overexpression systems, utilizing plasmid derived cloning vectors in bacteria, were discovered and developed. [2] *In vitro* studies on proteins have been remarkably advanced by the resulting large-scale production. In order to do protein overexpression, the gene of the target protein is inserted into a plasmid (a circular DNA vector), containing antibiotic resistance, promoters, and regulatory elements. A common system utilizes the *Lac* operator, promoter, and, which natively regulates lactose metabolism in *E. coli* and some other bacteria, to control the target protein overexpression (Fig II.1). The target gene can is inserted behind the *LAC* operation promoter, and in the absence of lactose, the *Lac* repressor, binds to the operator and suppresses the transcription. When cells are grown in the presence of lactose, allolactose (a metabolite of lactose) binds to the *LAC* repressor, changing its

conformation, and thus lowering its affinity for the *lac* operator. The target gene is then transcribed and the protein can be produced at high levels. [3]

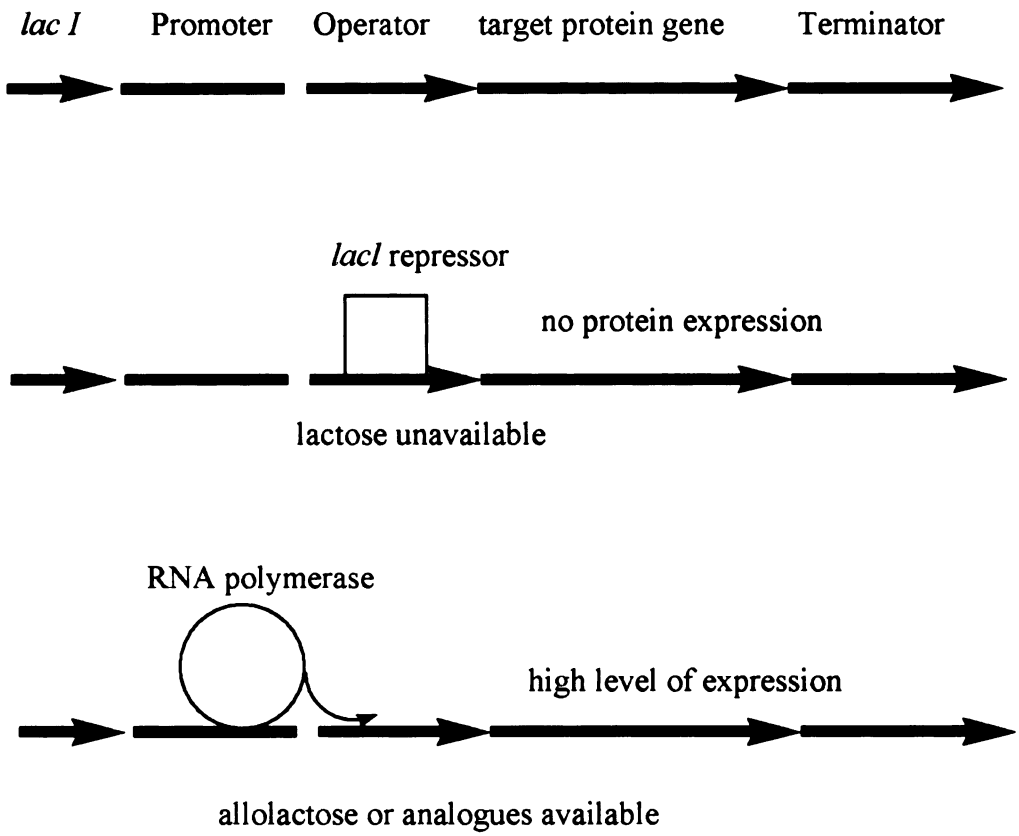

Figure II.1: Schematic diagram of protein expression controlled by *lac* promoter, operator and repressor. Little target protein is produced in the absence of lactose. Overexpression occurs when allolactose or analogues bind to the *lacI* repressor.

In practice, the allolactose analogue, isopropyl β-D-thiogalacto-pyranoside (IPTG) is commonly used to control protein overexpression, because it can bind to the lactose repressor like allolactose, but cannot be metabolized by *E. coli* (Fig II.2). Therefore, its concentration is constant during cell growth, and the rate and level of protein production is sustained during protein overexpression. An additional advantage is

that IPTG is transported into the cell efficiently, independent of the lactose transportation protein.

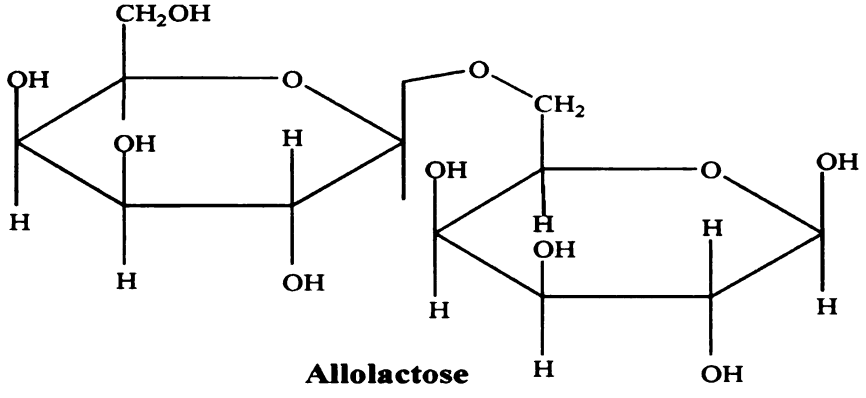

Allolactose

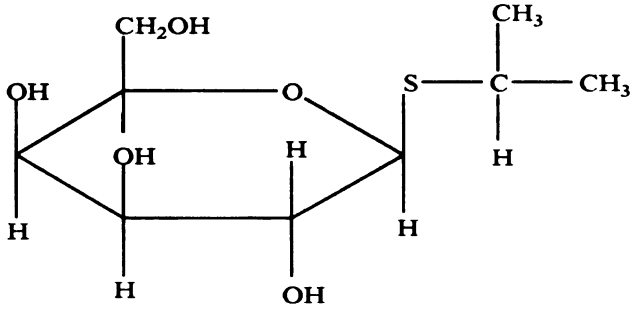

IPTG

Figure II.2: Structures of allolactose and IPTG. IPTG can bind to the *lac* repressor, but cannot be metabolized by the bacteria.

Once a protein is overexpressed, it generally must be isolated from all other cellular proteins. The soluble extract from the cells is a complicated mixture of hundreds of soluble proteins, although the overexpressed protein is ideally present at a much higher quantity than the others. Column chromatography is the most common method used to

purify the protein of interest from the extract. The instrumentation is usually comprised of pumps, an injecting/loading valve, a column, a spectrometer (generally UV-Vis) as the detector, a fraction collector and a computer as the control center. Gel filtration, ion exchange and affinity columns are widely used to purify based on the protein properties.

The gel filtration method was first developed by Porath and Flodin. [4] The so-called gel is composed of cross-linked dextran beads, which consist of an open three-dimensional molecular network. The bead form allows easy column packing and flow optimization. The pores in the beads have various sizes. Small molecules can penetrate all the pores, whereas large molecules, like proteins, can only pass through the pores bigger than their molecular size. The accessibility of the pores to different sizes of molecules ranges from 0 – 100%, with the coefficient K_{av} defining the proportion of the pores that can be penetrated by a specific molecule. One expression of the coefficient is that $K_{av} = (V_e - V_0)/(V_t - V_0)$, where V_t is the total column volume, V_0 (the void volume) is the volume outside of the bead, and V_e is the elution volume. [5] Bigger molecules occupy fewer pores, and therefore have smaller K_{av} values. That means large molecules, with less elution volume, will pass through a certain column with packed beads faster than small molecules. Thus the components in a mixture are separated by molecular size in gel filtration.

Ion exchange columns are another widely used method for protein purification. The net charges on proteins interact with the functional group embedded on the beads. [6] There are generally two types of ion exchangers, anion exchangers and cation exchangers. Anion exchangers have a positively charged matrix, interacting with the negative charges

on the protein surface. Cation exchangers, oppositely, have a negatively charged matrix to attract protein's positive charges.

Diethylaminoethyl (DEAE) and quaternary amino ethyl (QAE) substituents, connected to hydroxyl groups on the matrix, are commonly used anion exchangers. The positive charge is on the nitrogen atom of the exchangers. There are no dissociable protons for the quaternary amine, but in DEAE the proton on the nitrogen can leave, which makes DEAE partially positive charged at neutral pH. During the purification, it can act as a strong buffer, aiding the separation of proteins.

There are three classes of cation exchangers, the "weak" substituents carboxymethyl groups, the "strong" substituents sulfonate groups, and phosphate. The "weak" adsorbents are widely used above pH 4.5. For pH below 4, the "strong" substituents are required, as even at low pH they will not be protonated . Phosphate groups not only adsorb positive charges on the protein, but also interact with proteins that bind to phosphorylated substrates such as nucleic acids. [7]

The ion substituents on ion exchangers are neutralized by counterions. For instance, Cl^- is a common counterion for anion exchangers and H^+ is a common counterion for cation exchangers. The charges on proteins can replace the counterions on the substituents, and therefore the proteins are adsorbed on the matrix under appropriate conditions. To elute the adsorbed protein, salt gradients are usually applied. The salts can weaken the interaction between the protein and the adsorbents, which releases the protein into the buffer solution. Proteins with stronger adsorption are kept on the matrix longer and eluted out later than the protein with weaker adsorption, and thus proteins are separated by their interaction with the ion exchangers.

Hydrophobic interactions are also used in protein purification. [8] In aqueous solutions, the hydrophobic amino acid residues on protein's surface are attracted to the hydrophobic adsorbents on the matrix. The extent of binding of a specific protein to the matrix is dependent on the protein, the type and density of the substituents, and the buffer conditions. The hydrophobic adsorbents are usually short aliphatic chains (C_4 to C_{10}) or a benzyl group connected to the matrix by hydroxyl groups. High salt concentrations in the buffer promote the hydrophobic interaction. The separation in hydrophobic columns is usually poorer than in ion exchange columns due to more variations in this interaction.

II.2 Materials and methods

II.2.1 Chemicals, bacterial cells and plasmids

All chemicals were commercially purchased and of the highest quality except as noted otherwise. *E. coli* BL21(DE3)plysS competent cells were purchased from Novagen™. The plasmids pKK/pfl and pMG-AE [9] were generously donated by Dr. John Kozarich. The pKK/pfl was amplified in our lab as previously described, [10] and the AE gene from pMG-AE was engineered into the pCAL-n-EK expression vector (Stratagene) to produce pCAL-n-AE, which was amplified and stored as a stock solution. [10] Both of the pKK and pCAL-n-EK vectors carry the *lac* operator and ampicillin (AMP) resistance. SDS-PAGE gels were purchased from Bio-Rad Scientific.

II.2.2 Overexpression of PFL

The plasmid pKK/pfl (1 μL) was transformed into 50 μL of BL21(DE3)plysS competent cells. Luria Broth (LB) media (100 μL) was added to the cells thereafter. The

bacteria were incubated at 37 °C for 1 h. The growth was spread on 2 LB media plates containing 50 μg/mL AMP. The cells were incubated at 37 °C overnight. One single colony from the plates was used to inoculate 50 mL of LB media containing 50 μg/mL AMP. The cells were grown at 37 °C overnight. This saturated culture was added into 10 L of LB media with 50 μg/mL AMP. The 10 L growth was conducted in a fermentor (New Brunswick Scientific) at 37 °C, with 250 rpm stirring and 10 L/min air flow. The optical density (OD) of the culture, read as the absorption at 600 nm in the UV-Vis spectrometer (HP 8453), was used to monitor cell growth. When the OD_{600} reached 0.8, isopropyl β-D-thiogalacto-pyranoside (IPTG) was introduced into the growth to 1 mM final concentration. The culture was allowed to grow for another 2 h at 37 °C. The PFL overexpression was checked by SDS-PAGE. The cells were then harvested by centrifugation at 4 °C, 8000 rpm for 10 minutes in a Sorvall GS3 rotor. The cell pellet was weighed and stored at -80 °C.

II.2.3 Purification of PFL

The cell pellet was lysed in a lysis buffer (1 g cell paste / 2 mL buffer) at 4 °C. The buffer contained 20 mM HEPES, pH 7.2, 1 mM DTT, 1% (w/v) Triton X-100, 5% (w/v) glycerol, 10 mM $MgCl_2$, 1 mM PMSF, 0.2 mg/mL lysozyme, 0.002 mg/mL DNAse I and RNAse A. The suspension was stirred for 2 h until it was homogenized.

The mixture was centrifuged at 4 °C, 15,000 rpm for 30 minutes. The crude extract (50 mL) was loaded directly onto an AP-5 column (5 x 30 cm, Waters) packed with Accell Plus QMA anion exchange resin (Waters), and equilibrated with buffer A (20 mM HEPES, pH 7.2 and 1 mM DTT). The column was run isocratically with buffer A

for 60 min, followed by a linear gradient from 0% to 100% buffer B (20 mM HEPES, pH 7.2, 500 mM NaCl, and 1 mM DTT) over 180 min and isocratic 100% B for another 60 min. Fraction collection (10 mL/fraction) started at 180 min. The purification was conducted by a BioLogic HR workstation chromatography system at 4 °C, and a flow rate 5 mL/min. The fractions were analyzed by SDS-PAGE (12% Tris-HCl gel) to identify PFL and roughly quantify the relative amount of the protein in the fraction. The fractions containing >~ 75% of the soluble proteins as PFL were combined and concentrated to less than 10 mL on a Millipore YM-30 membrane using an Amicon™ concentrator.

The concentrated PFL was then purified by hydrophobic interaction chromatography at 4°C and 1.0 mL/min. Approximately 5 mL of concentrated PFL fractions were dialyzed against 3 L (2 x 1.5 L exchange) of buffer C (40 mM HEPES, pH 7.2, 1 M $(NH_4)_2SO_4$, and 1 mM DTT) for total 4 h. After the dialysis, PFL was loaded onto a Hi-load phenylsepharose hydrophobic interaction column (1.6 x 10 cm, Pharmacia) equilibrated with buffer C. The column was run isocratically with 100% C for 50 min, followed by a linear gradient to 100% buffer D (40 mM HEPES, pH 7.2 and 1 mM DTT) over the next 50 min and an isocratic wash at 100% buffer D for 50 min. The fraction collection (2 mL/fraction) started at 75 minutes. The fractions were analyzed by SDS-PAGE (12% Tris-HCl gel). Those with PFL >~ 95% of total soluble proteins were pooled together and concentrated. The concentrated protein was flash frozen in liquid N_2 and stored at -80 °C.

II.2.4 Overexpression of PFL-AE

Expression plasmid pCal-n-AE was transformed into 50 μL of BL21(DE3)plysS competent cells. LB media (100 μL) was added into the cells thereafter. The bacteria were incubated at 37 °C for 1 hour. The cells were spread on 2 LB media plates, containing 50 μg/mL AMP, and incubated at 37 °C overnight. One single colony from the plates was used to inoculate 50 mL of LB media containing 50 μg/mL AMP. The cells were grown at 37 °C overnight. This saturated culture was added into 10 L of minimal media with 50 μg/mL AMP and 34 μg/mL of chloramphenicol (CAM). [11, 12] The minimal media contained (per 10 L) 110 g Casamino acids, 84.2 g MOPS, 29.3 g NaCl, 8.0 g TRICINE, 16.0 g KOH, 5.1 g NH_4Cl, 40 g glucose, 2 mM KH_2PO_4, 0.276 mM K_2SO_4, 0.5 mM $CaCl_2$, 9 vitamins (biotin, thiamine, riboflavin, niacinamide, pantothenic acid, folic acid, vitamin B12, thioctic acid, pyridoxine, 10 mg of each), and trace amount of minerals (Fe^{2+}, BO_3^{3-}, Mn^{2+}, Co^{2+}, Cu^{2+}, Zn^{2+}, and MoO_4^{2-}). [11, 12] The 10 L growth was conducted in a fermentor (New Brunswick Scientific) at 37 °C, with 250 rpm stirring and 10 L/min air flow. When the OD_{600} reached 0.5, IPTG was introduced into the growth to 0.5 mM final concentration and 0.75 g $Fe(NH_4)_2(SO_4)_2$ was also added into the growth. The culture was allowed to grow for another 2 h aerobically. After 2 h the culture was cooled down to 30 °C, air flow was turned off, and N_2 passed through at 10 L/min while continuing to cool the culture. After 30 minutes, 0.75 g of $Fe(NH_4)_2(SO_4)_2$ was added. Once the temperature reached 20 °C, the fermentor was moved into a 4 °C refrigerator and N_2 was bubbled through the culture for at least 14 h at 4 °C. The cells were then harvested by centrifugation at 4 °C, 8000 rpm for 10 minutes in a Sorvall GS3 rotor. The cell pellet was weighed and stored at -80 °C.

II.2.5 Purification of PFL-AE

The entire purification of PFL-AE was carried out under strictly anaerobic conditions in a COY anaerobic chamber (COY Laboratories, Grass Lake, MI). Cell pellet (10 – 15 g) was suspended in 45 mL of lysis buffer, which contained 50 mM Tris-HCl, pH 7.5, 200 mM NaCl, 5% (w/v) glycerol, 1% (w/v) Triton X-100, and 10 mM $MgCl_2$. The buffer was degassed thoroughly on a Schlenk line before taking into the anaerobic chamber. To the anaerobic lysis buffer was added 39 mg DTT, 9 mg PMSF, 8 mg lysozyme, and 0.1 mg DNAseI and RNAseA. The pellet was then added to the buffer, and the mixture was stirred for 1 hour in an ice-water bath until it was totally homogenized. This suspension was centrifuged at 18,000 rpm at 4 °C for 30 minutes. The resulting crude extract (50 mL) was loaded onto an AP-5 column (5 x 60 cm, Waters) packed with Superdex-75 (Pharmacia) gel filtration resin. If the PFL-AE was well prepared, the crude extract would have a distinct dark brown color from the $[4Fe\text{-}4S]^{2+}$ clusters in the enzyme. The purification was conducted by an AKTA Basic 10 chromatography system (GE Healthcare).

The Superdex-75 column was pre-equilibrated with elution buffer (50 mM Tris-HCl, pH 7.5, 200 mM NaCl, and 1 mM DTT). Elution was carried out at room temperature with flow rate 5 mL/min. Fraction collection (10 mL/fraction) started at 2 h. The dark brown fractions were combined together and concentrated to about 10 mL on a Millipore YM-10 membrane in an Amicon™ concentrator. The concentrated fractions were flash frozen in liquid N_2 and stored at –80 °C. Usually three batches of the concentrated fractions were pooled together and loaded onto the same column again, and purified using the same method as the first time. The UV-Vis absorbance of the dark

brown fractions was measured at 426 nm, indicative of the $[4Fe\text{-}4S]^{2+}$ clusters, and at 280 nm, indicative of the protein concentration. Only the fractions with A_{426}/A_{280} ratio over 0.19 were combined together and concentrated to less than 10 mL. The purified enzyme was flash frozen in liquid N_2 and stored at -80 °C.

II.2.6. Determination of protein concentration

The concentration of the proteins was determined by the method of Bradford. [13] The absorbance at 595 nm of Bradford dye in the presence of protein was measured as the indicator of the protein concentration. Bovine serum albumin (BSA) was used as the standard. According to Beer's law, a standard curve of A_{595} corresponding to a series of BSA concentrations was established. The concentration of PFL or PFL-AE was calculated from the absorbance using the standard curve.

II.2.7. Determination of iron content in PFL-AE

Iron assays were conducted using the method of Fish or Beinert. [14, 15] The iron in PFL-AE were completely oxidized to Fe^{3+} using $KMnO_4$ (4.5% w/v) and 1.2 M HCl. The absorbance at 562 nm of ferrozine-Fe^{3+} complex was measured as the indicator of the iron concentration. $Fe(NO_3)_3$ or $FeCl_3$ solution was used as the standard. A standard curve of A_{562} corresponding to the ferrozine-Fe^{3+} complex concentrations was established. The iron concentration in PFL-AE was calculated from A_{562} using the standard curve.

II.3 Results and discussion

II.3.1 Overexpression and purification of PFL

The PKK/pfl plasmids were transformed into *E. coli* BL21(DE3)plysS strains. Usually 10 L of growth could produce 30 – 40 g of cell pellet. PFL was well expressed in the bacteria, determined by SDS-PAGE (Fig II.3). PFL showed a band at the monomeric molecular weight of 85 kDa.

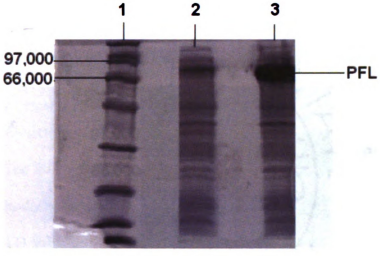

Figure II.3: SDS-PAGE of PFL overexpression. 1 mL of culture was taken out for the test. Lane 1 is the protein standard. Lane 2 is the growth before IPTG induction. Lane 3 is the growth 2 h after induction. PFL monomer band is at 85 kDa.

The ovexpressing cells were lysed using an enzymatic lysis procedure. The crude extract was first purified by an anion exchange column. The collected fractions containing PFL >~ 75% of total soluble proteins as identified by SDS-PAGE (12% Tris-HCl gel), were combined together and concentrated (Fig II.4). The concentrated fractions were purified by hydrophobic interaction chromatography. The PFL content in the collected fractions was determined by SDS-PAGE (12% Tris-HCl gel) again, and the fractions that had >~ 95% of soluble proteins as PFL were pooled together and concentrated (Fig II.5). A typical 10 L growth would yield 500 – 600 mg of purified PFL.

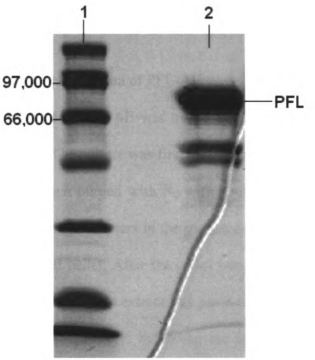

Figure II.4: SDS-PAGE of PFL obtained after anion exchange chromatography. Lane 1 is the protein standard. Lane 2 is PFL after the anion exchange column.

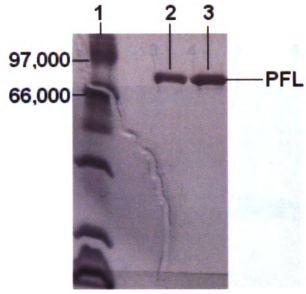

Figure II.5: SDS-PAGE of PFL obtained after hydrophobic interaction chromatography. Lane 1 is the protein standard. Lane 2 is 0.9 μg PFL loaded onto the gel. Lane 3 is 1.4 μg PFL loaded onto the gel

II.3.2 Overexpression and purification of PFL-AE

The PFL-AE plasmid pCal-n-AE was transformed into *E. coli* BL21(DE3)plysS to overproduce the enzyme. The culture was first grown aerobically to express the protein after IPTG induction, and then purged with N_2 with cooling. The process is thought to allow assembly of the $[4Fe\text{-}4S]^{2+}$ clusters in the presence of ferrous iron. A 10 L growth can produce 40 – 60 g of cell pellet. After the pellet was lysed in an anaerobic chamber by an enzymatic lysis buffer, the crude extract was passed through a gel filtration column. The fractions with a dark brown color, indicating the presence of iron-sulfur clusters, were pooled together and concentrated. The fractions were then purified by the same gel filtration column again. The fractions with A_{426}/A_{280} ratio over 0.19 were combined together and concentrated (Fig II.6). A typical 10 L growth can produce 250 – 350 mg of purified PFL-AE.

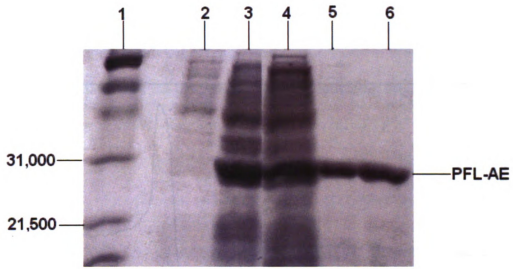

Figure II.6: SDS-PAGE showing the overexpression and purification of PFL-AE. Lane 1 is the protein standard. Lane 2 is PFL-AE growth before induction. Lane 3 is PFL-AE growth after IPTG induction. Lane 4 is the lysis of overpressing cells. Lane 5 is PFL-AE obtained after the first gel filtration column. Lane 6 is PFL-AE obtained after the second filtration column.

A successful growth and purification of PFL-AE has been found to produce protein containing close to 4 mol of Fe per mol of protein (3.8 – 4.0 Fe/PFL-AE for different high quality preparations). The state of the iron-sulfur cluster in the enzyme depends on how strictly anaerobic conditions were maintained during the growth and purification. The unique Fe in the $[4Fe\text{-}4S]^{2+}$ is highly sensitive to O_2, and exposure of the enzyme to air can deplete the unique Fe and form a $[3Fe\text{-}4S]^{+}$ cluster. [10, 12] After purification, PFL-AE is tested by EPR spectroscopy to monitor the state of the cluster. The $[4Fe\text{-}4S]^{2+}$ cluster is EPR silent, whereas $[3Fe\text{-}4S]^{+}$ cluster shows a strong and nearly isotropic signal at g = 2.02 (Fig II.7). [16] For the protein shown in Fig II.7, the spin quantification of the $[3Fe\text{-}4S]^{+}$ cluster, conducted according to the published method, [17] is

362 μM in a total protein concentration of 0.89 mM. High quality PFL-AE should have no such signal or a very small signal.

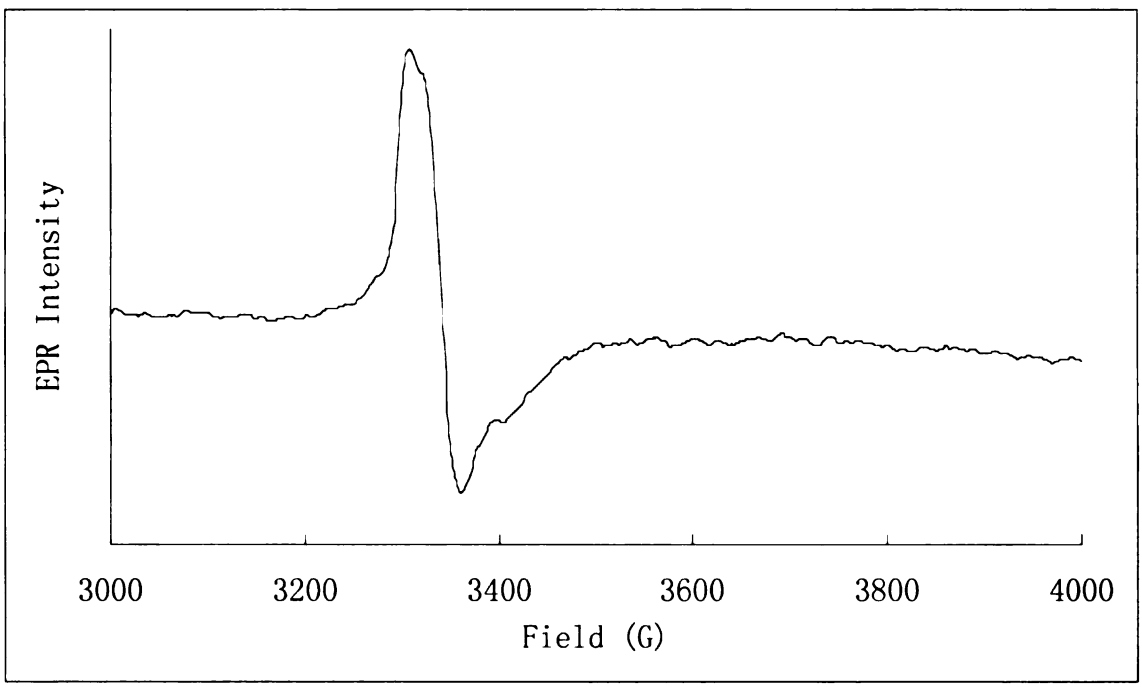

Figure II.7: X-band EPR spectrum of $[3Fe\text{-}4S]^{+}$ cluster in PFL-AE. Temperature 12 K, microwave power 1.9 mW, microwave frequency 9.36 GHz, modulation frequency 100 kHz, modulation amplitude 5 G, resolution 1024.

II. 4 Conclusions

PFL was successfully overexpressed in *E. coli* BL21(DE3)plysS strains. The protein was purified initially by anion exchange chromatography and subsequently by hydrophobic interaction chromatography. Purified PFL showed a monomeric molecular weight band at 85 kDa in SDS-PAGE. Although PFL is only active under anaerobic conditions, it can be prepared aerobically and is stable in the presence of air as an inactive form.

PFL-AE was successfully overexpressed in *E. coli* BL21(DE3)plysS strains. The protein was purified by gel filtration chromatography twice under strictly anaerobic conditions. The enzyme has a distinct dark brown color, which is from the $[4Fe\text{-}4S]^{2+}$ cluster. The absorption ratio A_{426}/A_{280} was used to choose the fraction that had most intact $[4Fe\text{-}4S]^{2+}$ cluster in PFL-AE. The purified protien showed a 28 kDa band on SDS-PAGE as the primary structure predicted [18]. The best preparation of PFL-AE had close to 4 mol of Fe per mole of protein, and had no $[3Fe\text{-}4S]^{+}$ cluster signal in the EPR spectrum.

References

1. Voet, D. V., J. G.,, *Biochemistry*. 2nd ed.; John Wiley & Sons: New York: 1995.

2. Winstanley, C. R., R., *Protein Derived Cloning Vectors. In Molecular Biomethods Handbook*. Eds. Humana Press: Totowa, New Jersey, 1998; p pp 165-179.

3. Jacob, F.; Monod, J., *J Mol Biol* **1961,** 3, 318-56.

4. Porath, J.; Flodin, P., *Nature* **1959,** 183, (4676), 1657-9.

5. Scopes, R., *Protein Purification*. 3rd ed.; Springer: 1993.

6. Muller, W., *Journal of Chromatography* **1990,** 510, 133-144.

7. Chilla, R.; Doering, K. M.; Domagk, G. F.; Rippa, M., *Arch Biochem Biophys* **1973,** 159, (1), 235-9.

8. Ochoa, J. L., *Biochimie* **1978,** 60, 1-15.

9. Parast, C. V.; Wong, K. K.; Lewisch, S. A.; Kozarich, J. W.; Peisach, J.; Magliozzo, R. S., *Biochemistry* **1995,** 34, (8), 2393-9.

10. Broderick, J. B.; Henshaw, T. F.; Cheek, J.; Wojtuszewski, K.; Smith, S. R.; Trojan, M. R.; McGhan, R. M.; Kopf, A.; Kibbey, M.; Broderick, W. E., *Biochemical and Biophysical Research Communications* **2000,** 269, (2), 451-456.

11. Garboczi, D. N.; Hullihen, J. H.; Pedersen, P. L., *J Biol Chem* **1988,** 263, (30), 15694-8.

12. Krebs, C.; Henshaw, T. F.; Cheek, J.; Huynh, B. H.; Broderick, J. B., *Journal of the American Chemical Society* **2000,** 122, (50), 12497-12506.

13. Bradford, M. M., *Anal Biochem* **1976,** 72, 248-54.

14. Fish, W. W., *Methods Enzymol* **1988,** 158, 357-64.

15. Beinert, H., *Methods Enzymol* **1978,** 54, 435-45.

16. Kennedy, M. C.; Kent, T. A.; Emptage, M.; Merkle, H.; Beinert, H.; Munck, E., *J Biol Chem* **1984,** 259, (23), 14463-71.

17. Aasa, R.; Vanngard, T.; Dunford, H. B., *Biochim Biophys Acta* **1975,** 391, (2), 259-64.

18. Roedel, W.; Plaga, W.; Frank, R.; Knappe, J., *European Journal of Biochemistry* **1988,** 177, (1), 153-8.

CHAPTER III

SULFUR LIGAND K-EDGE X-RAY ABSORPTION SPECTROSCOPIC STUDY OF PYRUVATE FOMATE-LYASE ACTIVATING ENZYME

III.1 Introduction

Under anaerobic conditions PFL-AE activates PFL via reductively cleaving AdoMet, [1-3] in which the electron required for the reduction is provided by the $[4Fe\text{-}4S]^{1+}$ cluster in PFL-AE and a putative deoxyadenosyl radical intermediate is generated. [4] This extremely reactive radical abstracts a pro-S hydrogen from Gly734 in PFL to yield a glycyl radical, [4, 5] thus activating PFL to its radical form. [6, 7] The cleavage of AdoMet occurs between the sulfonium sulfur and the 5' carbon, when one electron is transferred from the $[4Fe\text{-}4S]^{1+}$ cluster to AdoMet (Fig III.1). One interesting questions are how the interaction between AdoMet and the reduced cluster causes the electron transfer and which atom in the cluster, the unique iron or the bridging sulfide, ejects the electron to AdoMet. In another word, what is the mechanism behind the process?

Although previous evidence showed that AdoMet binds to the iron-sulfur cluster of PFL-AE through a unique Fe site by the carboxylate O and amino N, [8-11] the evidence of the interaction between the sulfonium S and the cluster is ambiguous. In the investigation of LAM, both the Se X-ray absorption spectroscopy (XAS) data of the interaction between Se-AdoMet and the iron-sulfur cluster and the crystal structure of LAM indicate that the Se of Se-Met is in the distance (2.7 Å away from an Fe site in Se XAS study and 3.2 Å away from the unique Fe in the crystal structure) to interact with

the unique Fe. [12, 13] However, Se XAS studies of Se-AdoMet in PFL-AE and BioB showed no evidence for a nearby iron to the Se, [14] and ENDOR studies of PFL-AE implied the sulfonium S in AdoMet had orbital overlap with the cluster, which could occur either via a bridging sulfide or through one of the iron atoms. [11]

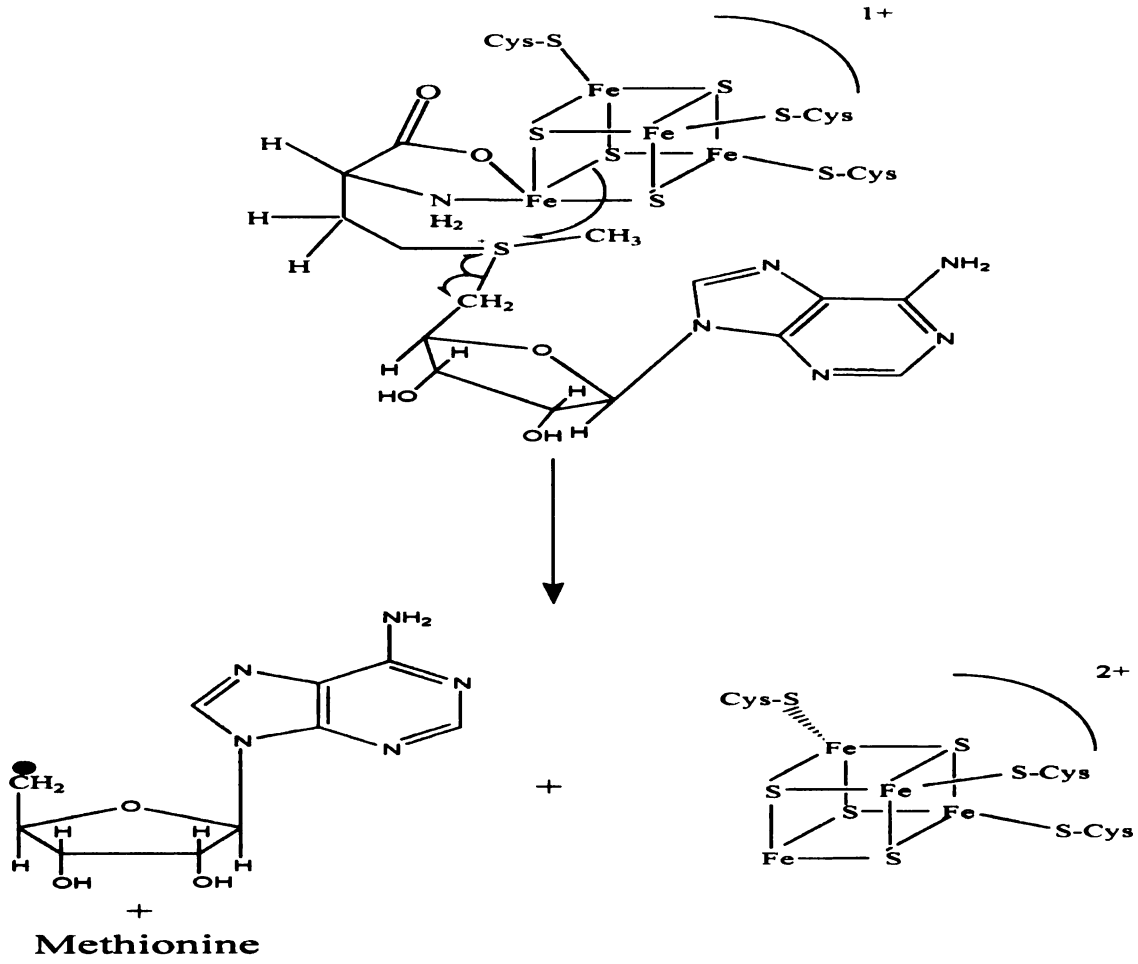

Figure III.1: The cleavage of AdoMet by radical SAM enzymes. One electron is transferred from $[4Fe\text{-}4S]^{1+}$ to sulfonium S. A deoxyadenosyl radical and a methionine are generated.

To illustrate the interaction between the sulfonium S and the cluster, a relatively new technique sulfur ligand K-edge XAS was used. This method is able to elucidate the covalency of iron-sulfur bonds, whose quantification demonstrates the exchange coupling between Fe 3d orbitals and S 3p orbitals, in Fe-S clusters. [15-17] Upon AdoMet binding, the

electronic property of the Fe-S bond in the cluster could be disturbed accordingly, which is partly due to the interaction between the sulfonium sulfur and the cluster. The calculation based on the change of the covalency in the absence and presence of AdoMet might illustrate the distance between the S^+ to the atoms in the cluster, and the orbital coupling between AdoMet and the cluster, which implies the mechanism of electron transfer from the cluster to the substrate.

A high-energy X-ray photon can be absorbed by an atom in a sample if the photon's energy matches the binding energy of an inner shell electron. The electron can be ejected into a vacant molecular orbital, which is related to the molecule's electronic structure and geometry. Hence, distinct absorptions provide information about the bonds surrounding the atom. A typical XAS spectrum shows a sharp rise in absorbance, a so-called edge, when the photon is absorbed. The absorption is sensitive to the electronic structure of the atom and demonstrates special features in the edge region. A scan of the X-ray photon energy range can provide several absorption edges for one atom as each photon energy is equal to the ionization potential of the inner shell electron. The different edges are called K, L, M, etc, whose names are derived from the shells of the Bohr atom (K edge for n = 1, L edge for n = 2, M edge for n = 3). The K-edge absorption of sulfur is at 2.5 keV.

The ligand—metal bond covalency can be estimated from a pre K-edge feature in the ligand K-edge X-ray absorption spectroscopy. [18] The ligand K-edge absorption is due to the ligand 1s → 4p transition. The ligand 4p orbitals can, however, covalently overlap with the unoccupied metal 3d antibonding orbitals, and the ligand filled 1s electrons are able to transit into the metal 3d orbitals, due to the electric dipole allowed ligand 1s → 4p

transition (Fig III.2). The intensity of the 1s → 3d forbidden transition, which occurs on the pre-edge region, depends on how much the ligand covalent character overlaps with the metal unfilled antibonding 3d orbital. Therefore, the intensity of the pre-edge feature can quantify the ligand—metal bond covalency. The energy position of the pre-edge transition is determined by both the shift of ligand 1s orbital energy and the energy of the lowest unoccupied molecular orbital (LUMO) of the complex. The shift of ligand 1s orbital energy is related to the effective charge on the nucleus (Z_{eff}) of the ligand. In addition, the 1s orbital shifts to lower energy due to the ligand electron density delocalization onto the metal in the complex bonds. Two primary factors contribute to the complex LUMO energy: the geometry of the ligand field affects the d orbital energy splitting, and the overall d energy can shift too, which is related to the coordination number and the Z_{eff} of the metal.

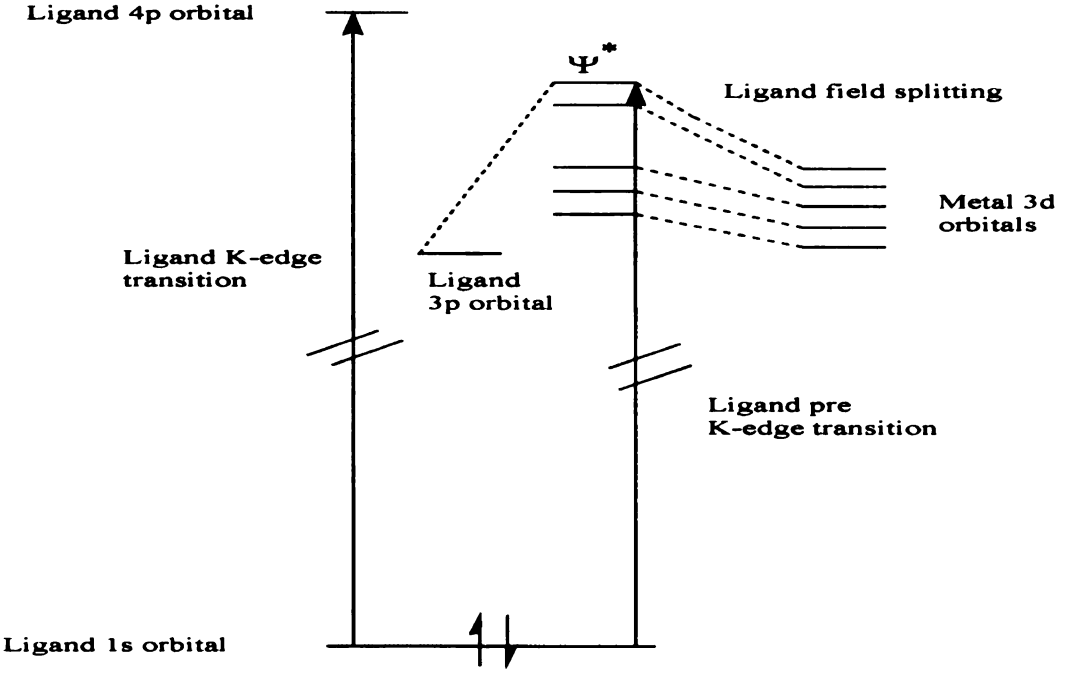

Figure III.2: Schematic representation of the ligand pre K-edge transition. The energy of the transition is determined by both the ligand 1s orbital and the metal unoccupied 3d antibonding orbital.

Sulfur K-edge XAS has been applied to investigate the characteristics of the Fe-S bonds and electron transfer in the active sites of various iron-sulfur proteins and their model complexes, such as rubredoxin, [19] Fe_2S_2 ferredoxin, [20] Fe_3S_4 ferredoxin, [21] Fe_4S_4 ferredoxin and high potential iron-sulfur protein (HIPIP). [16] In those XAS spectra, two major pre-edge features between 2469 eV and 2471 eV are deconvoluted from the absorption of each protein, except for rubredoxin which only has one pre-edge feature. The lower energy transition is from the bridging sulfide 1s → Fe 3d antibonding orbital, and the higher energy absorption is the transition between the terminal thiolate 1s → Fe 3d antibonding orbital. The primary edge rises after 2472 eV, which is assigned to the thiolate 1s to C—S σ^* transition. The covalency of the Fe-S bond is calculated from the pre-edge transition intensity.

Although the ligand pre K-edge XAS monitors the electron transfer from the ligand to the metal, its physical principles are different from ligand to metal charge transfer (LMCT). LMCT involves the transition of an electron from a complex bonding molecular orbital (MO) with primary ligand character to an antibonding MO with predominantly metal character. The electric dipole-allowed transfer shows a broad and intense absorption band in the UV-Vis region. In the ligand pre-edge XAS, the electron donor has only ligand character since the ligand 1s orbital has no overlap with the metal. Its transition dipole moment is oriented on the ligand alone, while the transition dipole moment in LMCT is mixed between the ligand and metal. Therefore, the LMCT is bond length dependent, but the ligand pre-edge XAS is not.

Another traditional method to investigate the ligand—metal bond and the coordination environment is EPR. EPR involves the spectroscopic detection of species

that have unpaired electrons. These species are either radicals or transition metal ions coordinated in complexes. A single electron has a magnetic moment because of its electronic spin. If the electron is surrounded by an external magnetic field, this magnetic moment can be aligned parallel or antiparallel to the external field, with parallel state having lower energy than the antiparallel state (Zeeman effect). The electron can resonantly absorb a photon, if the photon energy matches the separation between the parallel and antiparallel states (Fig III.3). This energy separation is $\Delta E = h\nu = g_e \mu_B B$, where g_e is called g factor, which is the ratio between the electron magnetic dipole momentum and the angular momentum, μ_B is the Bohr magneton, and the B is the external magnetic field. The g factor for a free electron in vacuum is 2.002319304386; the g factor can, however, deviate from this number if the environment changes. The actual g factor is, therefore, one indicator of the electronic structure surrounding the unpaired electron. The EPR signal is generally shown as a first derivative of the resonance absorbance, and the shape of the signal is frequently reflective of the geometry of the coordination environment. To enhance the resonance, EPR is usually measured at low temperature, due to the more favorable Boltzmann distribution and slower relaxation times.

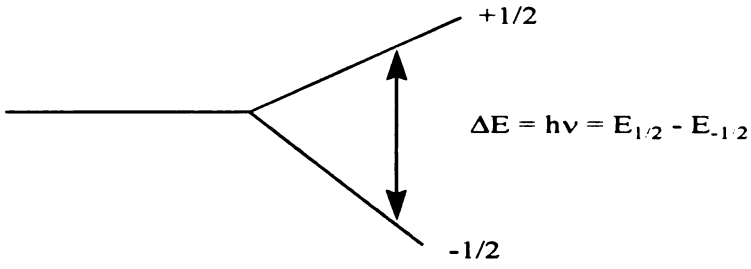

Figure III.3: Schematic representation of the energy separation of an electron magnetic moment placed in an external magnetic field.

The Fe_4S_4 cluster has been considered as a pair of two Fe_2S_2 subunits. [22] The electrons are delocalized between two irons in each subunit. [23] The $Fe^{3+}Fe^{2+}$ dimer has one electron shared, so the overall status of the subunit is two $Fe^{2.5+}$. The delocalized electron keeps the same spin state when it is in the presence of each iron site, and aligns antiparallel to the d^5 core electrons on the metal. Thus the spins of the d^5 electrons on each Fe^{3+} are aligned parallel, which is called ferromagnetic coupling (Fig III.4). The total spin of the Fe_2S_2 is S = +9/2. In the Fe_4S_4 cluster, the two Fe_2S_2 subunits are coupled antiferromagneticlly, meaning the delocalized electrons are aligned antiparallel. The $[4Fe\text{-}4S]^{2+}$ has a total spin S = 0 and is EPR silent, since each Fe_2S_2 cluster has a spin S = 9/2. In the reduced $[4Fe\text{-}4S]^{1+}$ cluster, one more electron is delocalized in one of the Fe_2S_2 subunits, and makes the overall spin of the Fe_4S_4 cluster S = + 1/2. This cluster is observable in EPR.

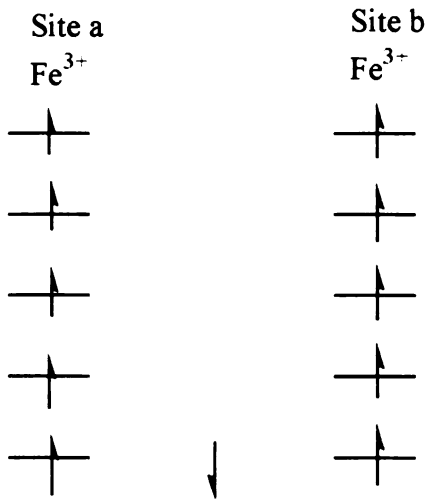

Ferromagnetic coupling in a Fe_2S_2 subunit

Figure III.4: Schematic representation of an electron delocalization in a $Fe^{2.5}Fe^{2.5}$ dimer. The spin state of the unit is S = +9/2.

III.2 Materials and methods

III.2.1 Chemicals and materials

All chemicals were commercially purchased and of the highest quality except as noted otherwise. *E. coli* BL21 (DE3)plysS competent cells were purchased from Novagen™. The pCAL-n-EK expression vector was purchased from Stratagene. pMG-AE plasmid was inserted into the expression vector to produce the pCAL-n-AE plasmid. SDS-PAGE gels were purchased from Bio-Rad Scientific.

III.2.2 Overexpression and purification of PFL-AE

Growth and purification of PFL-AE were carried out following the procedure previously described in II.2.4 and II.2.5, except the modification that the reducing agent in the purification buffer was 1 mM ascorbic acid instead of 1 mM DTT. Because the sulfur XAS measures the absorbance from all types of S, DTT in the buffer would likely have interfere with the XAS results and thus was avoided.

III.2.3 Synthesis of S-adenosylmethionine

AdoMet was synthesized in a reaction catalyzed by SAM synthetase (scheme III.1). A crude extract of cells expressing SAM synthetase was used in the reaction. The reaction was carried out in 10 mL of 100 mM Tris-HCl pH 8.0 buffer, containing 50 mM KCl, 26 mM $MgCl_2$, 13 mM adenosine triphosphate (ATP), 8% (v/v) β–mercaptoethanol, 1 mM EDTA, 10 mM methionine, 2.5 μL of inorganic pyrophosphatase (0.25 U) and 1 mL of SAM synthetase crude lysate. It was stirred at room temperature for 16 hours and terminated by adding 1 mL of 1 M HCl. The solution was centrifuged at 18,000 rpm, 4 °C

for 30 minutes to remove the proteins. The clear solution (6 mL) was loaded onto a Source 15S cation exchange column (Pharmacia, 1 cm x 10 cm), precharged with 1 M HCl and equilibrated with H_2O. The purification of AdoMet was conducted at room temperature with flow rate 2 mL/min. The column was run isocratically at 100% A (MQ H_2O) for 14 min, followed by a linear gradient to 10% B (1 mM HCl)over 5 min and then isocratically at 10% B for 8 min. A linear gradient from 10% to 100% B over 60 min was used to elute the AdoMet. The column was then washed with 100% B for 10 min followed by re-equilibration with buffer A. The eluate between 40% and 60% B was collected. The fractions were lyophilized on a Shlenk line and weighed after being completely dried. The solid was then dissolved in 50 mM Tris-HCl pH 7.5 in the anaerobic chamber (Mbraun). NaOH (1 M) was used to adjust the pH to near 7.0.

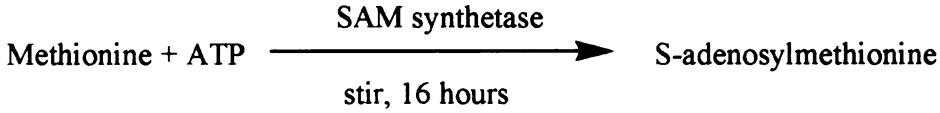

Scheme III.1: Schematic representation of AdoMet synthesis catalyzed by SAM synthetase.

III.2.4 Sample preparation for sulfur XAS

All procedures were carried out in the anaerobic glove box (Mbraun) with O_2 levels under 1 ppm. PFL-AE (300 μL of 3.4 mM) was mixed with 50 μL of 70 mM AdoMet to make the final concentration of PFL-AE 2.9 mM and AdoMet 10 mM. PFL-

AE (300 μL of 3.4 mM) alone as well as the prepared PFL-AE and AdoMet mix were flash frozen in liquid N_2 in the box and stored at –80 °C.

III.2.5 PFL-AE photo-reduction

All procedures were carried out in EPR tubes in the anaerobic glove box (Mbraun). Photoreduction was carried out in two identical samples, 300 μL each, containing 100 mM Tris-HCl pH 7.5, 100 mM KCl, 50 μM PFL-AE, 100 μM 5-deazariboflavin (the photo reducing agent), and 100 μM dithionite. A 300 W halogen lamp was put 5 cm away from the sample to conduct the photo reduction. The EPR tubes were placed in an ice-water bath (4 °C) to prevent over heating the samples. After illumination, one sample was flash frozen in liquid N_2. AdoMet (1.6 μL, 55 mM) was added into the other sample to make the final AdoMet concentration 150 μM. The sample was then flash frozen in liquid N_2.

Another set of samples was photoreduced following the same procedure above. The samples contained either 10 mM DTT or 10 mM cysteine in addition during the illumination, after which AdoMet (final concentration 150 μM) was added into one of the two identical samples.

The buffer (300 μL of 100 mM Tris-HCl, 100 mM KCl, pH 7.5) was illuminated at the same condition as the blank sample for the background measurement in EPR.

III.2.6 UV-Vis spectroscopy

UV-Vis spectra were recorded on an HP-8453 diode-array spectrometer. PFL-AE was diluted in 100 mM Tris-HCl, 100 mM KCl, pH 7.5 to final concentration 100 μM in

the anaerobic glove box (Mbraun). The diluted samples (300 μL) were loaded into a quartz cuvette with 1 mm optical path length. The cuvette was sealed with a rubber septum in the box. The absorbance between 200 and 1100 nm was measured in the spectrometer at room temperature. During the measurement, a nitrogen flow was purging from a funnel on top of the cuvette.

III.2.7 EPR spectroscopy

EPR spectra were recorded in a Bruker ER-200D-SRC spectrometer at 12 K. X-band microwave frequency 9.37 GHz was used. The microwave power was 1.9 mW. The external magnetic field was scanned from 2000 to 4000 G. The static field was 2000 G. The modulation frequency was 100 kHz, and modulation amplitude was 5 G. Two scans were accumulated.

III.2.8 Sulfur K-edge XAS

The XAS spectra were recorded at the Stanford Synchrotron Radiation Laboratory under ring conditions of 3 GeV and 60-100 mA. The experiments were performed on the 54-pole wiggler beam line 6-2 operating in high field (10 kG) mode with a fully tuned Si(111) double crystal monochromator followed by a Ni-coated harmonic rejection mirror. The X-ray beam was optimized for low-energy studies, with all optical elements under a differentially-pumping maintained vacuum, and with a single, in-hutch 127-μm beryllium window separating the experiment from ring vacuum. This Be window is protected from oxidation by a ~4" He gas path terminated with a 6.35-μm polypropylene window. The beam thereafter passes in a He gas atmosphere through aperturing slits, an

ionization chamber for I_0 measurements, and a 6.35-μm polypropylene window into the sample compartment (Fig III.5).

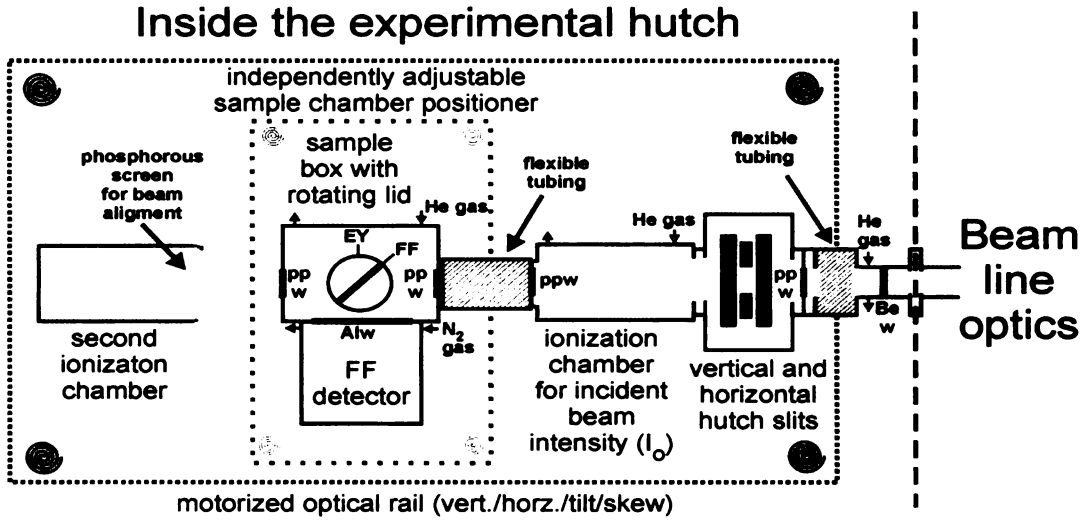

Figure III.5: Schematic representation of the experimental setup of X-ray absorption spectrometer (ppw: polypropylene window, Alw: aluminized Mylar window, Bew: Beryllium window, EY: electron yield , FF: fluorescence). [24]

For fluorescence measurements, a N_2-filled Lytle detector is used without filter or Soller slits. Due to the high absorption at low energies (2-4 keV), external energy calibration using $Na_2S_2O_3 \cdot 5H_2O$ as the standard was performed before and after each sample. The sharp maximum of the first K-edge feature is assigned at 2472.02 eV. The monochromator step size over the edge region was 0.08 eV, the energy resolution was ~0.5 eV, and the reproducibility in energy determination was ~0.1 eV, as determined from repeated calibration and sample measurements during separate experimental runs.

Protein samples (~300 μL) were transferred into a Pt-coated Al block sample cell, sealed with a polypropylene window on the front and with septum-sealed loading and

gas-release holes on the top. The samples were maintained at ~ 4 °C by passing pre-cooled N_2 through the sample cell block.

Pre- and post-data calibration scans were compared and the energy scale of the data is adjusted accordingly. The acceptable data scans were then averaged, and a smooth second-order polynomial background was fit to the pre-edge region and subtracted from the entire spectrum. Normalization of the data was accomplished by fitting a flattened second-order polynomial or straight line to the post-edge region and normalizing to an edge jump of 1.0 at 2490 eV. The protein spectra were re-normalized by the ratio of the total sulfurs (including the cysteines and methionines) and the contributing absorbers for the covalency determinations. Energy positions of features in the normalized spectrum were obtained from the minima in the second derivative of the data.

III.3 Results and discussion

III.3.1 Overexpression and purification of PFL-AE

PFL-AE has been successfully overexpressed in *E. coli* strains BL21(DE3)plysS. After purification in the presence of 1 mM ascorbic acid, the enzyme showed a distinct dark brown color. The protein was over 95% pure as determined by densitometry of an SDS-PAGE gel (Fig III.6). The concentration of the protein was 3.4 mM and one mole of PFL-AE contained 3.7 mole of Fe.

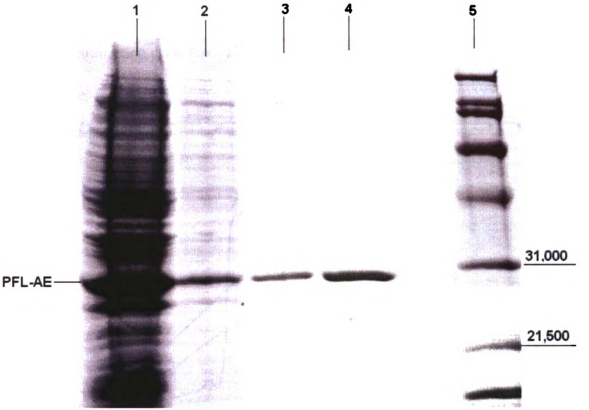

Figure III.6: SDS-PAGE gel of PFL-AE purified in the presence of 1 mM ascorbic acid. Lane 1: *E. coli* cells overexpressing PFL-AE after IPTG induction; Lane 2: Soluble lysate of cells expressing PFL-AE. Lane 3: PFL-AE after 1st run over gel filtration column; Lane 4: PFL-AE after 2nd run over gel filtration column; Lane 5: Protein standard.

III.3.2 Synthesis of S-adenosylmethionine

AdoMet synthesis and purification followed the procedure described in the experimental methods. AdoMet was eluted out from the cation exchange column as a broad and intense peak between 40% and 60% B monitored by UV absorbance at 260 nm (Fig III.7). After lyophilization, AdoMet was a colorless solid. A total of 36 mg of product was obtained, corresponding to a 72% yield. Since AdoMet eluted between 0.4

and 0.6 M HCl, the solution made from the solid dissolved in the buffer was still acidic, and thus neutralization using NaOH (1M) was necessary.

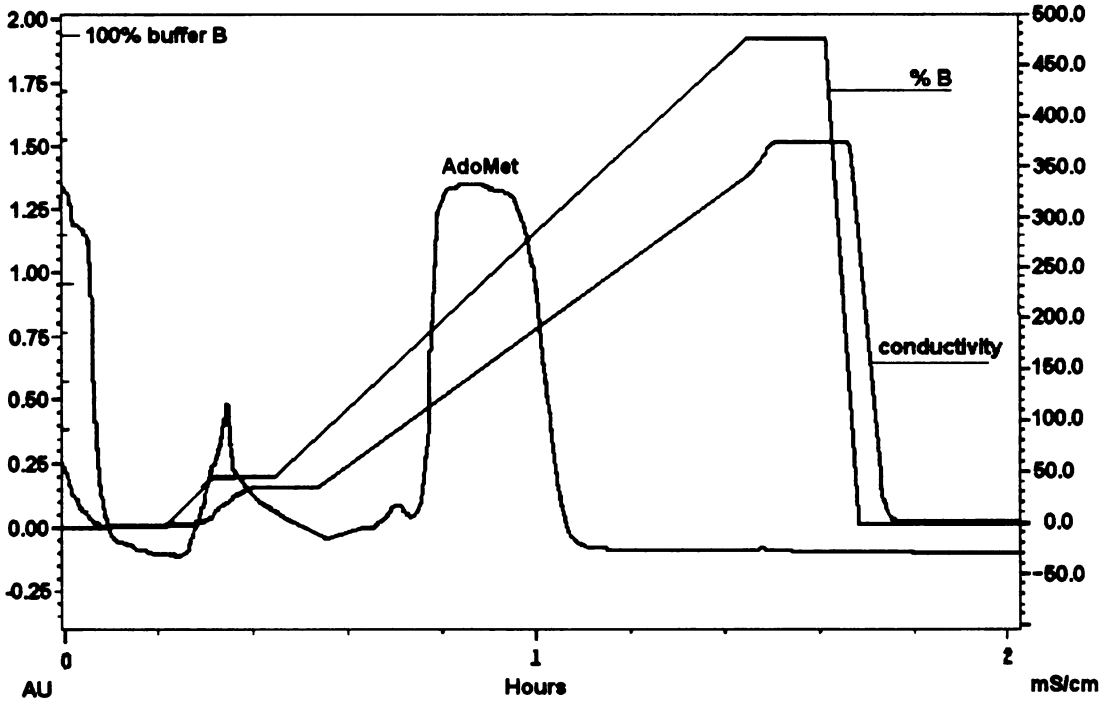

Figure III.7: Chromatography of AdoMet elution from the Source 15S cation exchange column. The AdoMet peak eluted between 0.4 and 0.6 M HCl.

III.3.3 UV-Vis spectra of PFL-AE purified in ascorbic acid and DTT

UV-Vis spectra of the purified PFL-AE showed a broad absorption band, with a shoulder from 410 nm (Fig III.8). This type of feature is characteristic of iron-sulfur cluster proteins. [25, 26] The spectrum of PFL-AE purified in the presence of 1 mM ascorbic acid was almost the identical to that of PFL-AE purified in the presence of 1 mM DTT, suggesting that the change in reductant did not significantly effect cluster composition.

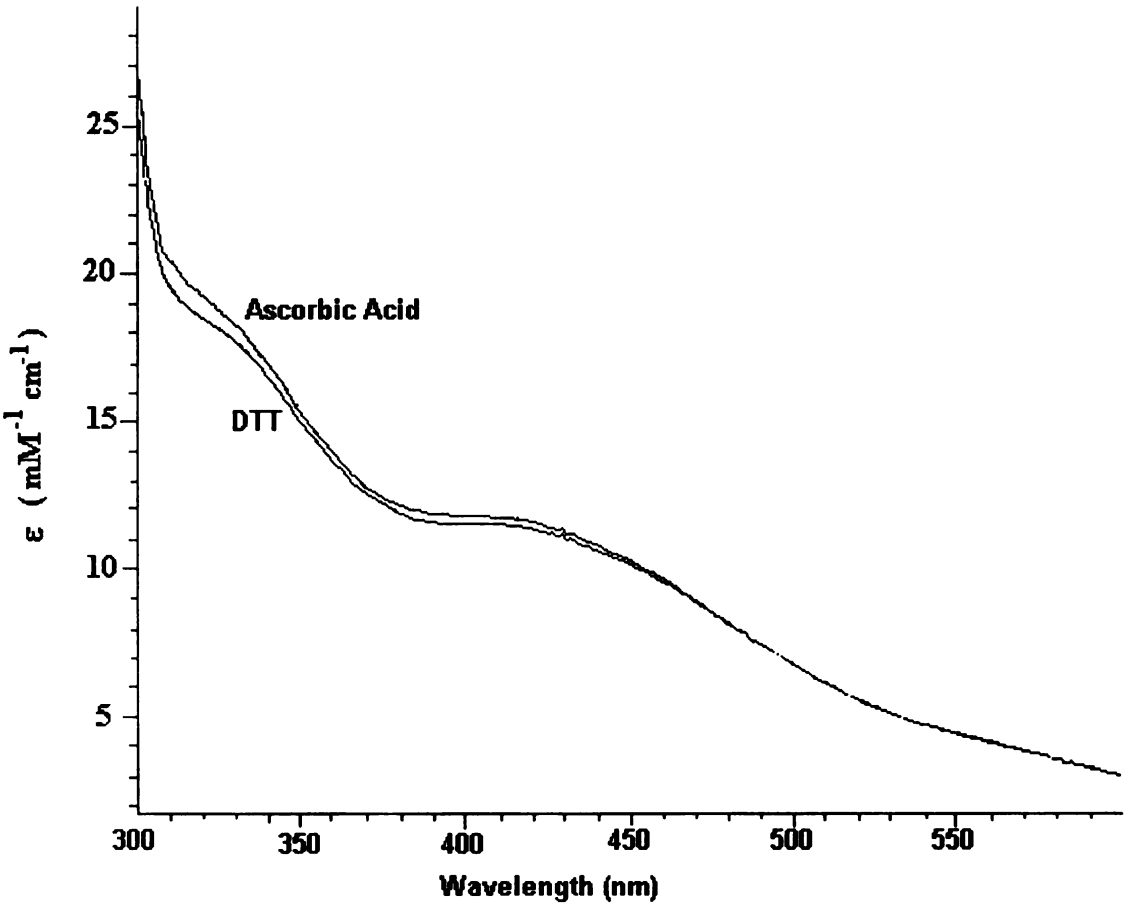

Figure III.8: UV-Vis spectra of PFL-AE purified in ascorbic acid and DTT. The protein was 100 μM in a quartz cuvette with 1 mm optical path length. The spectra were recorded under anaerobic condition at room temperature.

To test the possibility that excess thiols in the buffer might bind to the unique Fe of the Fe_4S_4 cluster in PFL-AE, the UV-Vis spectra of the protein in the presence of 10 mM DTT or 10 mM cysteine were also recorded. The reason to conduct this experiment is to compare PFL-AE with Fe_4S_4 cluster model compounds and other Fe_4S_4 cluster proteins (each Fe was coordinated by 4 sulfurs), whose S pre-edge spectra were published previously. [16, 17] The difference spectra (PFL-AE/10 mM RSH – PFL-AE) showed only slight changes upon adding excess thiols (Fig III.9), while the EPR spectra of reduced PFL-AE and reduced PFL-AE with excess thiols are different (shown in III.3.4),

indicating that UV-Vis absorption spectroscopy may not be sensitive enough to detect the Fe_4S_4 cluster structural change under the conditions.

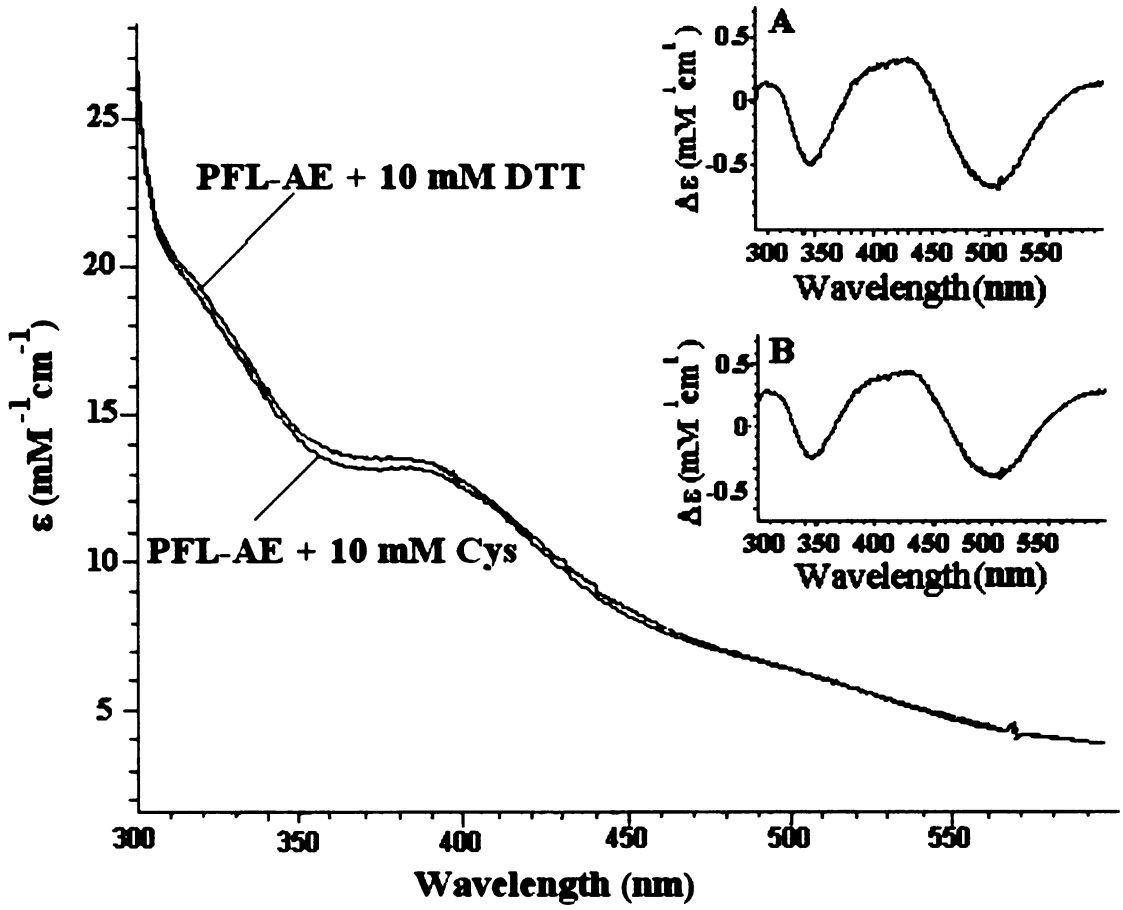

Figure III.9: UV-Vis spectra of PFL-AE with exogenous thiols (10 mM DTT or 10 mM Cys). The protein was purified in the presence of 1 mM ascorbic acid. Protein concentrations were 100 μM and RSH concentrations were 10 mM. The inset spectra are difference spectra of PFL-AE/RSH – PFL-AE (purified in the presence of ascorbic acid). A. RSH = DTT. B. RSH = Cys. All the spectra were recorded under anaerobic conditions at room temperature.

III.3.4 EPR spectra of photo-reduced PFL-AE

The reduced $[4Fe\text{-}4S]^{1+}$ cluster (S = +1/2) of PFL-AE purified in the presence of 1 mM ascorbic acid had a rhombic EPR signal (g = 2.01, 1.92 and 1.87, Fig III.10.A). The shape of the signal and the g values were very similar to the published EPR spectrum (g =

2.02, 1.94, 1.88) of PFL-AE purified in the presence of 1 mM DTT. [10] For both the DTT and ascorbic acid purified proteins, the presence of AdoMet resulted in a dramatic change to a more rhombic signal (g = 2.00, 1.92 and 1.89, Fig III.10.B). This effect demonstrates a significant perturbation of the cluster electronic environment by AdoMet, consistent with the direct interaction between the substrate and the active site previously demonstrated. [8-11]

When the protein was photoreduced in the presence of exogenous thiol (10 mM DTT or 10 mM cysteine), the $[4Fe\text{-}4S]^{1+}$ cluster exhibited a more axial EPR signal compared to the protein in the absence of thiol (Fig III.11). The axial signal indicates the cluster has a more symmetric electronic environment, implying that the exogenous thiol might coordinate to the unique Fe. In addition, there were subtle differences in the g values and line shape depending on whether PFL-AE was reduced in the presence of DTT (g = 2.03, 1.93) or cysteine (g = 2.00, 1.93). These slight difference are consistent with the possibility of DTT and cysteine coordinating to the cluster, as they are distinct molecules with different electron density on the sulfurs.

To compare PFL-AE purified in the presence of DTT with PFL-AE purified in the presence of ascorbic acid, the former was photoreduced in the presence of 10 mM cysteine or DTT. The EPR spectra and g values (g = 2.03, 1.93 in the presence of 10 mM DTT and g = 2.00, 1.93 in the presence of 10 mM cysteine) were very similar to the protein purified in the presence of ascorbic acid (Fig III.11). The results further demonstrate that the electronic structure of PFL-AE/$[4Fe\text{-}4S]^{1+}$ purified in ascorbic acid is similar to that purified in DTT.

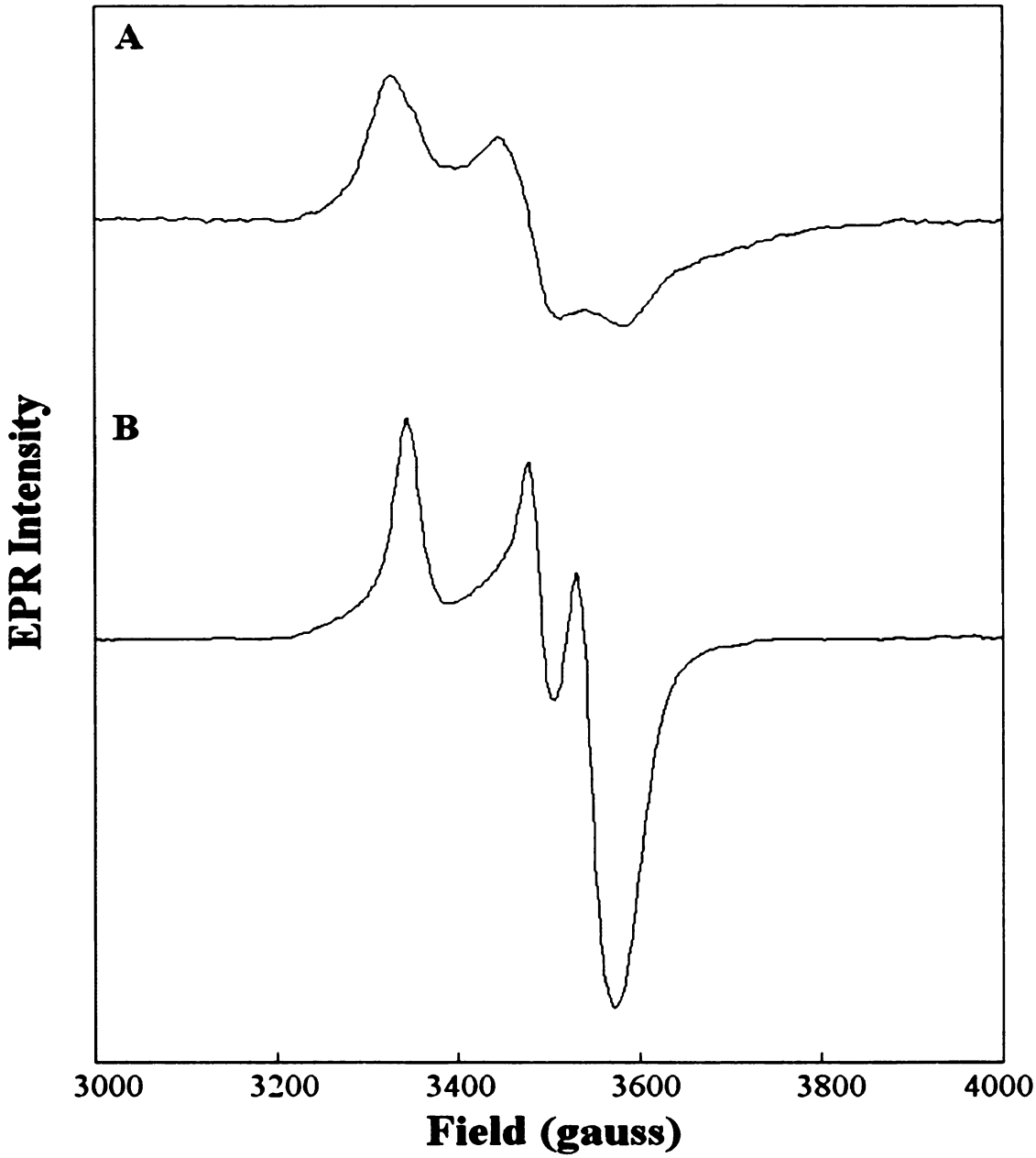

Figure III.10: X-band EPR spectra of reduced PFL-AE and reduced PFL-AE with 3 equivalents of AdoMet added. The protein was purified in 1 mM ascorbic acid. The buffer in both A and B contained 100 mM Tris-HCl pH 7.5, 100 mM KCl, 50 μM 5-deazariboflavin and 100 μM dithionite. A. PFL-AE (50 μM) was photoreduced for 1 h. B. PFL-AE (50 μM) with 150 μM AdoMet added after photoreduction for 1h. EPR parameters: T = 12 K, frequency 9.37 GHz, microwave power 1.9 mW, magnetic field scanned from 2000 to 4000 G, static field 2000 G, modulation frequency 100 kHz, modulation amplitude 5 G, scan twice.

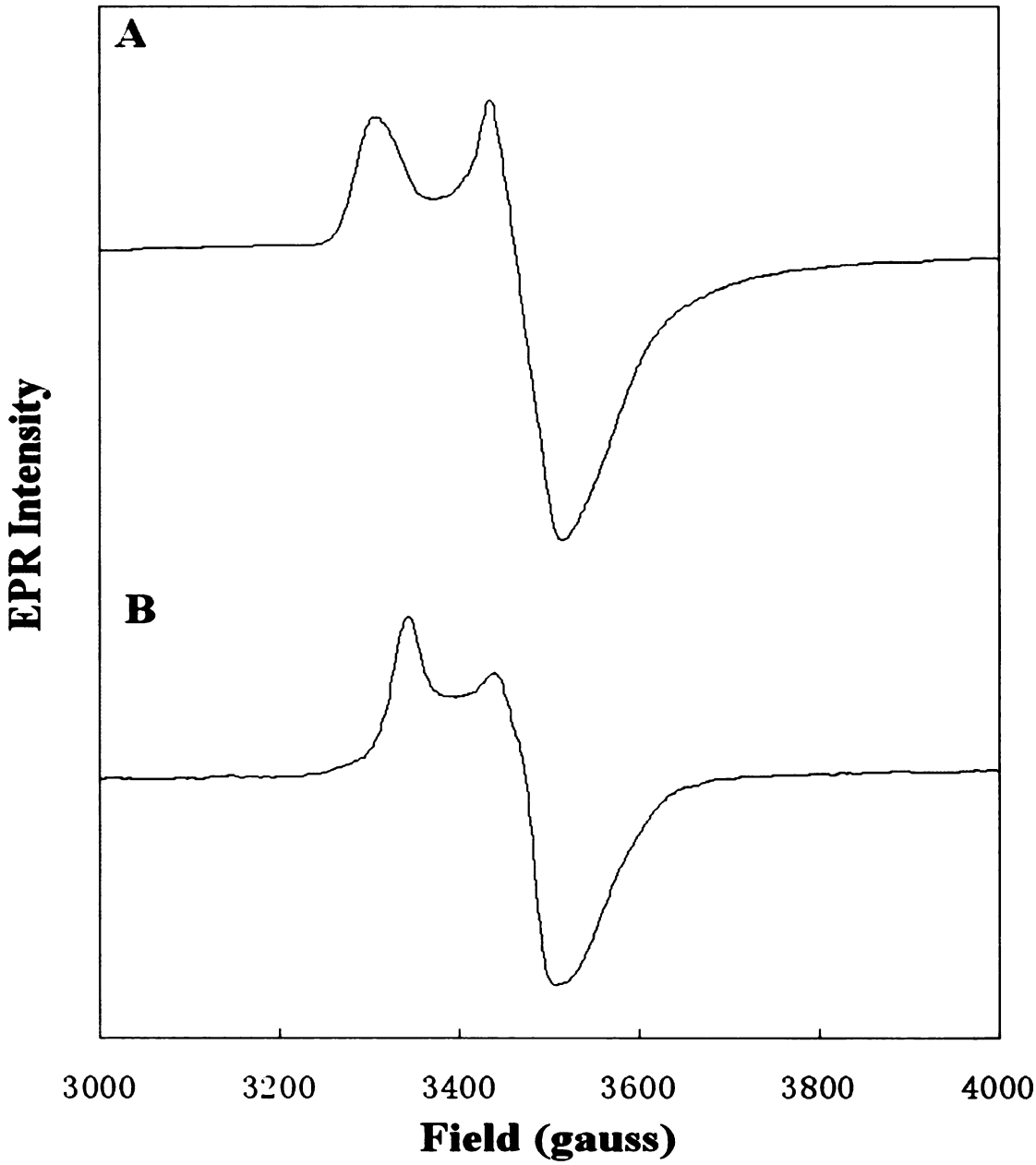

Figure III.11: X-band EPR spectra of PFL-AE (purified in the presence of 1 mM ascorbic acid) photoreduced in the presence of exogenous thiols. The buffer in both A and B contained 100 mM Tris-HCl pH 7.5, 100 mM KCl, 50 μM 5-deazariboflavin and 100 μM dithionite. A. PFL-AE (50 μM) photoreduced for 1 h with 10 mM DTT. B. PFL-AE (50 μM) photoreduced for 1h with 10 mM cysteine. EPR parameters: T = 12 K, frequency 9.37 GHz, microwave power 1.9 mW, magnetic field scanned from 2000 to 4000 G, static field 2000 G, modulation frequency 100 kHz, modulation amplitude 5 G, scan twice.

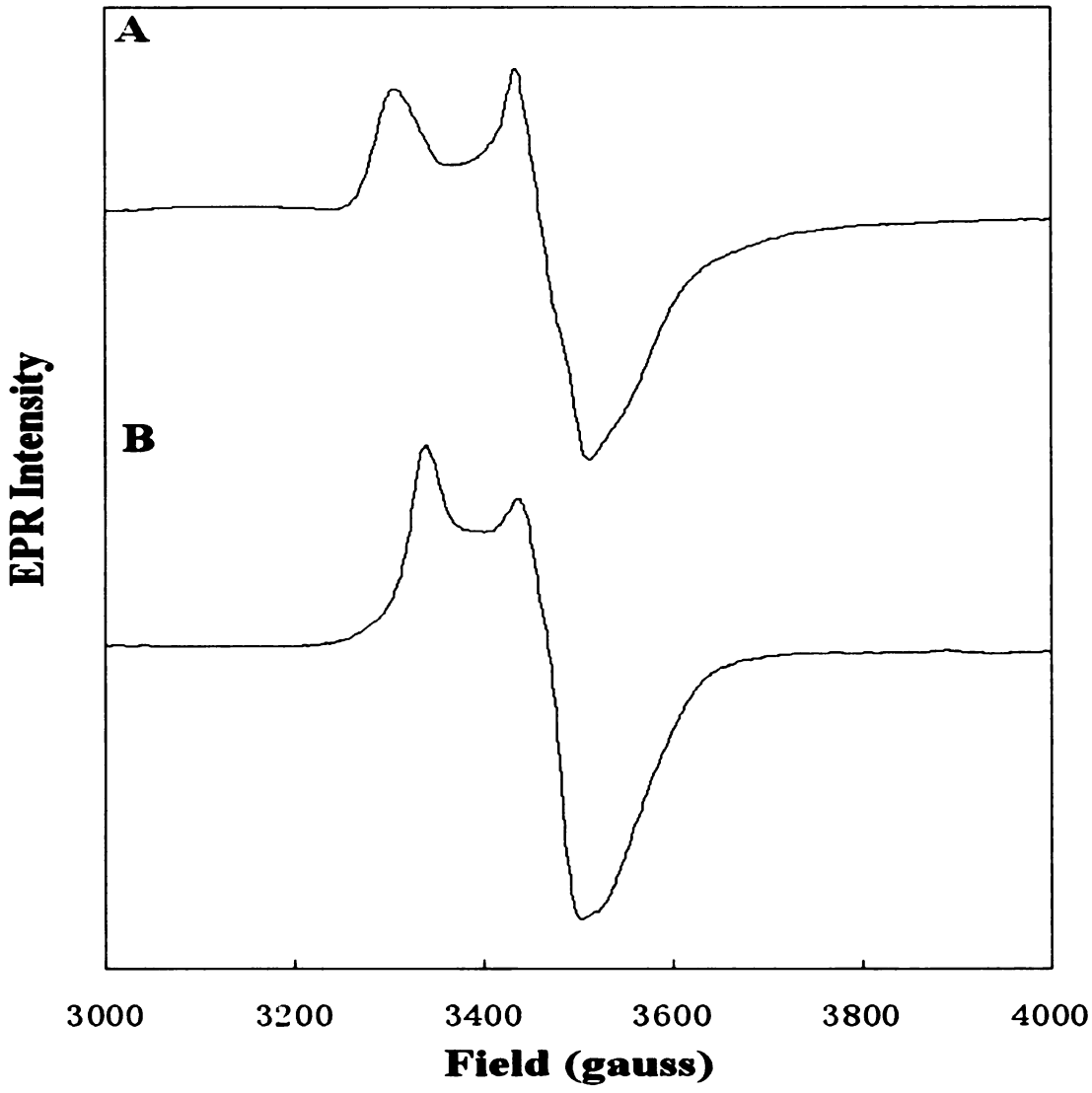

Figure III.12: X-band EPR spectra of PFL-AE (purified in 1 mM DTT) and photoreduced with exogenous thiol. The buffer in both A and B contained 100 mM Tris-HCl pH 7.5, 100 mM KCl, 50 μM 5-deazariboflavin and 100 μM dithionite. A. PFL-AE (50 μM) photoreduced for 1 h with 10 mM DTT. B. PFL-AE (50 μM) photoreduced for 1h with 10 mM cysteine. EPR parameters: T = 12 K, frequency 9.37 GHz, microwave power 1.9 mW, magnetic field scanned from 2000 to 4000 G, static field 2000 G, modulation frequency 100 kHz, modulation amplitude 5 G, scan twice.

For more comparisons between the PFL-AE purified in the presence of ascorbic acid and the PFL-AE purified in the presence of DTT, AdoMet (3 equivalents) was added

after the PFL-AE was photoreduced in the presence of exogenous thiol. The spectra of the protein purified in the presence of ascorbic acid (Fig III.13.A and Fig III.13.B) are almost identical to the spectra of the protein purified in the presence of DTT (Fig III.13.C and Fig III.13.D). The results demonstrate that AdoMet binds to PFL-AE the same way in all cases, regardless of the reductant (DTT or ascorbic acid) used during purification, and regardless of the presence of excess thiols in the sample. Together with the UV-vis results and the EPR spectra of the proteins without AdoMet, these results demonstrate that the Fe_4S_4 cluster of PFL-AE purified in the presence of ascorbic acid has a similar electronic structure as that of PFL-AE purified in the presence of DTT. Thus, the sulfur K-edge XAS investigation of PFL-AE purified in the presence of ascorbic acid (described in the next section) is directly relevant to previous studies of PFL-AE purified in the presence of DTT.

The spectra in Fig III.13 are distinct from those in Fig III.11 and Fig III.12, indicating that the $[4Fe\text{-}4S]^{1+}$ cluster in PFL-AE has a different electronic structure upon AdoMet binding. The results are consistent with AdoMet binding to the cluster, suggesting that AdoMet might replace an exogenous thiol ligand, even though the thiol (10 mM) was in a much higher concentration than AdoMet (150 μM). The spectra in Fig III.13 are similar to the spectrum in Fig III.10.B, which was photoreduced PFL-AE (without 10 mM thiols) with AdoMet added after illumination. The results demonstrate that the $[4Fe\text{-}4S]^{1+}$ cluster in PFL-AE has the same electronic structure in the presence of AdoMet, regardless of the presence of large excesses of thiols. These results suggest that AdoMet may be able to coordinate to the unique iron of the cluster, even though some other ligands in large excess possibly bind to that iron in the absence of AdoMet.

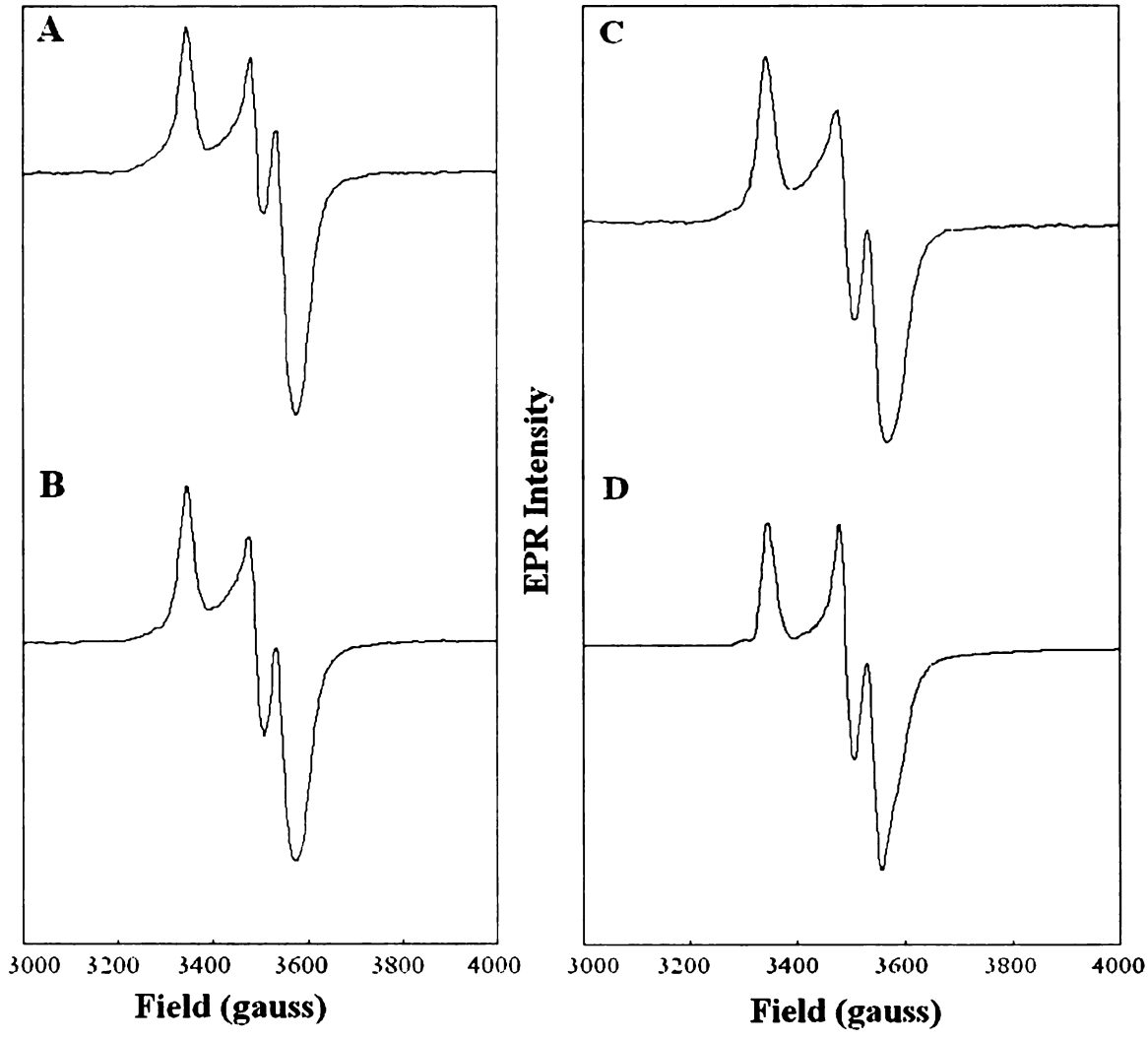

Figure III.13: X-band EPR spectra of photoreduced PFL-AE in the presence of 10 mM exogenous thiol with 3 equivalents of AdoMet added after illumination. The PFL-AE in panel A and B was purified in the presence of 1 mM ascorbic acid. The PFL-AE in panel C and D was purified in the presence of 1 mM DTT. The buffer contained 100 mM Tris-HCl pH 7.5, 100 mM KCl, 50 μM 5-deazariboflavin and 100 μM dithionite. AdoMet (150 μM) was added into each sample after the PFL-AE was photoreduced for 1 h. A. PFL-AE (50 μM, 1 mM ascorbic acid) photoreduced with 10 mM DTT + AdoMet (150 μM). B. PFL-AE (50 μM, 1 mM ascorbic acid) with 10 mM cysteine + AdoMet (150 μM). C. PFL-AE (50 μM, 1 mM DTT) with 10 mM DTT + AdoMet (150 μM). D. PFL-AE (50 μM, 1 mM DTT) with 10 mM cysteine + AdoMet (150 μM). EPR parameters: T = 12 K, frequency 9.37 GHz, microwave power 1.9 mW, magnetic field scanned from 2000 to 4000 G, static field 2000 G, modulation frequency 100 kHz, modulation amplitude 5 G, and scan twice.

III.3.5 Sulfur K-edge XAS spectra of PFL-AE and PFL-AE with AdoMet

The S K-edge XAS data on PFL-AE (Fig. III.14.A) show an intense pre-edge transition at ~2470 eV characteristic of a $[4Fe\text{-}4S]^{2+}$ cluster. [17, 24] This broad feature envelops transitions to all the un-occupied Fe_{3d} based orbitals from the 1s orbitals of four $\mu_3S_{sulfide}$ and three $S_{thiolate}$ ligands. The *rising-edge* (at 2473.5 eV) is comprised of S 1s to C-S σ^* transitions of all bound and unbound cysteines and methionines present in the protein. The data for the protein upon AdoMet binding (Fig. III.14.A, dotted line) show an increase in the intensity of the pre-edge feature as well as the rising-edge feature. While the increase in the rising-edge features is expected as there are additional 3 equivalents of AdoMet (AdoMet has three C-S bonds), the increase in pre-edge feature must result from AdoMet binding to the cluster as AdoMet has no feature at 2470 eV (Fig. III.14.A, grey line). This increase is demonstrated in Fig. III.14.B, where the renormalized difference spectrum shows a clear peak at 2470.3 eV. This increase in the pre-edge intensity could originate from a change of cluster ligation, AdoMet interaction with $\mu_3S_{sulfide}$, or other effects. To evaluate these effects, geometry optimized DFT calculations were used.

The calculated covalency shows that substituting a OH^- ligand (a proposed exogenous ligand to the unique Fe in the absence of AdoMet) on the cluster with AdoMet results in a 37% increase in S_{3p} character in the Fe_{3d} manifold (Table III.1, row 1 and 2). This increase does not occur when substituting OH^- by a glycine or a methionine bound form (Table III.1, rows 3 and 4). This computational result is consistent with the increased experimental observation of pre-edge intensity upon AdoMet binding. One interesting result is that 25% of the 37% increase is derived from the Fe-thiolate

covalency (Table III.1, rows 1 and 2, column 2) although AdoMet is proposed to have more interaction with the Fe-S^b bonds than with the Fe-S^t bonds.

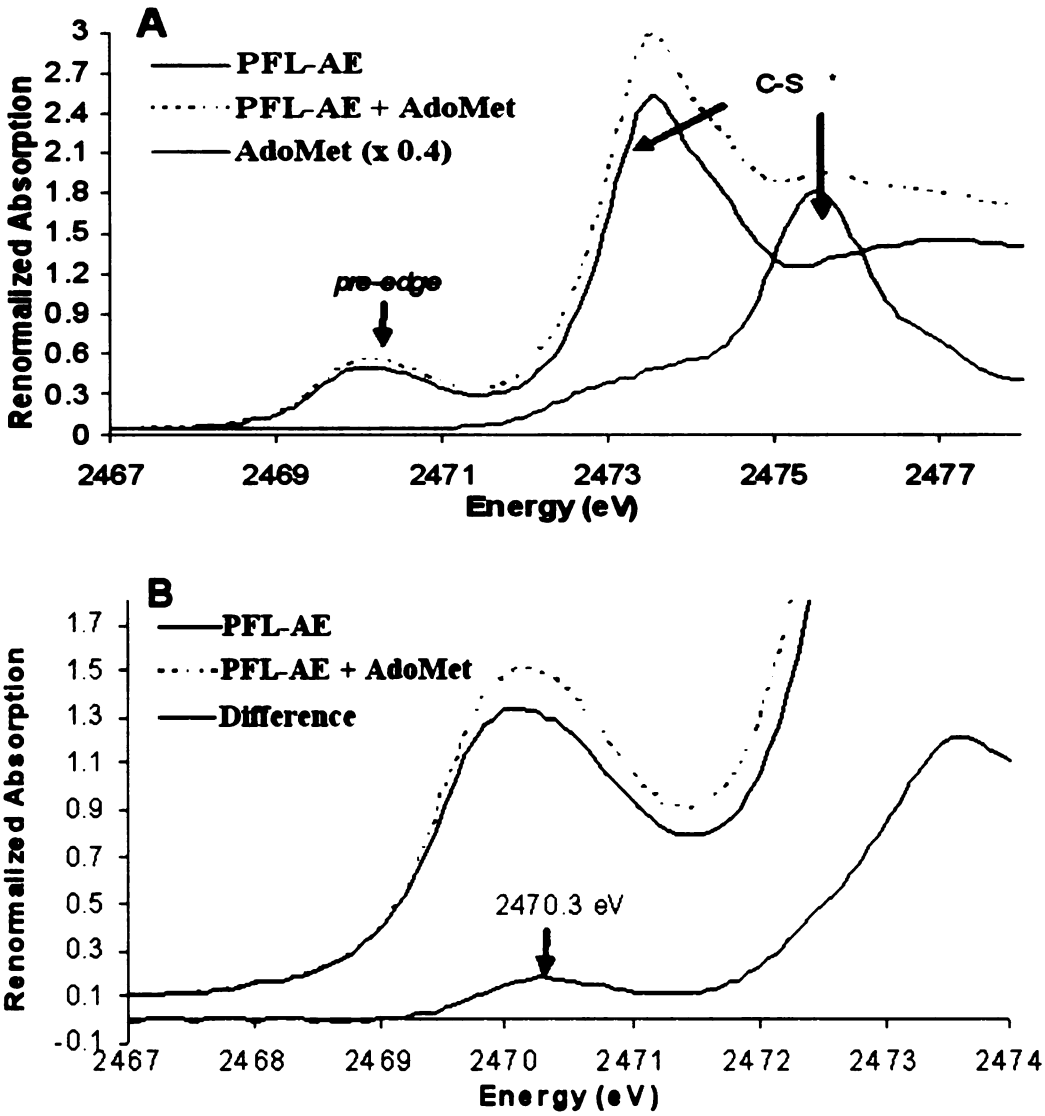

Figure III.14. Sulfur K-edge XAS spectra of PFL-AE, PFL-AE + AdoMet and AdoMet (A) and difference spectrum PFL-AE/AdoMet – PFL-AE (B). A. Black solid line is the absorbance of PFL-AE (3.4 mM). Black dashed line is the absorbance of PFL-AE (2.9 mM)+ AdoMet (10 mM). The grey line is the absorbance of AdoMet (20mM). B. The black solid line is the absorbance of PFL-AE (3.4 mM). The black dashed line is the absorbance of PFL-AE (2.9 mM) + AdoMet (10 mM). The grey line is the difference spectrum PFL-AE/AdoMet – PFL-AE. XAS parameters: The XAS spectra were recorded in Stanford Synchrotron Radiation Laboratory under ring conditions of 3 GeV and 60-100 mA at 4 °C. The X-ray beam was optimized for low-energy studies. The monochromator step size over the edge region was 0.08 eV, and the energy resolution was ~0.5 eV. Solid $Na_2S_2O_3 \cdot 5H_2O$ was used as the standard to calibrate the spectra.

$[Fe_4S_4]^{2+}(SMe)_3L$	μ_3Sulfide	Thiolate	Total	Δ
L = OH	369	90	459	
L = AdoMet	381	115	496	37
L = Glycine	375	85	460	1
L = Methionine	370	80	450	-9

Table III.1 DFT calculated covalencies (%) of $[4Fe\text{-}4S]^{2+}$ cluster in PFL-AE with different exogenous ligands.

The optimized structure of AdoMet bound $[4Fe\text{-}4S]^{2+}$ cluster (Fig. III.15, left) shows close contact between the AdoMet sulfonium S and the recent cluster bridging sulfide (3.78 Å) and the unique Fe (3.45 Å). This is consistent with our crystal structure study (manuscript in preparation) and ENDOR studies of PFL-AE. [9-11] Energy levels of the AdoMet bound $[4Fe\text{-}4S]^{2+}$ cluster indicate that in addition to Fe_{3d} based acceptor orbitals present in a resting cluster, there are three AdoMet C-S σ* orbitals in the same energy region as these Fe_{3d} based orbitals. These orbitals are ~3 eV higher in energy relative to the C-S σ* of a thiolate (feature at 2473.5 eV) due to the positive charge on the S atom in AdoMet. The AdoMet C-S σ* orbital between the sulfonium S and 5'-C has back-bonding interactions with filled Fe-sulfide orbitals of the cluster. This shifts the charge density to the C-S σ* orbital from the cluster bridging sulfide, making the later a poorer donor to the cluster. The reduced donation by the sulfide is compensated by enhanced donation from the terminal thiolates which become more covalent. Although the sulfide becomes a poorer donor to the cluster, its overall donation increases due to its donation to the C-S σ* orbital. Thus the pre-edge feature of the AdoMet bound $[4Fe\text{-}4S]^{2+}$ cluster includes transitions from the sulfide and the thiolate to the Fe_{3d} based

orbitals and the sulfide to the C-S σ* orbitals of AdoMet (which now has S_{3p} character of sulfide mixed in due to back-bonding), increasing the overall pre-edge intensity of the AdoMet bound cluster relative to a native cluster.

Figure III.15. DFT optimized structures of AdoMet bound cluster in the $[4Fe\text{-}4S]^{2+}$ state (left) and its one electron reduced form $[4Fe\text{-}4S]^{1+}$ (right).

III.4 Conclusions

PFL-AE purified in the presence of 1 mM ascorbic acid had very similar UV-Vis and EPR spectroscopic properties as the PFL-AE purified in the presence of 1 mM DTT, the latter of which has been intensely investigated in our lab. Upon addition of exogenous thiols (10 mM DTT or 10 mM cysteine), the EPR signals from both the proteins became axial, indicating that the electronic structure of the cluster was more symmetric. This would be consistent with coordination of the exogenous thiols to the unique site of the

cluster to form a Fe_4S_4 cluster with 4 sulfur ligands (3 bridging sulfide and 1 terminal thiolate) to each iron. Upon addition of AdoMet, the EPR spectra of the reduced PFL-AE (purified in the presence of 1 mM ascorbic acid or 1 mM DTT) became rhombic, suggesting that AdoMet significantly perturbed the cluster electronic structure, presumably due to the carboxylate O and amine N coordinating to the unique iron. [9-11] Therefore AdoMet appears to bind the unique Fe of the Fe_4S_4 cluster even in the presence of excess thiols as possible exogenous ligands. The results that PFL-AE purified in the presence of ascorbic acid had very similar UV-Vis and EPR spectra to those of PFL-AE purified in the presence of DTT indicate that the electronic structures in the two proteins are the same.

The sulfur K-edge XAS data of PFL-AE showed a K-edge feature at 2473.5 eV and a broad pre-edge feature at ~2470 eV, characteristic of $[4Fe\text{-}4S]^{2+}$ clusters. The K-edge is due to all sulfur (including all cysteines and methionines) 1s electrons to C-S σ^* transitions, and the pre-edge feature is due to the transitions from 1s electrons in bridging sulfide and terminal thiolates to unoccupied Fe_{3d} orbitals. Both the K-edge absorbance and the pre-edge feature had intensity increase upon addition of 3 equivalents of AdoMet. The increase of the K-edge intensity is due to the absorbance from AdoMet, however the increase of the pre-edge intensity is from the covelancy change in the cluster in the presence of AdoMet, as AdoMet itself has no absorbance in this region. The DFT calculation shows a 37% covalency increase of the Fe-S bonds, in which 25% is contributed from the terminal thiolate, although the interaction between AdoMet and Fe-S^b bonds is proposed more than the interaction between AdoMet and Fe-S^t bonds.

To explain this result, a model structure was constructed based on the DFT calculation, and the energy level diagram indicates that the AdoMet C-S σ^* orbital between the sulfonium S and 5'-C has back-bonding interaction with filled Fe-sulfide orbitals of the cluster. This effect shifts charge density from the sulfide to the C-S σ^* orbital, causing bridging sulfide to be a weaker donor to the cluster. The enhanced donation from the terminal thiolate compensates for this change, inducing more covalency into the Fe-S bonds. The pre-edge feature has the characters of sulfur to Fe_{3d} antibonding transition and bridging sulfide to AdoMet 5'C-S^+ σ^* transition, and therefore, the overall donation from the $\mu_3$sulfide increases because of the back-bonding from AdoMet. The XAS results demonstrate the interaction between the Fe-S bonds and the 5'C-S^+ bond, the position to be reductively cleaved to generate the putative deoxyadenosyl radical. The charge shift from the cluster to AdoMet might be the initial step to eject one electron from the cluster to the substrate, triggering the catalysis.

References

1. Knappe, J.; Schmitt, T., *Biochemical and Biophysical Research Communications* **1976,** 71, (4), 1110-17.

2. Knappe, J.; Schacht, J.; Moeckel, W.; Hoepner, T.; Vetter, H., Jr.; Edenharder, R., *European Journal of Biochemistry* **1969,** 11, (2), 316-27.

3. Conradt, H.; Hohmann-Berger, M.; Hohmann, H. P.; Blaschkowski, H. P.; Knappe, J., *Archives of Biochemistry and Biophysics* **1984,** 228, (1), 133-42.

4. Henshaw, T. F.; Cheek, J.; Broderick, J. B., *Journal of the American Chemical Society* **2000,** 122, (34), 8331-8332.

5. Frey, M.; Rothe, M.; Wagner, A. F. V.; Knappe, J., *Journal of Biological Chemistry* **1994,** 269, (17), 12432-7.

6. Knappe, J.; Neugebauer, F. A.; Blaschkowski, H. P.; Gaenzler, M., *Proceedings of the National Academy of Sciences of the United States of America* **1984,** 81, (5), 1332-5.

7. Knappe, J.; Elbert, S.; Frey, M.; Wagner, A. F. V., *Biochemical Society Transactions* **1993,** 21, (3), 731-4.

8. Krebs, C.; Broderick, W. E.; Henshaw, T. F.; Broderick, J. B.; Huynh, B. H., *Journal of the American Chemical Society* **2002,** 124, (6), 912-913.

9. Walsby, C. J.; Ortillo, D.; Broderick, W. E.; Broderick, J. B.; Hoffman, B. M., *Journal of the American Chemical Society* **2002,** 124, (38), 11270-11271.

10. Walsby, C. J.; Ortillo, D.; Yang, J.; Nnyepi, M. R.; Broderick, W. E.; Hoffman, B. M.; Broderick, J. B., *Inorganic Chemistry* **2005,** 44, (4), 727-741.

11. Walsby, C. J.; Hong, W.; Broderick, W. E.; Cheek, J.; Ortillo, D.; Broderick, J. B.; Hoffman, B. M., *Journal of the American Chemical Society* **2002,** 124, (12), 3143-3151.

12. Cosper, N. J.; Booker, S. J.; Ruzicka, F.; Frey, P. A.; Scott, R. A., *Biochemistry* **2000,** 39, (51), 15668-73.

13. Lepore, B. W.; Ruzicka, F. J.; Frey, P. A.; Ringe, D., *Proceedings of the National Academy of Sciences of the United States of America* **2005,** 102, (39), 13819-13824.

14. Cosper, M. M.; Cosper, N. J.; Hong, W.; Shokes, J. E.; Broderick, W. E.; Broderick, J. B.; Johnson, M. K.; Scott, R. A., *Protein Science* **2003,** 12, (7), 1573-1577.

15. Glaser, T.; Rose, K.; Shadle, S. E.; Hedman, B.; Hodgson, K. O.; Solomon, E. I., *J Am Chem Soc* **2001,** 123, (3), 442-54.

16. Dey, A.; Glaser, T.; Couture, M. M.; Eltis, L. D.; Holm, R. H.; Hedman, B.; Hodgson, K. O.; Solomon, E. I., *J Am Chem Soc* **2004,** 126, (26), 8320-8.

17. Dey, A.; Roche, C. L.; Walters, M. A.; Hodgson, K. O.; Hedman, B.; Solomon, E. I., *Inorg Chem* **2005,** 44, (23), 8349-54.

18. Glaser, T.; Hedman, B.; Hodgson, K. O.; Solomon, E. I., *Acc Chem Res* **2000,** 33, (12), 859-68.

19. Rose, K. S., S. E.; Eidsness, M. K.; Kurtz, D. M., Jr.; Scott, R. A.; Hedman, B.; Hodgson, K. O.; Solomon, E. I., *Journal of American Chemical Society* **1998,** 120, (41), 10743-47.

20. Rose, K. S., S. E.; Glaser, T.; de Vries, S.; Cherepanov, A.; Canters, G. W.; Hedman, B.; Hodgson, K. O.; Solomon, E. I., *Journal of American Chemical Society* **1999,** 121, (11), 2353-63.

21. Dey, A.; Glaser, T.; Moura, J. J.; Holm, R. H.; Hedman, B.; Hodgson, K. O.; Solomon, E. I., *J Am Chem Soc* **2004,** 126, (51), 16868-78.

22. Louis Noodleman, J. G. N., , Jr. Joseph H. Osborne, Arie Aizman, David A. Case, *Journal of American Chemical Society* **1985,** 107, (12), 3418-26.

23. Beinert, H.; Holm, R. H.; Munck, E., *Science (Washington, D. C.)* **1997,** 277, (5326), 653-659.

24. Solomon, E. I., Hedman, B., Hodgson, K. O., Dey, A., Szilagyi, R. K., *Coordination Chemistry Reviews* **2005,** 249, 97-129.

25. Broderick, J. B.; Duderstadt, R. E.; Fernandez, D. C.; Wojtuszewski, K.; Henshaw, T. F.; Johnson, M. K., *Journal of the American Chemical Society* **1997,** 119, (31), 7396-7397.

26. Ollagnier-de Choudens, S.; Fontecave, M., *FEBS Lett* **1999,** 453, (1-2), 25-8.

CHAPTER IV

NUCLEAR RESONANCE VIBRATIONAL SPECTROSCOPY STUDY OF PYRUVATE FORMATE-LYASE ACTIVATING ENZYME

IV.1 Introduction

PFL-AE utilizes a Fe_4S_4 cluster to catalyze the reductive cleavage of AdoMet to form a putative deoxyadenosyl radical. [1, 2] The cluster is coordinated to the enzyme by three cysteines, Cys-29, Cys-33, and Cys-36. [3] This CX_3CX_2C binding motif of the cluster is highly conserved in all radical SAM superfamily enzymes. [4, 5] Three of the four irons in the cluster are coordinated by these three conserved cysteines, while the fourth iron is coordinated by a non-cysteined ligand, making it chemically and spectroscopically unique. The 4th iron binds AdoMet to anchors the substrate, however, the identity of the exogenous ligand in the absence of AdoMet is unknown (scheme IV.1). [6-9]

Another Fe_4S_4 cluster enzyme, aconitase, also uses a site-differentiated Fe_4S_4 cluster to catalyze its reaction, although it is not a radical SAM superfamily protein. [10] ENDOR and resonance Raman spectroscopic evidence for aconitase show that a hydroxide ion from the solvent binds to the unique Fe site in the absence of the substrate. [11, 12] The crystal structure of aconitase with the substrate isocitrate bound demonstrated that the unique Fe was coordinated by one hydroxyl group, and one carboxylate group from isocitrate as well as one H_2O to form a six ligand coordination environment. [13, 14] It has been proposed that the hydroxide ligand was protonated by a histidine and changed

position to let the substrate enter the active site. [8] The coordination of the unique Fe in aconitase therefore changes from 4 to 6 ligands upon substrate binding.

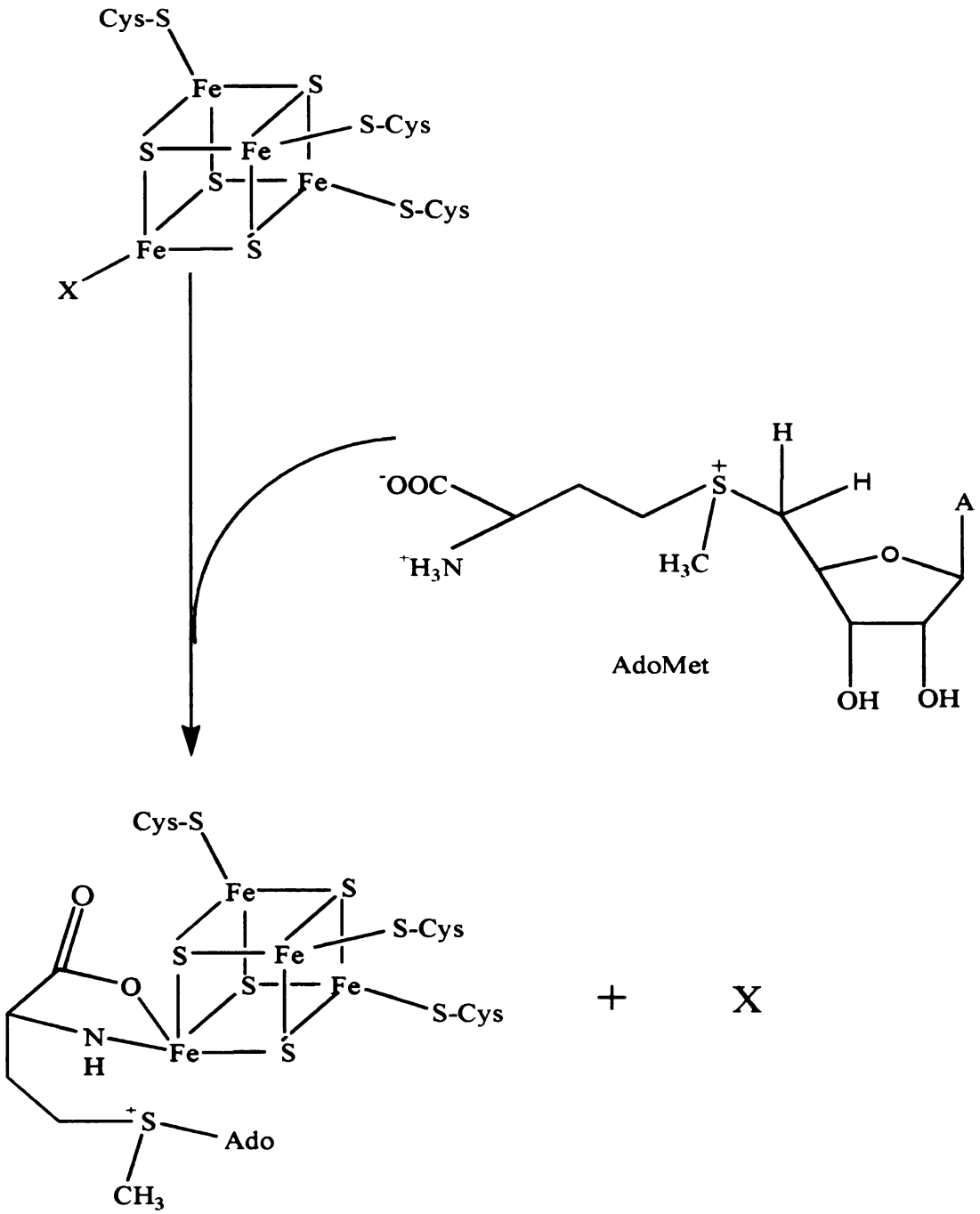

Scheme IV.1: Schematic representation of AdoMet binding to the unique iron of PFL-AE. The fourth ligand to the unique Fe in the absence of AdoMet is unknown. AdoMet replaces the unknown ligand when it binds to the Fe site.

Evidence suggests that PFL-AE has a similar change in coordination of the unique Fe upon substrate binding. [6] To investigate whether a solvent hydroxide might bind to the unique Fe and be replaced by AdoMet, a relatively new vibrational spectroscopic method, nuclear resonance vibrational spectroscopy (NRVS), was used.

Vibrational spectroscopy provides some important information on the structure and dynamics of the active sites in metalloproteins. [15] Resonance Raman (RR) in particular has provided powerful insights into Fe_4S_4 cluster model compounds and proteins. [16] However, RR spectroscopy is restricted by the selection rules, and as a site-select technique it is sensitive only to those vibrations that are coupled to electronic excitations. NRVS, sometimes called nuclear resonant inelastic X-ray scattering, detects the complete vibrational spectrum of a Mössbauer-active nucleus, such as ^{57}Fe. [17-19] This technique couples nuclear excitation and molecular vibrations. A recoil-free absorption of a photon can happen if the energy of the photon equals the energy difference between the ground and excited nuclear states, as discovered by Mössbauer in 1958; [20] this energy is 14.413 keV for ^{57}Fe. [21] A typical NRVS scan usually starts from –20 meV below the recoil-free resonance energy and ends at +100 meV above that energy (-160 cm^{-1} – 800 cm^{-1}). Photons that have energy equal to the nuclear excitation state plus or minus vibrational states (Stokes or anti-Stokes shift) can be absorbed by the nuclei (Fig IV.1). Although this is an absorption spectroscopy, the detection is via measuring the resulting 6.4 keV atomic fluorescence emitted from the excited ^{57}Fe atoms. The intensity of the signal is directly related to the magnitude and direction of the vibration.

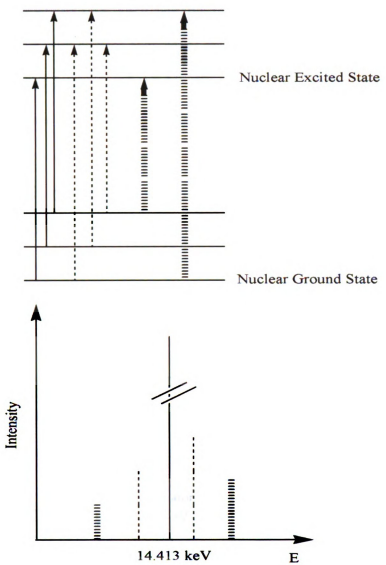

Figure IV.1: Schematic representation of NRVS photon absorption in ^{57}Fe. The solid line is recoil-free energy absorption. The dashed line is the absorption involving one phonon creation or annihilation. The broken line is the absorption involving two phonons creation or annihilation.

Although this type of resonance absorption was predicted in 1960, [22] the initial experiment was not reported until the mid 1990's. [23] Technical difficulties arise from the fact that the shifts of the vibrational bands are on the order of 1 meV, therefore requiring source velocity of hundreds of meters per second to produce incident radiation of

appropriate energy (see late discussion of conventional Mössbauer spectroscopy). This is not plausible with current Mössbauer instrumentation. Another technical difficulty arises from that the intensity of the NRVS absorption is only about 1% of the recoil-free resonance, and therefore an ultra bright source is required. These difficulties have been overcome by a new generation synchrotron X-ray source. The bandwidth of the excitation X-ray beam (with energy around 14.4 keV) can be narrowed down to 1.0 meV via two monochromators, a diamond crystal as the premonochromator and a Si crystal as the high-resolution monochromator. The wavelength (energy) of the X-ray is tuned according to the Bragg reflection of the single crystal, $n\lambda = 2d\sin\theta$, where λ is the wavelength, d is the separation between the lattice planes, θ is the angle of incidence and $n = 1$ is the fundamental reflection. The corresponding resolution of the spectrum is 7 – 8 cm^{-1}, (Fig IV.2).

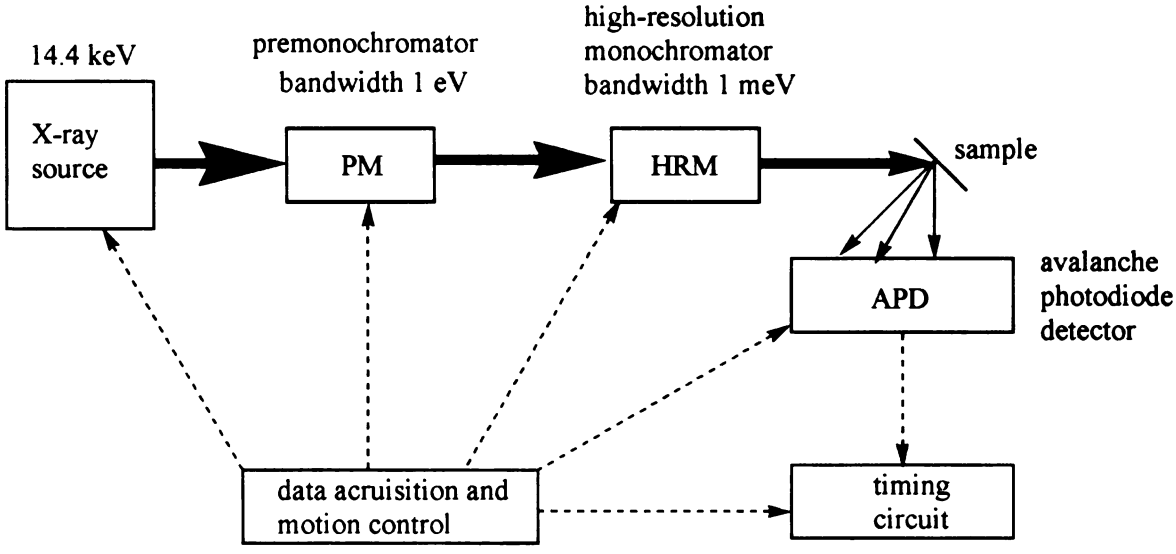

Figure IV.2: Schematic diagram of NRVS experimental set-up. The bandwidth of the irradiation beam is cut down to 1 meV by two monochromators. The APD is turned off during the X-ray pulse in order to remove the elastically scattered photons. It is controlled by the timing circuit to collect the delayed atomic fluorescence corresponding to the nuclear absorption.

The relevant transition for ^{57}Fe is from the nuclear spin state I = 1/2 to the spin state I = 3/2, corresponding to an energy of 14.413 keV. Conventional Mössbauer spectroscopy monitors the electronic structure of ^{57}Fe produced by the interaction between the nucleus and electrons. [24] The excitation source is ^{57}Co, with decay to ^{57}Fe to generating the 14.413 keV incident radiation with a bandwidth of $4.7x10^{-9}$ eV. To probe the different energy transitions of the sample, the source is moved to produce a Doppler shift of the incident radiation. A movement at a velocity of 1 mm/sec toward the sample can increase the energy of the beam by $4.8x10^{-8}$ eV, 10 times the original bandwidth. This velocity, called the isomer shift, is used as the unit in Mössbauer spectroscopy. The actual spectrum is a plot of transmission counts versus the isomer shift.

There are several significant interactions between the nucleus and the electrons, including the electrostatic attraction. The excited ^{57}Fe nucleus is 0.1% smaller than the ground state nucleus, and therefore the interaction between the electrons and nucleus changes upon excitation. The difference in electron density on the nucleus therefore can shift the Mössbauer transition energy, and is recorded as the isomer shift. The 1s and 2s electrons are not affected significantly by the electronic environment of the ^{57}Fe, but the 3d electrons shield the 3s electrons and decrease the electron density on the nucleus. The isomer shift therefore decreases when there are more delocalized 3d electrons. The 4s character in the bonding orbital also reduce the isomer shift, which makes interpretation of results more complicated. [25]

The excited state of ^{57}Fe has quadrupole degeneracies, and the ground state has double degeneracies in the absence of external electric field. The quadrupole degeneracies can be partially lifted if the nucleus is surrounded by a low symmetric

electric field, due to the interaction of the nuclear quadrupole moment and the electric field gradient. In the absence of magnetic interactions, the nuclear excited state is split into two degenerate doublets. The ground state can have transitions to both of the doublets that are separated by the quadrupole splitting energy (ΔE).

The nuclear spin also possesses a magnetic moment, which can be influenced by the external electron magnetic field, a sum of the magnetic moments from the unpaired electrons. For ^{57}Fe, the electron magnetic perturbation at the nucleus is approximately proportional to the sum of the 3d electron interference. However, the 4s character in the bonding orbitals mixes with the filled molecular orbital made from 3d orbitals, which makes the calculation more complicated. Therefore, the values of the magnetic interaction are determined empirically in many cases. [26] Mössbauer spectroscopy, combining these three factors, can provide information on the oxidation state, spin state, and coordination environment of the atom.

The NRVS spectra of ^{57}Fe complexes are often compared with the resonance Raman spectra of the same compounds. In Raman spectroscopy, an incident beam excites a molecule from a ground vibrational state to a virtual excited vibrational state. The re-emitted photon keeps the same energy if the molecule returns to the ground vibrational state ($\nu = 0$); this is called Raleigh scattering. If the molecule returns to the lowest excited vibrational state ($\nu = 1$), the re-emitted photon will have less energy than the incident photon; this is referred as Stokes scattering. If the molecule transits from the $\nu = 1$ state to $\nu = 0$ state because of the irradiation, the scattered photon will have more energy than the incident photon, a phenomenon called anti-Stokes scattering. Stokes and anti-Stokes scatterings are two types of Raman scattering (Fig IV.3 A). Raman scattering can be

greatly enhanced (10^2 to 10^6 times) if the energy of the incident photon matches the difference between the electronic ground state and excited state of the molecule (Fig IV.3 B). This is resonance Raman spectroscopy. Resonance Raman is a very powerful method to study active sites in metalloproteins, as proteins in aqueous solution in the concentration range of μM to mM can be investigated due to resonance enhancement. Secondly, only the vibrational modes coupled to the electronic transitions are enhanced in resonance Raman, which provides high selection for the metal center even in very large proteins. However, resonance Raman also has some significant restrictions. Only the vibrations that change the polarizability of the molecule are Raman active, which means some vibrational modes are not observable in Raman spectroscopy. A further limitation of resonance Raman is that not all the Raman active vibrations are enhanced because the intensity increase of the bands is due to the electronic state transition induced polarizability change. Those vibrations coupled with molecular geometry change of the excited state are promoted, but others are not.

Resonance Raman of iron-sulfur cluster proteins utilizes excitation at the absorption wavelength range of the sulfur to iron charge transfer. [16] Therefore, the Raman bands involving Fe-S vibrations are enhanced, however the intensity of the vibration between the unique iron and a non-sulfur ligand such as OH^- or H_2O may not be increased. In fact, no Fe to exogenous ligand vibration has been detected yet in radical SAM superfamily proteins. On the other hand, NRVS is not subject to the selection rule or the electronic absorption enhancement, since it directly monitors the all movements of the ^{57}Fe nucleus. Thus, it provides a greater opportunity to observe the unique ^{57}Fe vibration involving the exogenous ligand.

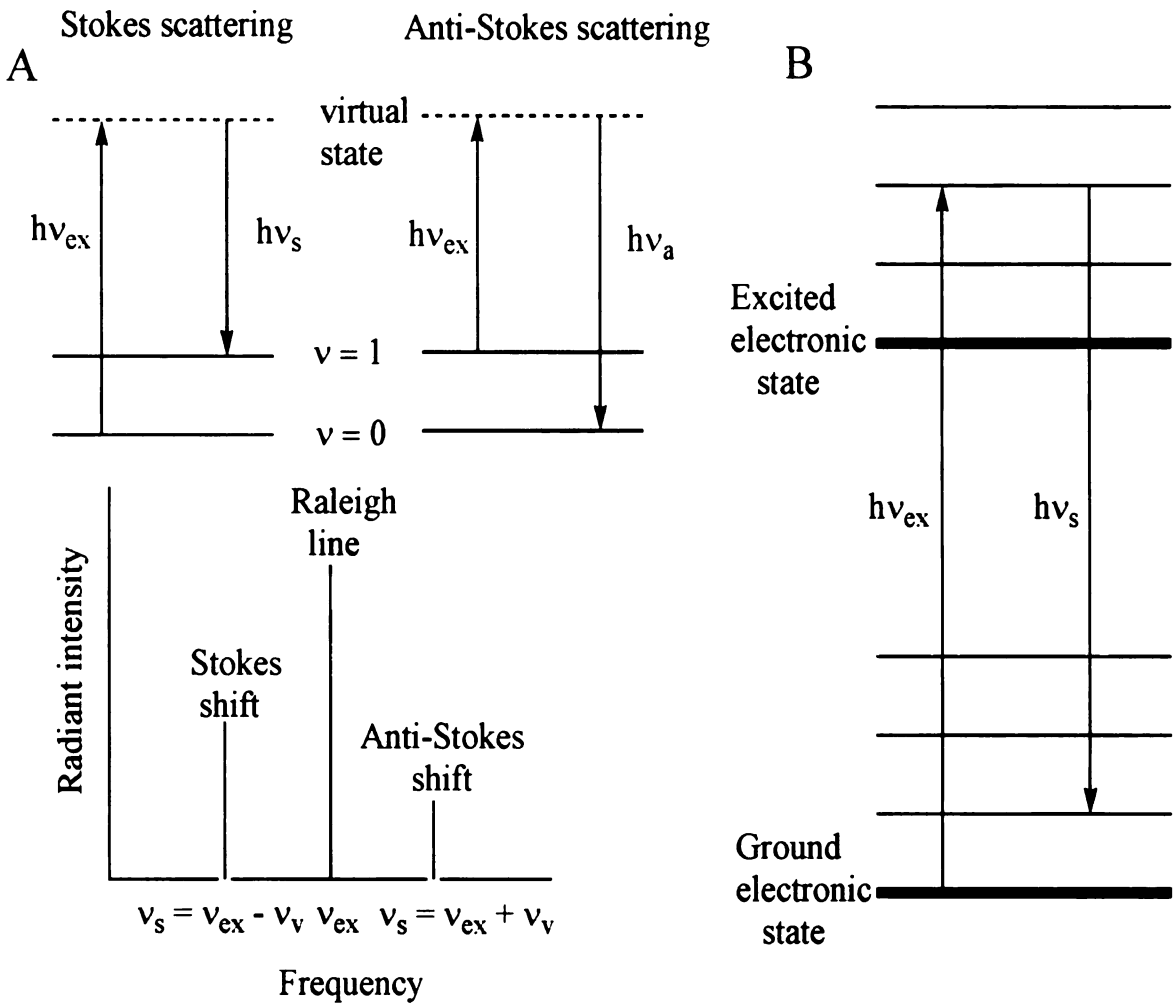

Figure IV.3: Schematic diagrams of Raman scattering. A: Raleigh (ν_{ex}), Stokes ($\nu_{ex} - \nu_v$) and anti-Stokes ($\nu_{ex} - \nu_v$) scattering from the incident beam. B: Resonance Raman scattering. The Raman shift ($\nu_{ex} - \nu_v$) is enhanced by the electronic absorption.

IV.2 Materials and methods

IV.2.1 Chemicals and materials

All chemicals were purchased from commercial sources and were of the highest quality except as noted otherwise. The isotope ^{57}Fe metal powder was purchased from Cambridge Isotope Laboratories. The solution of $^{57}FeSO_4$ was prepared by dissolving the metal in 3:1 H_2O:H_2SO_4. The pH of the solution was adjusted to 6.5 by 6 M NaOH. The

Fe concentration was determined by the method described in chapter II. Natural abundance ^{56}Fe PFL-AE was overexpressed and purified following the procedure described in chapter II.

IV.2.2 Preparation of ^{57}Fe labeled PFL-AE

Preparation of unique-iron site ^{57}Fe labeled PFL-AE. All procedures were carried out under strictly anaerobic conditions. Purified natural abundance PFL-AE (1 mL) was loaded on an Amersham HiTrap Desalting column and eluted with buffer (50 mM Tris, 200 mM NaCl, pH 8.5) to remove DTT. The colored fraction was collected. The protein concentration and Fe content were determined via the methods described in chapter II. Three equivalents of $K_3Fe(CN)_6$ (in H_2O, 1.9 mM final conc, relative to $[4Fe\text{-}4S]^{2+}$ cluster) were added into the protein and one equivalent of EDTA was added 10 minutes later. The oxidized protein was gel filtered through the same column again after 10 minutes to remove EDTA, extra oxidizing agent and released iron. The Fe content was determined by the same method again. $^{57}FeSO_4$, 1.1 equivalent relative to the $[3Fe\text{-}4S]^{1+}$ cluster (converted from Fe content, determined by Fe assay as described in Chapter II, presumably in $[3Fe\text{-}4S]^{1+}$ state), was then introduced into the protein to reconstitute the $[4Fe\text{-}4S]^{2+}$ cluster. To provide reducing environment, DTT (10 mM final conc) was added after 10 minutes. The protein was concentrated on a YM-10 ultra filtration membrane (Millipore). The final concentration of the reconstituted protein was 3.6 mM and the Fe content was 4.3 Fe/PFL-AE.

Preparation of all sites ^{57}Fe labeled PFL-AE. PFL-AE was overexpressed and purified as described in Chapter II except that $^{57}FeSO_4$, as the only iron source, was

introduced into the cell growth to a final concentration of 20 μM. The final concentration of purified [^{57}Fe]PFL-AE was 1.8 mM and the Fe content was 3.1 Fe/PFL-AE. The purified PFL-AE was concentrated on YM-10 centrifugal filters (Millipore) at 10,000 rpm for 1 hour at 4 °C under anaerobic conditions to make final concentration 10 mM.

IV.2.3 NRVS sample preparation

All procedures were carried out under strictly anaerobic conditions. For ^{57}Fe unique site labeled PFL-AE, protein alone (3.6 mM) or protein (3.5 mM) plus AdoMet (6.9 mM) were loaded into NRVS cells. The same samples were used for Mössbauer and resonance Raman spectroscopy. For ^{57}Fe all sites labeled PFL-AE, 10 mM PFL-AE or 6.5 mM PFL-AE plus 19.3 mM AdoMet were loaded into NRVS cells. The sample cells were sealed with Teflon washers and sapphire windows, and stored at –80 °C.

IV.2.4 Mössbauer spectroscopy

Mössbauer spectra were recorded at Emory University in a strong field spectrometer at 4.2 K in a magnetic field of 50 mT applied parallel to the incident beam. The spectrometer operated in a constant acceleration mode in a transmission geometry. The zero velocity of the spectra refers to the centroid of a room temperature spectrum of a metallic iron foil.

IV.2.5 Resonance Raman spectroscopy

The resonance Raman spectra were recorded at Northeastern Univeristy. The samples were excited by a laser beam at 413.3 nm from a Kr^+ laser source (Coherent

Innova 302C), and measured at 20 K in a helium flow cryostat (Oxford Instruments). The Raman scattering was collected in a LabRam HR800 spectrometer (JY Horiba). The laser power to excite the PFL-AE sample was 3.3 mW. The collection time was 4 minutes and spectra were accumulated 12 times. The laser power to excite the sample of PFL-AE with AdoMet was 5.3 mW. The collection time was 4 minutes and spectra were accumulated 11 times.

IV.2.6 NRVS spectroscopy

The NRVS measurement was conducted at sector 3-ID of the Advanced Photon Source at Argonne National Laboratory. A high-resolution X-ray beam with energy around 14.4 keV and resolution of 0.85 meV (7 cm^{-1}) was used. The beam energy was scanned above and below the nuclear excitation energy of ^{57}Fe. The bandwidth was narrowed by a diamond premonochromator followed by a dispersive pair of asymmetric Si crystals. An APD detector with a 1 cm^2 area was used to collect the atomic fluorescence from the sample. Pulses from the APD were recorded by a counter that discriminated the fluorescence photons 140 ns later than the strong coincident X-ray scattering. The sample was cooled down to 20 K in a He flow cryostat.

IV.3 Results and discussion

IV.3.1 Mössbauer spectra of PFL-AE

The Mössbauer spectrum of the unique site ^{57}Fe labeled PFL-AE showed 84% of total ^{57}Fe was in the $[4Fe\text{-}4S]^{2+}$ state (isomer shift δ = 0.42 mm/sec, quadrupole splitting

ΔE_Q = 1.12 mm/sec), and 16% of the total ^{57}Fe was in the solution as free ferrous (data not shown). It was not possible to distinguish the unique Fe from the other irons in the cluster in the absence of AdoMet, as the electronic environment was almost the same for each iron in the cluster. In the presence of AdoMet, the spectrum indicated 16% of the total ^{57}Fe was in the unique iron site with AdoMet bound (isomer shift δ = 0.72 mm/sec, quadruple splitting ΔE_Q = 1.19 mm/sec) (Fig IV.4). The increase of the isomer shift and quadrupole splitting of the unique Fe implied an increase of coordination number to the Fe due to AdoMet binding, as we have previously published. [6] However, the unique Fe signal was not separated clearly from the irons in the other positions of the cluster, which indicated that the AdoMet binding was not complete. Compared to previously published Mössbauer spectra, [6] it was estimated that 15 – 55% of the $[4Fe\text{-}4S]^{2+}$ cluster was not bound to AdoMet. In the current experiments 68% of the total ^{57}Fe was in other positions of the cluster, or in the unique site without AdoMet bound.

The Mössbauer data demonstrated that ^{57}Fe was reconstituted not only into the unique site, but also into other sites in the cluster. Earlier Mössbauer experiments with PFL-AE showed no exchange between the unique site and the other iron sites. [6] In these earlier experiments, the ^{57}Fe labeled sample was flash frozen in liquid N_2 immediately after it was reconstituted. However, in the NRVS sample preparation, the protein was concentrated for more than 30 minutes after the reconstitution, providing more time for exchange of iron between sites. This implies that the cluster is not a static structure, but rather dynamic under the reducing conditions (10 mM DTT).

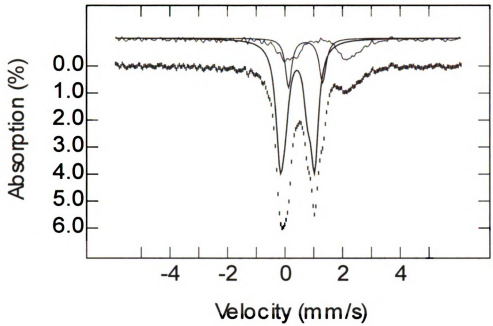

Figure IV.4: Mössbauer spectrum of ^{57}Fe labeled unique site PFL-AE in the presence of AdoMet. Data were recorded at 4.2 K in a magnetic field of 50 mT parallel to the incident beam. The black dashed line is the experimental signal. The black solid line is the deconvoluted ^{57}Fe in the $[4Fe\text{-}4S]^{2+}$ cluster other than the unique site. The dark grey solid line is the deconvoluted ^{57}Fe in the unique site. The light grey line is the free ferrous ^{57}Fe.

IV.3.2 Resonance Raman spectra of PFL-AE

Resonance Raman spectra of PFL-AE and PFL-AE with AdoMet showed typical $[4Fe\text{-}4S]^{2+}$ signals (Fig IV.5), compared to published $[4Fe\text{-}4S]^{2+}$ model compounds and proteins [1, 27-29]. The strongest band at 338 cm^{-1} is the totally symmetric breathing mode of the Fe_4S_4 cubane. [1, 16, 29] The band at 370 cm^{-1} is assigned to the asymmetric stretching mode of the bond between iron and the terminal sulfur. [28, 29] The band at 396 cm^{-1} is the symmetric stretching mode of the bond between iron and the terminal sulfur. [28, 29] The bands at 290 cm^{-1} and 320 cm^{-1} are the stretching modes of the bond between iron and the bridging sulfide. [27-29]

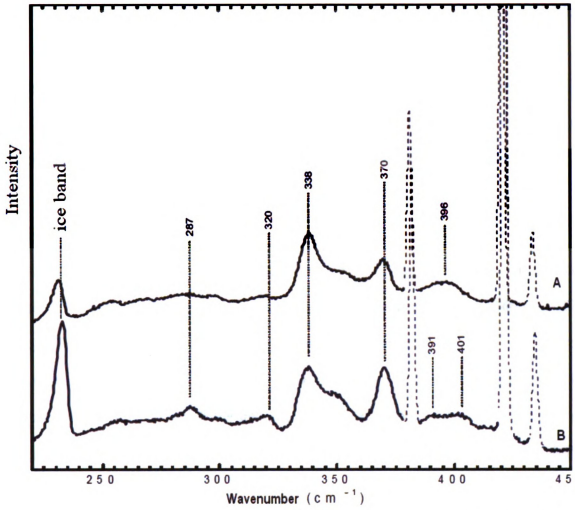

Figure IV.5: Resonance Raman spectra of PFL-AE and PFL-AE with AdoMet. The spectra were recorded at 20 K. The excitation wavelength was 413.3 nm. The solid bands were the vibrational modes from the protein, and the dashed bands were from the sapphire window of the sample cell. A: Spectrum of PFL-AE. Excitation power 3.3 mW. 48 min accumulation. B: Spectrum of PFL-AE with AdoMet. Excitation power 5.3 mW. 44 min accumulation.

In the presence of AdoMet, the resonance Raman spectrum of PFL-AE did not change signifcantly. The band at 396 cm^{-1} split to two bands at 391 and 401 cm^{-1}. AdoMet binding to the unique Fe changes the coordination number of this site, which decreases the symmetry of the cluster and might lead to splitting of this band. The relative intensity of the bands at 338 cm^{-1} and 370 cm^{-1} also changes upon addition of

AdoMet, with intensity of the band at 370 cm^{-1} increasing in the presence of AdoMet. These two changes point to some differences in the Fe-S^t bonds when AdoMet is coordinated to the unique Fe. Upon AdoMet binding, the intensities of the bands at 287, 320 and ~345 cm^{-1}, mainly Fe-S^b stretching modes, are also increased. Coordination of AdoMet might induce more tense in the [4Fe-4S] cube, changing the Fe-S^b bonds.

IV.3.3 NRVS spectra of PFL-AE

The NRVS spectra of ^{57}Fe reconstituted PFL-AE and PFL-AE with AdoMet reveal the complete vibrational modes of the $[4Fe\text{-}4S]^{2+}$ cluster from 0 – 660 cm^{-1} (Fig IV.6). The experimental recording shows the inelastic nuclear absorption of synchrotron radiation as a function of energy of the incident radiation. Various features contributes to the energy spectrum, in which the inelastic absorption is accompanied by excitation or annihilation of different vibrational states. To obtain the spectrum corresponding to single vibrational state change, decomposition of multiple probabilities of vibrational states density is used to deconvolute the spectrum (both the experimental spectra and deconvoluted spectra are shown in Fig IV.6). Four major features are observed: a triplet between 340 and 390 cm^{-1}, a doublet between 250 and 300 cm^{-1}, a strong band at 160 cm^{-1}, and a broad band below 100 cm^{-1}. The vibrations above 200 cm^{-1} are assigned to Fe-S bond stretching modes, the vibrations between 100 and 200 cm^{-1} are assigned to S-Fe-S' bending modes, and those below 100 cm^{-1} are assigned to cubane twist modes. [30] The detailed assignments are listed in table IV.1, compared with calculated normal modes of model compounds. [30, 14]

Upon AdoMet binding, there were some changes in the vibrational modes. The intensity of the band at 432 cm^{-1}, which is the Fe-ligand plus Fe-S^t stretching mode, increased dramatically, indicating that the coordination of the amino N and carboxylate O in AdoMet to the unique Fe enhanced the Fe-ligand vibration. The intensity of the bands at 388 cm^{-1} (Fe-S^t stretching) and 158 cm^{-1} (S-Fe-S' bending) also increased, indicating that the magnitude of these two vibrations was increased. There was a split of the peak at 278 cm^{-1}, also a Fe-S^t stretch. As with the resonance Raman spectra, AdoMet binding causes some change to the Fe-S^t bonds. Since the terminal sulfur ligands to the cluster in PFL-AE are three cysteines, this indicates that the details of cluster coordination to the protein may change in the presence of AdoMet.

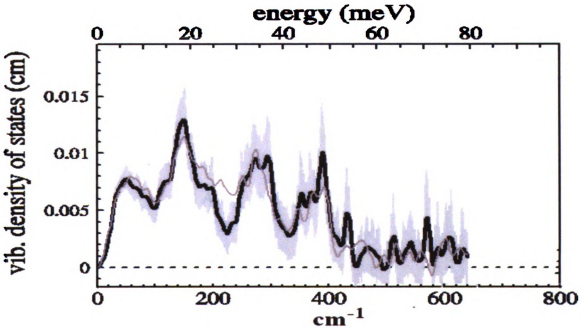

Figure IV.6: NRVS spectra of ^{57}Fe reconstituted PFL-AE and PFL-AE with AdoMet. The shadow line is the experimental data of PFL-AE with AdoMet. The black line was the deconvoluted spectrum of PFL-AE with AdoMet. The grey line was the deconvoluted spectrum of PFL-AE.

The stretching of the Fe-O bond between the unique Fe and the exogenous OH^- in aconitase was predicted to occur at 408 cm^{-1} in aconitase. [12] However, resonance Raman

spectroscopy has never detected this type of vibration in either aconitase or radical SAM superfamily proteins, presumably because the Fe-O stretching might not be enhanced by the excitation of sulfur to iron charge transfer absorption. The resonance Raman spectra of PFL-AE were no exception. On the other hand, NRVS is not limited by the requirement for resonance enhancement. The increase in intensity of the peak at 432 cm^{-1} and the up-shift of the band at 458 cm^{-1} in the presence of AdoMet could be indicative of a change in the exogenous ligand. The ligands from AdoMet could cause stronger and more rigid vibrations than the vibrations between the unique iron and the (non-AdoMet) exogenous ligand.

Mode	Symmetry	Wavenumber (cm^{-1})		
		PFL-AE	PFL-AE + AdoMet	Calculated
Fe-Ligand + Fe-S^t stretch	E	432	432	429.3
Fe-S^t stretch	A_1	390	388	390.4
Mainly Fe-S^t stretch	B_2	368	364	361.0
Fe-S^b stretch	A_1	344	348	347.1
	A_1		300	299.9
	A_2	278	278	278.4
	E	254		266.1
S-Fe-S' bend	A_1	180	184	179.0
	E	160	160	157.2
Cubane twist	B_1	58	60	54.3

Table IV.1 NRVS normal mode assignments of PFL-AE and PFL-AE with AdoMet, compared with published calculations.

The NRVS spectrum of all sites labeled [^{57}Fe]PFL-AE is different from that of the unique site labeled sample (Fig IV.7). The most intense band shifts from 160 cm^{-1} to 142 cm^{-1}. The peak at 278 cm^{-1} is broader and has a small split. The peaks at 368 and 390 cm^{-1} combine to form a broad band. The intensity of the bands above 400 cm^{-1} are decreased. The difference observed between the all-sites labeled and unique labeled samples might be due to different forms of iron-sulfur clusters existing in the protein. The Fe content of the purified all-sites labeled enzyme was only 3.1 Fe/PFL-AE. Previous Mössbauer studies of PFL-AE with similar iron content showed that there were $[2Fe\text{-}2S]^{2+}$, $[3Fe\text{-}4S]^{1+}$ and $[4Fe\text{-}4S]^{2+}$ clusters present. [25] Unfortunately, we did not obtain Mössbauer data on the current sample, so we cannot be certain as to the cluster content. However it is reasonable to suspect that the sample also had several cluster forms. The assignment of the vibrational modes would thus be very difficult due to the lack of quantification of different clusters present.

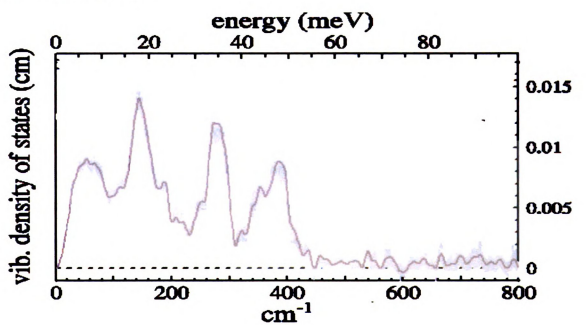

Figure IV.7: NRVS spectrum of all sites labeled [^{57}Fe]PFL-AE. The shadow line was the experimental signal. The grey solid line was the deconvoluted spectrum of the protein.

IV.4 Conclusions

The isotope ^{57}Fe has been reconstituted into the $[4Fe\text{-}4S]^{2+}$ cluster in PFL-AE after the purified protein was oxidized to the $[3Fe\text{-}4S]^{1+}$ state under controlled conditions. The Mössbauer spectrum showed that 84% of the total ^{57}Fe was incorporated into the cluster, and 16% of the total iron was in the solution as free ferrous. The Mössbauer spectrum of PFL-AE with AdoMet bound demonstrated that only 16% of the ^{57}Fe occupied the unique site with AdoMet bound, while the other 68% of ^{57}Fe was scrambled into other sites of the cluster and/or on the unique site without AdoMet bound. We have previously show that ^{57}Fe could be taken into the $[3Fe\text{-}4S]^{1+}$ cluster to form the $[4Fe\text{-}4S]^{2+}$ cluster, however the prolonged incubation in the presence of 10 mM DTT utilized in the current experiment may have resulted in scrambling of the ^{57}Fe into all sites of the cluster. The mechanism of label scrambling is unknown.

The resonance Raman spectra of PFL-AE and PFL-AE with AdoMet bound are typical $[4Fe\text{-}4S]^{2+}$ signals. There are strong symmetric Fe-S stretching modes and weak asymmetric Fe-S stretching modes. In the presence of AdoMet, there are small changes in the vibrational modes of $Fe\text{-}S^{t}$ stretching, but nothing that definitively identifies the unique site ligand in the absence of AdoMet.

The NRVS spectra of the protein and the protein with substrate provide a complete set of the cluster vibrational movements, including the Fe-ligand stretching, Fe-S stretching, S-Fe-S' bending, and the cubane twist. Compared with resonance Raman spectra, NRVS not only demonstrates the vibrations that are missing in Raman spectroscopy, but also provides more detailed information of the modes. Upon AdoMet binding, significant changes of $Fe\text{-}S^{t}$ vibrations are observed. The resonance Raman and

NRVS results imply the coordination of the cluster to the protein is altered when AdoMet binds, based on the increases of the intensity and energy shift of the bands.

NRVS spectra show the vibrational information between Fe and exogenous ligands above 400 cm^{-1}, which are missing in the resonance Raman results. The changes of the bands at 432 and 458 cm^{-1} in the presence and absence of AdoMet binding might provide clues as to identify the exogenous ligand to the unique Fe site.

The NRVS spectrum of all sites labeled [^{57}Fe]PFL-AE is different from the ^{57}Fe reconstituted protein. The explanation might be that the former spectrum is a mixture of the vibrations of $[2Fe\text{-}2S]^{2+}$, $[3Fe\text{-}4S]^{1+}$ and $[4Fe\text{-}4S]^{2+}$ clusters. Without the Mössbauer quantification of each cluster form, it is difficult to interpret these results.

References

1. Broderick, J. B.; Duderstadt, R. E.; Fernandez, D. C.; Wojtuszewski, K.; Henshaw, T. F.; Johnson, M. K., *Journal of the American Chemical Society* **1997,** 119, (31), 7396-7397.

2. Henshaw, T. F.; Cheek, J.; Broderick, J. B., *Journal of the American Chemical Society* **2000,** 122, (34), 8331-8332.

3. Kulzer, R.; Pils, T.; Kappl, R.; Huttermann, J.; Knappe, J., *Journal of Biological Chemistry* **1998,** 273, (9), 4897-4903.

4. Sofia, H. J.; Chen, G.; Hetzler, B. G.; Reyes-Spindola, J. F.; Miller, N. E., *Nucleic Acids Research* **2001,** 29, (5), 1097-1106.

5. Cheek, J.; Broderick, J. B., *Journal of biological inorganic chemistry : JBIC : a publication of the Society of Biological Inorganic Chemistry* **2001,** 6, (3), 209-26.

6. Krebs, C.; Broderick, W. E.; Henshaw, T. F.; Broderick, J. B.; Huynh, B. H., *Journal of the American Chemical Society* **2002,** 124, (6), 912-913.

7. Walsby, C. J.; Ortillo, D.; Broderick, W. E.; Broderick, J. B.; Hoffman, B. M., *Journal of the American Chemical Society* **2002,** 124, (38), 11270-11271.

8. Walsby, C. J.; Hong, W.; Broderick, W. E.; Cheek, J.; Ortillo, D.; Broderick, J. B.; Hoffman, B. M., *Journal of the American Chemical Society* **2002,** 124, (12), 3143-3151.

9. Walsby, C. J.; Ortillo, D.; Yang, J.; Nnyepi, M. R.; Broderick, W. E.; Hoffman, B. M.; Broderick, J. B., *Inorganic Chemistry* **2005,** 44, (4), 727-741.

10. Beinert, H.; Kennedy, M. C.; Stout, C. D., *Chemical Reviews (Washington, D. C.)* **1996,** 96, (7), 2335-2373.

11. Werst, M. M.; Kennedy, M. C.; Beinert, H.; Hoffman, B. M., *Biochemistry* **1990,** 29, (46), 10526-32.

12. LaTonya K. Kilpatrick, M. C. K., Helmut Beinert, Roman S. Czernuszewicz, Thomas G. Spiro, Di Qiu, *Journal of American Chemical Society* **1994,** 116, (9), 4053-61.

13. Lauble, H.; Kennedy, M. C.; Beinert, H.; Stout, C. D., *Biochemistry* **1992,** 31, (10), 2735-48.

14. Lauble, H.; Kennedy, M. C.; Beinert, H.; Stout, C. D., *J Mol Biol* **1994,** 237, (4), 437-51.

15. Barth, A.; Zscherp, C., *Q Rev Biophys* **2002,** 35, (4), 369-430.

16. Spiro, T. G. C., Roman S., *Resonance Raman spectroscopy. Physical Methods in Bioinorganic Chemistry*. University Science Books: Sausalito, CA, 2000; p pp 97 - 112.

17. Chumakov, A. I., Sturhahn, W., *Hyperfine Interactions* **1999,** 123/124, 781-808.

18. Leu, B. M.; Zgierski, M. Z.; Wyllie, G. R.; Scheidt, W. R.; Sturhahn, W.; Alp, E. E.; Durbin, S. M.; Sage, J. T., *J Am Chem Soc* **2004,** 126, (13), 4211-27.

19. Scheidt, W. R., Durbin, S. M., Sage, J. T., *Journal of Inorganic Biochemistry* **2005,** 99, 60-71.

20. Mössbauer, R., *Z. Physik* **1958,** 151, 124-143.

21. Edwards, P. R., Johnson, C. E. and Williams, R. J. P., *J. Chem. Phys.* **1967,** 47, 2074-82.

22. A. Rahman, K. S. S., and A. Sjölander, *Phys. Rev.* **1960,** 120, (4), 1093-1102.

23. Sturhahn, W.; Toellner, T. S.; Alp, E. E.; Zhang, X.; Ando, M.; Yoda, Y.; Kikuta, S.; Seto, M.; Kimball, C. W.; Dabrowski, B., *Physical Review Letters* **1995,** 74, (19), 3832-3835.

24. Cranshaw, T. E., Dale, B. W., Longworth, C. O. and Johnson, C. E., *Mössbauer Spectroscopy and its Applications*. Cambridge Univ. Press.: 1985.

25. Greenwood, N. N. a. G., T. C., *Mössbauer Spectroscopy*. Chapman and Hall: London, 1971.

26. Lang, G. a. M., W., *Proc. Phys. Soc.* **1966,** 87, 3-34.

27. Johnson, M. K.; Czernuszewicz, R. S.; Spiro, T. G.; Ramsay, R. R.; Singer, T. P., *J Biol Chem* **1983,** 258, (21), 12771-4.

28. Vittal K. Yachandra, J. H., Andrew Gewirth, Roman S. Czernuszewicz, T. Kimura, Richard H. Holm, Thomas G. Spiro, *Journal of American Chemical Society* **1983,** 105, 6462-6468.

29. Roman S. Czernuszewicz, K. A. M., Michael K. Johnson, Andrew Gewirth, Thomas G. Spiro, *Journal of American Chemical Society* **1987,** 109, (23), 7178-87.

30. Xiao, Y.; Koutmos, M.; Case, D. A.; Coucouvanis, D.; Wang, H.; Cramer, S. P., *Dalton Trans* **2006**, (18), 2192-201.

CHAPTER V

STRUCTURAL CHANGE IN PYRUVATE FORMATE-LYASE DURING ACTIVATION

V.1 Introduction

Pyruvate formate-lyase (PFL) utilizes a glycyl radical on Gly-734 to initiate catalysis. [1-3] This radical is generated by a putative 5'-deoxyadenosyl (5'-dAdo) radical intermediate, which is produced from the reductive cleavage of AdoMet catalyzed by PFL-AE. [4, 5, 6] There has been no direct detection of the putative 5'-dAdo radical as yet, although an allylic analogue of the deoxyadenosyl radical was identified by EPR during LAM catalysis. [7] PFL is a homodimer, with each monomer comprising a 10 strand β/α barrel. [8, 9] A short loop containing Gly-734 is buried in the non-radical form of PFL, with Gly-734 8 Å from the surface. [8-10] Considering the extremely high reactivity expected for the deoxyadenosyl radical intermediate, it is expected that it must be generated in the immediate vicinity of Gly-734 of PFL. A major unresolved question is how the PFL-AE active site accesses Gly-734 of PFL to catalyze activation.

The structure of PFL is similar to subunit R1 of the class I ribonucleotide reductase (RNR), [7, 11] which uses a thiyl radical in catalysis. The activation of class I RNR is initiated by a tyrosyl radical in subunit R2, 35 Å apart from the thiyl radical. [12] It has been proposed that there is a long-range proton-coupled electron transfer to transport the radical from the tyrosine to the cysteine. [13] Ten residues total are proposed to be involved in the pathway. However, PFL probably has a different mechanism for

activation. Direct hydrogen transfer from Gly-734 to the product of AdoMet cleavage was observed, [14] by which a direct interaction between the Gly-734 residue and the putative deoxyadenosyl radical intermediate was proposed. This implies that PFL must undergoe a conformational change prior to activation, in which the glycine loop is moved out from the protein core. [10]

EPR Spin quantification of the glycyl radicals in activated PFL, activity assays of the enzyme, and circular dichroism (CD) spectroscopy were used to investigate the proposed mechanism of PFL activation. The experiments provide evidence to support a PFL conformational change. An examination of the published PFL crystal structure suggests possible residues which may be involved in the glycine loop position change.

V.2 Materials and methods

V.2.1 Chemicals and materials

All chemicals were commercially purchased with the highest quality except as noted otherwise. AdoMet was synthesized according to the procedure described in chapter III. Overexpression and purification of PFL and PFL-AE, as well as protein and iron assays were carried out following the procedures in chapter II.

V.2.2 PFL activation

All procedures were carried out under strictly anaerobic conditions (Mbraun glove box, O_2 level < 2 ppm). All components were degassed completely on a Shlenk line before the reaction. An activation mix contained 100 mM Tris/HCl pH 7.6, 100 mM KCl,

10 mM oxamate, 10 mM DTT, 50 or 100 μM PFL, 0.5 – 100 μM PFL-AE, 10 equivalents of AdoMet relative to PFL, and 100 μM 5-deazariboflavin. The mix was transferred into an EPR tube and illuminated by a 300 W halogen light approximately 5 cm away from the tube for different time periods. The EPR tube was put in an ice-water bath (4 °C) to keep the protein from over-heating by the lamp. The mix was flash frozen in liquid N_2 immediately after illumination and later examined by using EPR spectrocopy.

V.2.3 EPR spectroscopy

EPR spectra were recorded at X-band (9.37 GHz) in a Bruker ER-200D-SRC spectrometer at 60 K. The microwave power was 19 μW. The external magnetic field was scanned from 3000 to 4000 G. The static field was 1000 G. The modulation frequency was 100 kHz, and modulation amplitude was 5 G. The resolution was 1024. $K_2(SO_3)_2NO$ was used as a standard to determine the quantity of the PFL glycyl radical, according to the published method. [6, 15]

V.2.4 Hydrogen-deuterium exchange of activated PFL in D_2O

All the procedures were conducted under strictly anaerobic conditions. After the EPR spectra were measured, the samples were thawed. Buffer (150 μL of 100 mM Tris/DCl, 100 mM KCl in D_2O, pD 8.2) was added into 150 μL of the EPR samples with PFL to PFL-AE ratios of 100:1, 10:1 and 1:1. Immediately after mixing, the sample was pipetted into an EPR tube and flash frozen in liquid N_2. Another sample was prepared by adding 225 μL of the D_2O buffer into 75 μL of the same EPR sample, following the procedure above.

V.2.5 PFL activity assay

All the procedures were conducted under strictly anaerobic conditions. The protein activity was measured by using a modification of published procedures. [16] The rate of acetyl-CoA production was monitored by a coupled enzymatic reaction (Fig V.1). Completely activated PFL (1 μL of 100 μM), as determined by EPR, was added to 99 μL of buffer (100 mM Tris/HCl, pH 7.6, 100 mM KCl). This diluted sample (5 μL) was mixed with 795 μL of the coupling enzyme mix, containing 100 mM Tris-HCl pH 8.1, 10 mM pyruvate, 55 μM CoA, 10 mM malate, 3 mM NAD^+, 0.1 mg BSA, 300 U malic dehydrogenase and 20 U citrate synthase. The NAD^+ reduction rate, recorded as the increase in absorption at 340 nm due to production of NADH, was used as the indicator of PFL activity. As can be seen in Fig V.1, the reduction of NAD^+ to NADH by malic dehydrogenase is at equilibrium if the oxaloacetate concentration remains stable. In the presence of acetyl-CoA (produced by PFL), citrate synthase converts oxaloacetate to citrate, which shifts the equilibrium to the right. The only source of acetyl-CoA is from PFL catalysis, so the rate of NADH production could be converted to PFL activity.

The rate of production of NADH was recorded at 340 nm in an HP-8453 diode-array spectrometer. The reaction is considered as a zero order reaction. The experiment was conducted under anaerobic conditions at room temperature.

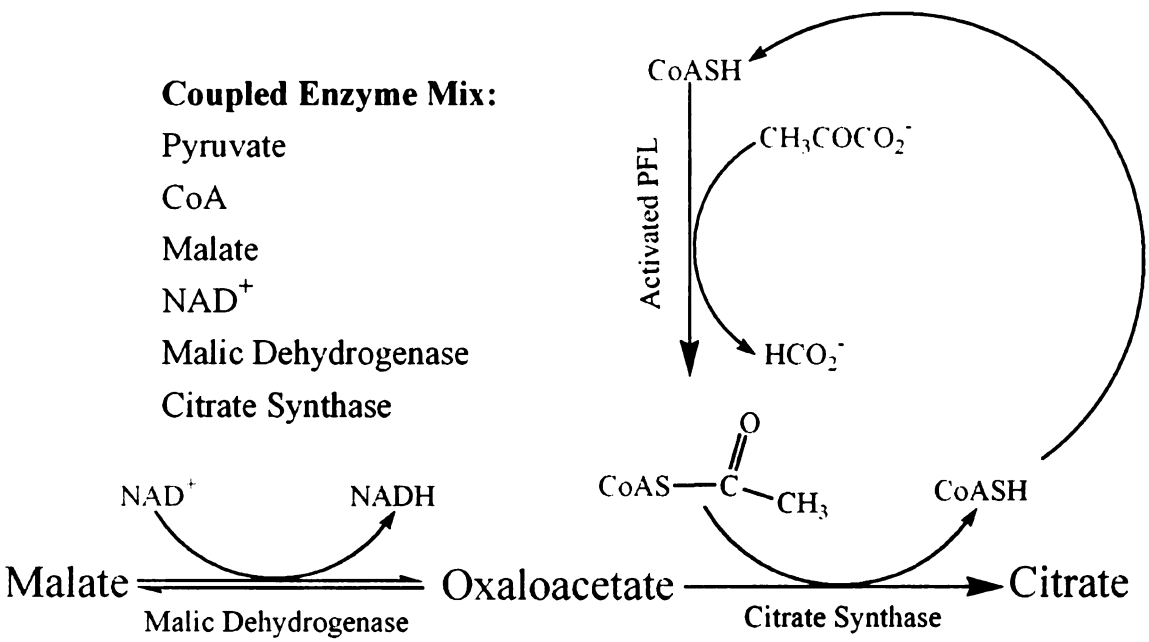

Figure V.1: Schematic representation of PFL activity assay. Activated PFL was mixed with pyruvate, CoA, and two coupling enzymes. The rate of NADH production was converted to PFL activity.

V.2.6 CD sample preparation

All procedures were carried out under strictly anaerobic conditions. The EPR samples described previously were thawed after experiments. PFL samples (35.3 μL of 50 μM) were mixed with 64.7 μL of 10 mM phosphate buffer, pH 7.5 to make the final concentration of PFL 3 mg/mL. Samples were then frozen in liquid N_2. Each sample was loaded into a 0.1 mm optical-path CD measuring cell immediately after it was thawed in an anaerobic chamber (COY). The cells were sealed by rubber septa in the chamber, and taken out for measurement

To subtract the CD absorption of PFL-AE in the PFL activation mix, background solutions were prepared. The background solutions contained everything in the PFL activation mix except PFL itself. They had the same concentration of PFL-AE as those

used to activate PFL, and were illuminated for the same time as for PFL activation. After illumination, 35.3 μL of the solution was mixed with 64.7 μL of 10 mM phosphate buffer, pH 7.5. The mixture was stored and measured the same way as PFL samples.

V.2.7 CD spectroscopy

CD spectra were measured by using a JASCO J-710 spectropolarimeter at room temperature. The spectra were recorded in the wavelength range 170 – 300 nm. The scan speed was 50 nm/min. The data pitch was 0.1 nm. The band width was 0.5 nm and 4 scans were accumulated. To keep anaerobic conditions during the measurement, the spectrometer was purged with N_2 gas at 60 L/min, and the measuring chamber was purged with N_2 from a separate line.

V.3 Results and discussion

V.3.1 Spin quantification of glycyl radical in activated PFL

PFL (50 μM) was activated for 2 h in the presence of 0.5, 5, 10, 20, 30, 40, 50, and 100 μM of PFL-AE, as described in Materials and Methods. The EPR spectra of these samples (having PFL to PFL-AE ratio of 100:1, 10:1, 5:1, 5:2, 5:3, 5:4, 1:1, and 1:2) are shown in Fig V.2.A, and the spin quantifications are shown in Fig V.2.B and Table V.1. At higher PFL to PFL-AE ratios (100:1 and 10:1), the PFL is fully activated after 2 h illumination, showing 50 (±5) and 49 (±5) μM spin for 50 μM PFL respectively. The smaller the PFL to PFL-AE ratio, the less glycyl radical was present after a 2 h activation. These results were initially unexpected, because one would expect the most rapid and

complete activation to occur with higher ratios of catalyst (PFL-AE) to substrate. Repeating this experiment, however, revealed that the results were very reproducible. We thus began to suspect that these unexpected results might be telling us some important information about the interaction of PFL-AE with its substrate PFL. We hypothesized that when these two proteins interact, the glycine loop of PFL might be pulled out of the core of the PFL structure, so that it is accessible to the PFL-AE active site. This would leave the glycyl radical more exposed to solvent and more prone to quenching, resulting in less glycyl radical being present after a 2 h illumination (activation) reaction. In this model, the lower glycyl radical quantification at lower PFL:PFL-AE ratios reflects not incomplete activation, but rather complete activation followed by faster quenching process occurring in the presence of more PFL-AE.

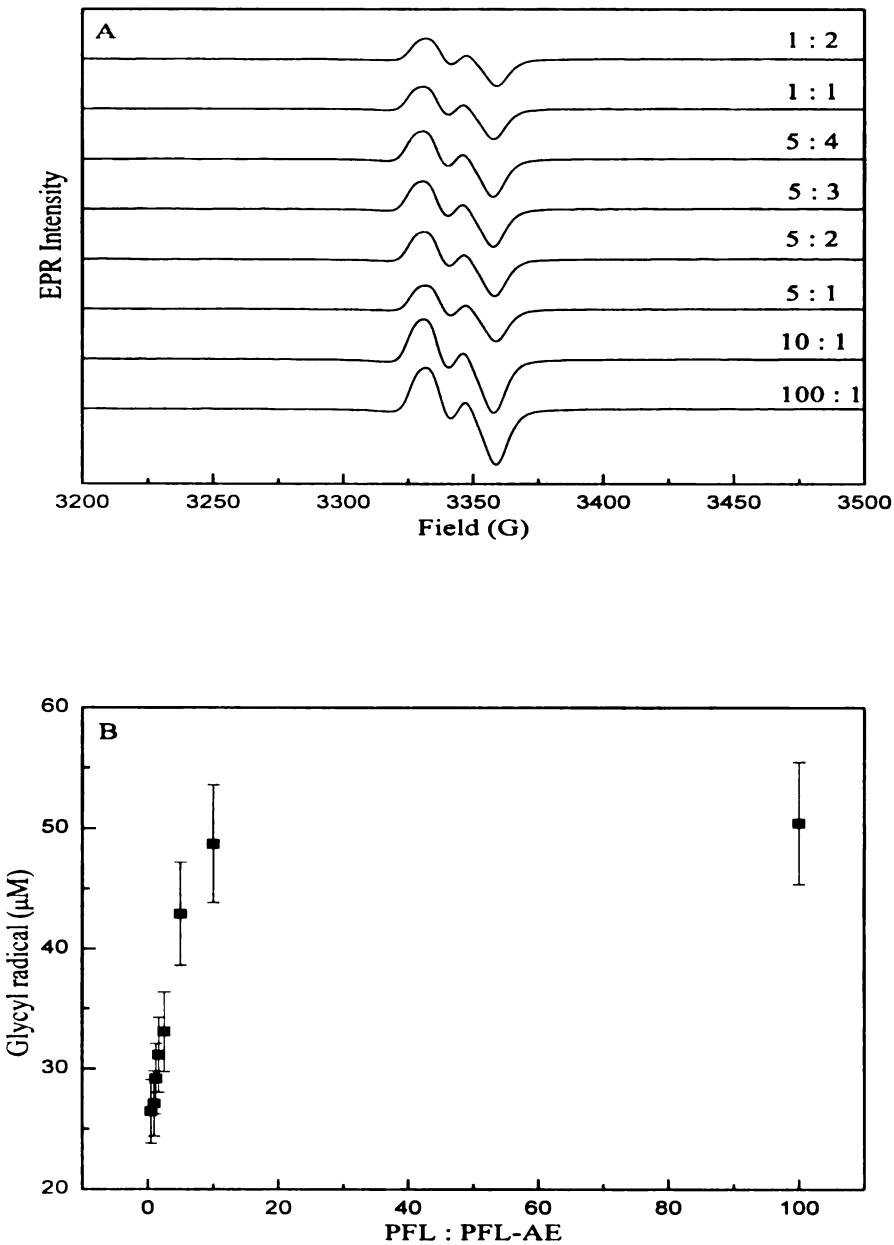

Figure V.2: EPR spectra (top) and spin quantification (bottom) of 50 μM PFL activated with different amounts of PFL-AE for 2 h. A. EPR spectra of 50 μM PFL activated by 0.5, 5, 10, 20, 30, 40, 50, and 100 μM of PFL-AE, 500 μM AdoMet, and 100 μM 5-deazariboflavin for 2 h, in a buffer containing 100 mM Tris/HCl pH 7.6, 100 mM KCl, 10 mM oxamate, and 10 mM DTT. B. Spin quantification of the glycyl radicals in panel A. EPR parameters: T = 60 K, microwave frequency 9.37 GHz, power 19 μW, modulation amplitude 5 G, scan twice.

PFL : PFL-AE ratio	[Gly·] (μM)
100:1	50
10:1	49
5:1	43
5:2	33
5:3	31
5:4	29
1:1	27
1:2	26

Table V.1: Spin quantification of glycyl radical in 50 μM PFL activated with 0.5, 5, 10, 20, 30, 40, 50, and 100 μM PFL-AE, 500 μM AdoMet, and 100 μM 5-deazariboflavin in a buffer containing 100 mM Tris/HCl pH 7.6, 100 mM KCl, 10 mM oxamate, and 10 mM DTT, after 2 h illumination.

In order to further examine this hypothesis, we illuminated 1:1 and 100:1 PFL:PFL-AE for times ranging from 0 to 120 min. Specifically, 50 μM PFL with either 0.5 μM or 50 μM PFL-AE was illuminated for 0, 20, 40, 60, 80, 100 and 120 minutes. The spin quantifications of glycyl radicals in PFL activated by PFL-AE in a 100:1 ratio increase during illumination (Fig V.3.A). The spin quantifications of glycyl radicals in PFL activated by 1 equivalent of PFL-AE are maximum at the shortest time points but decrease with longer illumination time (Fig V.3.B). The spin quantifications of the two samples are listed in Table V.2. The results show that PFL is completely activated by 0.01 equivalent of PFL-AE in 100 minutes, and is stable up to 120 minutes. In the

presence of a 1:1 ratio of PFL-AE, however, the fully activated PFL present at 20 minutes is slowly inactivated during subsequent illumination.

The spin quantification demonstrated that a 1:1 ratio of PFL to PFL-AE resulted in rapid and complete activation of PFL, as expected based on previous results. [6] However, the activated PFL was deactivated with continuing incubation. On the other hand, the glycyl radical in PFL activated with 0.01 equivalents of PFL-AE was stable after PFL was fully activated. The results rule out the possibility that the glycyl radicals are destroyed by intense photo illumination, but are consistent with the hypothesis that the presence of PFL-AE changes the environment of the glycyl radical loop, such that it is more solvent exposed and thus more prone to quenching.

The PFL activated with 1 equivalent of PFL-AE for 2 h had 21 μM glycyl radical, less than that shown in Fig V.2. The difference could be due to a slight difference in experimental procedure. For the experiments in Fig V.3, all the samples were illuminated in one preparation. After each time point, the sample was frozen in liquid N_2, which took approximately 2 – 3 minutes, while rest of the samples were kept in dark. Therefore, each PFL sample was exposed to the solvent longer than the illumination time.

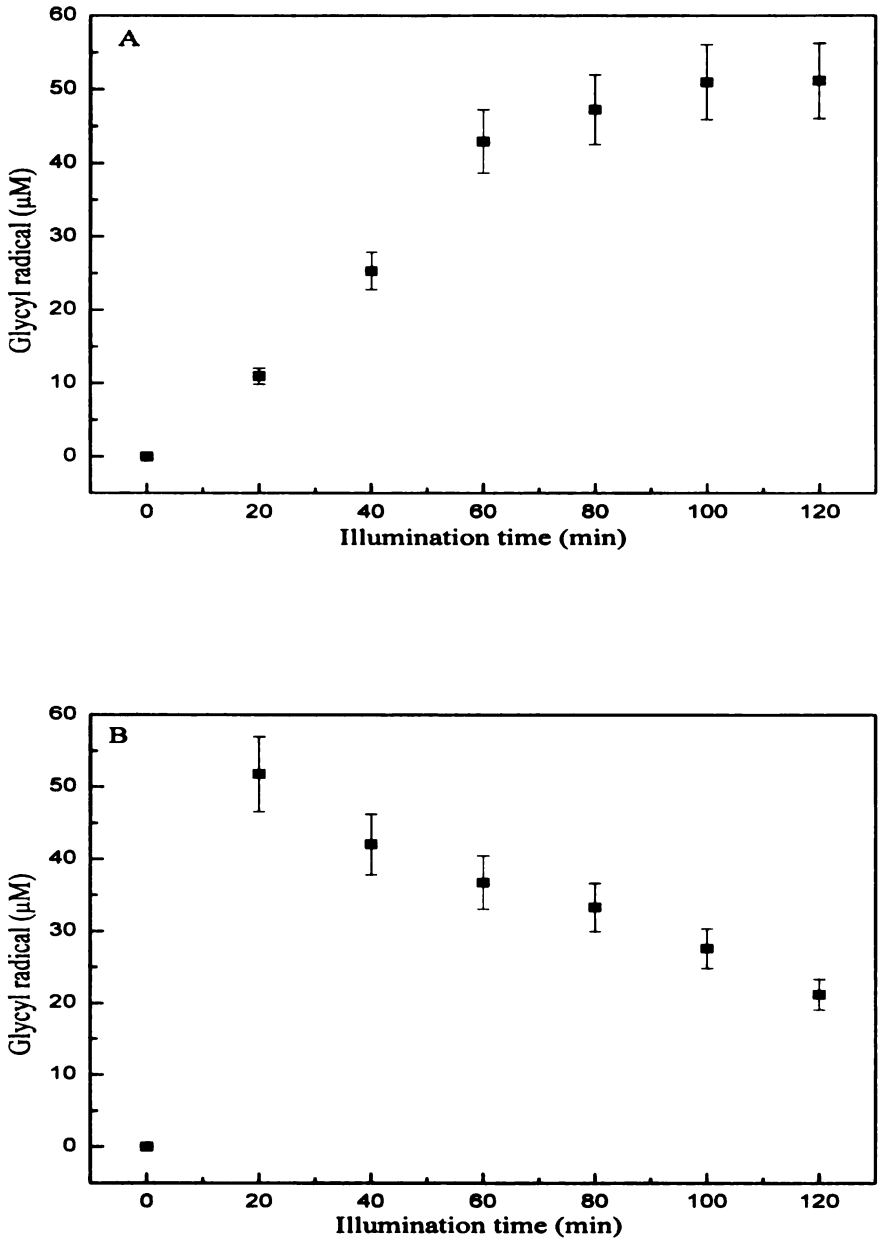

Figure V.3: Spin quantification of glycyl radicals in PFL activated by different ratios of PFL-AE as a function of time. PFL (50 μM) was illuminated with 0.5 μM (A) or 50 μM (B) PFL-AE, 500 μM AdoMet, and 100 μM 5-deazariboflavin in a buffer containing 100 mM Tris/HCl pH 7.6, 100 mM KCl, 10 mM oxamate, and 10 mM DTT. Samples were activated for 0, 20, 40, 60, 80, 100, 120 minutes. EPR paramaters: T = 60 K, microwave frequency 9.37 GHz, power 19 μW, modulation amplitude 5 G, scan twice.

Illumination time (min)	[Gly·] (μM)	
	PFL:PFL-AE (100:1)	PFL:PFL-AE (1:1)
0	0	0
20	11	52
40	25	42
60	43	37
80	47	33
100	51	28
120	51	21

Table V.2: Spin quantification of glycyl radical in 50 μM PFL activated by 0.5 and 50 μM PFL-AE, 500 μM AdoMet, and 100 μM 5-deazariboflavin in a buffer containing 100 mM Tris/HCl pH 7.6, 100 mM KCl, 10 mM oxamate, and 10 mM DTT.

In order to investigate the effect of AdoMet, PFL (50 μM) was activated for 2 h by 50 μM PFL-AE with 500, 250, 200, 100, and 50 μM AdoMet (Fig V.4, Table V.3). The results are similar to those in Fig V.2 and demonstrated that AdoMet does not completely protect the glycyl radical from quenching. However, more radical is present when there was more AdoMet present. This could be explained by AdoMet partially protecting the glycyl radical from quenching or by reactivating of PFL after quenching by reduced PFL-AE and excess AdoMet.

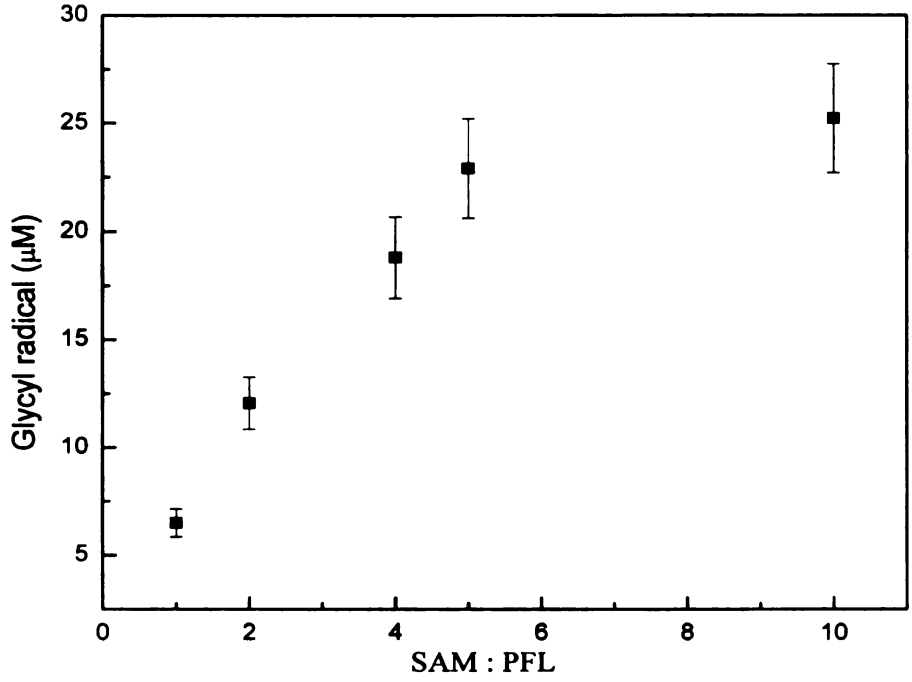

Figure V.4: Spin quantification of glycyl radicals in 50 μM PFL activated for 2 hours by 50 μM of PFL-AE with 50, 100, 200, 250 and 500 μM of AdoMet, and 100 μM 5-deazariboflavin in a buffer containing 100 mM Tris/HCl pH 7.6, 100 mM KCl, 10 mM oxamate, and 10 mM DTT. EPR parameters: T = 60 K, microwave frequency 9.37 GHz, power 19 μW, modulation amplitude 5 G, scan twice.

AdoMet concentration (μM)	**[Gly·] (μM)**
50	7
100	12
200	19
250	23
500	25

Table V.3: Spin quantification of glycyl radicals in 50 μM PFL illuminated for 2 hours by 50 μM of PFL-AE with 50, 100, 200, 250 and 500 μM of AdoMet, and 100 μM 5-deazariboflavin in a buffer containing 100 mM Tris/HCl pH 7.6, 100 mM KCl, 10 mM oxamate, and 10 mM DTT.

V.3.2 Hydrogen-deuterium exchange of activated PFL in D_2O

As previously reported, [2, 17, 18] the α-H on the Gly-734 radical can exchange with solvent, as evidenced by the doublet EPR signal becoming a singlet in D_2O (Fig V.5). The doublet EPR signal of the glycyl radical is due to the interaction between the radical electronic spin (S = 1/2) and the glycine hygrogen nuclear spin (I = 1/2). When the glycyl hydrogen is replaced by a deuteron (I = 1), the doublet signal becomes a singlet. The active site residue Cys-419 was shown to be essential for the H/D exchange at Gly-734, as the mutant C419A-PFL showed no exchange. [16] A similar Gly-734/Cys-419 radical transfer is believed to occur in the PFL catalytic mechanism. [18, 19, 20] The H/D exchange has been explained by the glycyl radical abstracting a hydrogen from Cys-419 to generate a thiyl radical. Because the thiol hydrogen is exchangeable with solvent, the glycyl radical will abstract either H (in H_2O) or D (in D_2O).

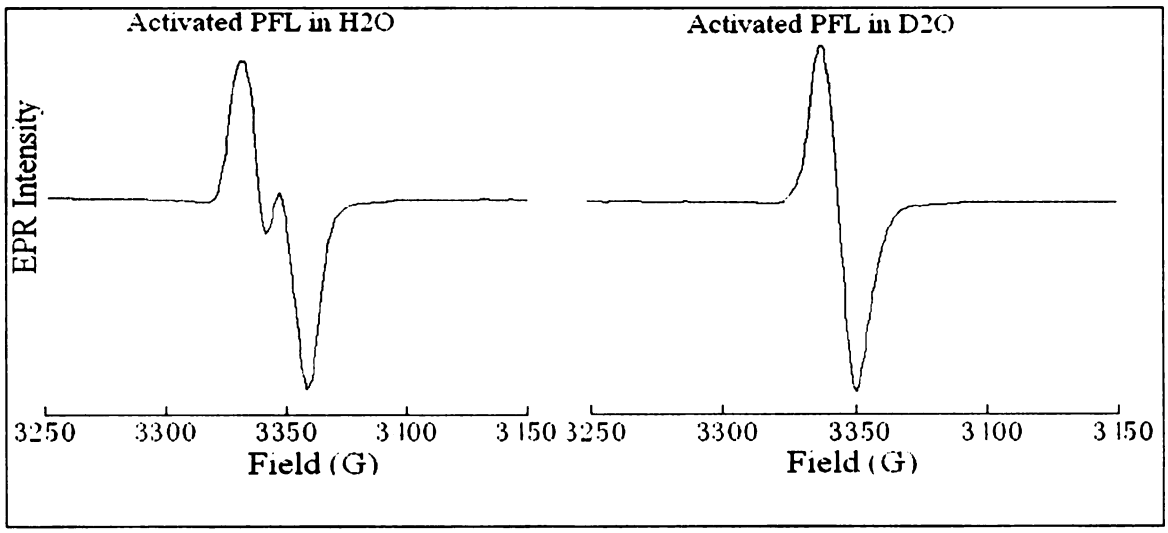

Figure V.5: EPR spectra of activated PFL in H_2O and D_2O. PFL (50 μM) was activated by 50 μM PFL-AE and 500 μM AdoMet in either H_2O or D_2O buffer, containing 0.1 M Tris-HCl pH 7.6 (in H_2O) or pD 8.2 (in D_2O), 0.1 M KCl, 10 mM oxamate, 10 mM DTT, 100 μM 5-deazariboflavin. The spin quantification of glycyl radical of PFL in H_2O is 39 μM, and the spin quantification of glycyl radical of PFL in D_2O is 33 μM. EPR parameters: T = 60 K, microwave frequency 9.37 GHz, power 19 μW, modulation amplitude 5 G, scan twice.

Based on our previously stated hypothesis that interaction with PFL-AE perturbs the position of the Gly-734 loop, we proposed that this position change might be reflected in the H/D exchange results. If PFL-AE perturbs the position of the glycine loop, we would expect less H/D exchange at higher PFL-AE to PFL ratios. We therefore fully activated 100 μM PFL with either 1, 0.1 or 0.01 equivalents of PFL-AE and then mixed the sample with D_2O to examine H/D exchange by EPR. Fig V.6.A shows the change in EPR signal of activated PFL mixed with one volume of D_2O (final $[D_2O]$ = 50%). The PFL activated with 1 equivalent of PFL-AE has a partial doublet signal, which is decreased in PFL activated with 0.1 and 0.01 equivalent of PFL-AE. Fig V.6.B shows the change in EPR signal of activated PFL mixed with 3 volumes D_2O (final $[D_2O]$ = 75%). The signal of PFL activated with 1 equivalent of PFL-AE is broader than those of PFL with 0.1 and 0.01 equivalents of PFL-AE. The results demonstrate that glycyl α-hydrogen exchange to deuteron is slower in PFL with 1:1 PFL-AE than that in PFL with only 0.1 and 0.01 equivalents of PFL-AE, supporting our hypothesis that interaction with PFL-AE pulled the glycine loop away from its position in the active site of PFL.

The EPR signal change of PFL diluted in 3 volumes of D_2O was more significant than the PFL diluted in 1 equivalent volume of D_2O, due to the greater extent of H/D exchange in the former case.

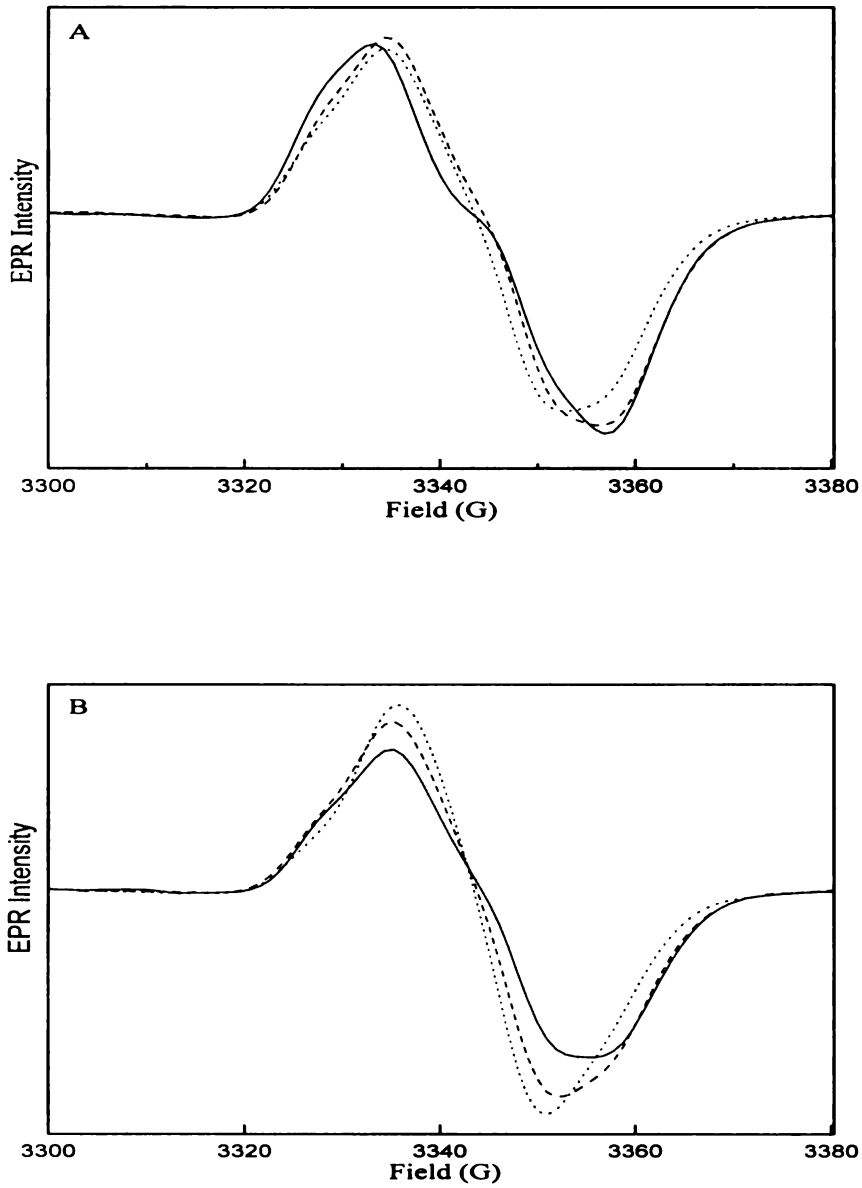

Figure V.6: EPR spectra of PFL activated with PFL-AE and then mixed with D_2O. In both A and B, the solid line is 100 μM PFL activated by 100 μM PFL-AE for 30 min; dashed line is 100 μM PFL activated by 10 μM PFL-AE for 2 h; dotted line is 100 μM PFL activated by 1 μM PFL-AE for 2 h. The PFL activation mix contained 100 mM Tris-HCl pH 7.6, 100 mM KCl, 500 μM AdoMet, 100 μM 5-deazariboflavin, 10 mM oxamate, and 10 mM DTT. A. D_2O buffer (150 μL, 100 mM Tris/HCl pD 8.2) was added into 150 μL of 100 μM activated PFL B. The D_2O buffer (225 μL, 100 mM Tris/HCl pD 8.2) was added into 75 μL of 100 μM activated PFL. EPR condition: T = 60 K, microwave frequency 9.37 GHz, power 19 μW, modulation amplitude 5 G, scan twice.

V.3.3 PFL activity assay

In order to further examine our hypothesis that the position of the glycine loop changes when PFL interacts with PFL-AE, the activity of PFL activated with 1, 0.1 or 0.01 equivalents of PFL-AE was investigated. It has been shown that Cys-418 and Cys-419, both on another loop separated from the glycine loop, are required for PFL catalysis.[8, 18, 21] It has been proposed that the bond cleavage of pyruvate is initiated by a thiyl radical on one of the cysteines, transferred from the glycyl radical. If the glycine loop is pulled out of the core of PFL structure during the interaction with PFL-AE, the contact between Gly-734 and Cys-419 (remaining in its position in the PFL active site) will be lost, and the thiyl radical will not be generated. Therefore, in PFL activated with higher ratio of PFL-AE, there might be less thiyl radical transfer to the Cys-419, and PFL would have less activity accordingly. The experiments were designed such as to obtain maximal PFL activation for each PFL to PFL-AE ratio. Thus 100 μM PFL was activated with 100 μM PFL-AE for 30 min, and in the two other samples 100 μM PFL was activated with either 10 μM or 1 μM PFL-AE for 2 h. The spin quantifications of the glycyl radicals in the activated PFL were 98 (PFL:PFL-AE 1:1), 105 (PFL:PFL-AE 10:1) and 102 μM (PFL:PFL-AE 100:1). The specific activities of the three PFL samples were 6.6 (PFL:PFL-AE 1:1), 21.7 (PFL:PFL-AE 10:1), and 22.6 (PFL:PFL-AE 100:1) U/nmol PFL (1U = 1 μmol pyruvate turnover/min) respectively (Table V.4). Although the samples have similar quantities of glycyl radical, the activity of PFL activated with 1 equivalent of PFL-AE, is only approximately 30% of the that observed for other two PFL samples activated with 0.1 and 0.01 equivalents of PFL-AE. The data are consistent with our hypothesis that more interaction between PFL and PFL-AE results in a greater

population of the PFL molecules having the glycine loop in the exposed position, which reduces the contact between Gly-734 and Cys-419, generates less thiyl radical, and results in less PFL activity.

PFL:PFL-AE	Illumination (min)	[Gly·] (μM)	Activity (U/nmol PFL)
1:1	30	98	6.6
10:1	120	105	21.7
100:1	120	102	22.6

Tabel V.4: Activities of 100 μM PFL that was completely activated by 100, 10, and 1 μM of PFL-AE, 500 μM AdoMet, and 100 μM 5-deazariboflavin in the buffer containing 100 mM Tris/HCl pH 7.6, 100 mM KCl, 10 mM oxamate, and 10 mM DTT.

V.3.4 CD spectra of PFL activated with different amounts of PFL-AE

To provide more evidence for the position change of PFL glycine loop during interaction with PFL-AE, circular dichroism (CD) spectroscopy, a technique providing information on g the secondary structures of proteins, [22] was used. The movement of Gly-734, from the center of PFL into the active site of PFL-AE, requires a conformational change of PFL, which might be observed in CD. Fig V.7 shows the CD spectra of PFL in the activation mix with no PFL-AE in present, and PFL activated with 0.01 to 2 equivalents of PFL-AE (from bottom to top). Each spectrum is the result of taking the spectrum of activated PFL with PFL-AE subtracted by the activation mix background (no PFL in present) spectrum. The intensity of the negative peak at 209 nm, one of the indicators of α-helical structure, [22] consecutively decreases as the amount of PFL-AE increases. We were unable to obtain CD signal below 200 nm, the spectral region which

contains another α-helix indicator. The reason could be that the absorption from either DTT, AdoMet, or 5-deazariboflavin saturated the detector.

The CD spectra demonstrated that PFL lost some of its α-helical structure during interaction with PFL-AE. More PFL-AE might promote conversion of PFL to an open .conformation with the Gly loop removed from the PFL core, and thus results in change of PFL secondary structure as observed in the CD spectra.

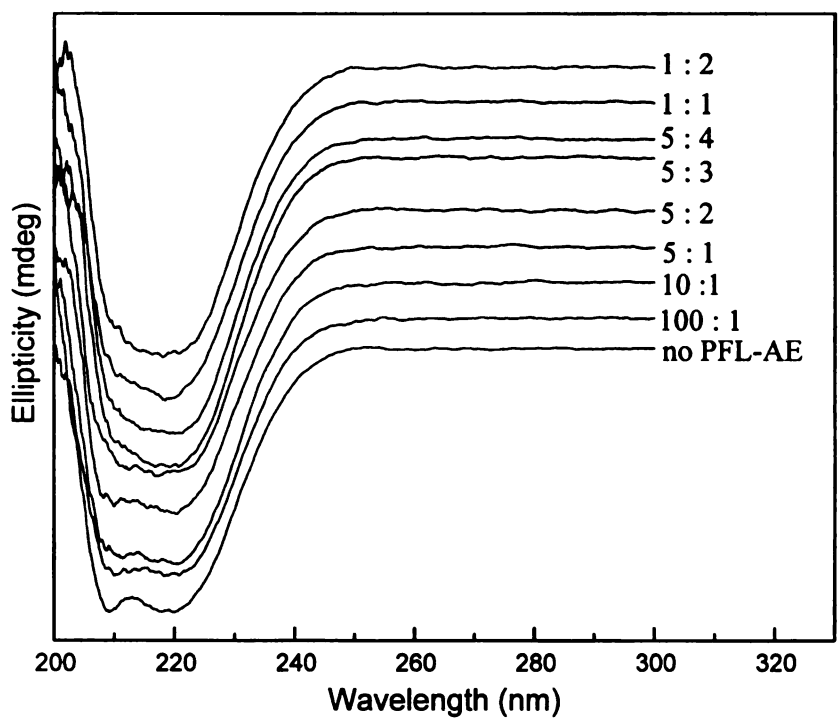

Figure V.7: CD spectra of 50 μM PFL activated by 0.5, 5, 10, 20, 30, 40, 50,100 μM of PFL-AE, 500 μM AdoMet, and 100 μM 5-deazariboflavin in the buffer containing 100 mM Tris-HCl pH 7.6, 100 mM KCl, 10 mM oxamate, and 10 mM DTT for 2 h. Each line was made from the spectrum of PFL (3mg/mL) in activation mix subtracted by the background of the same activation mix in the absence of PFL. The ratios are between PFL and PFL-AE. CD parameters: wavelength range 170 – 300 nm, scan speed 50 nm/min, data pitch 0.1 nm, band width 0.5 nm, 4 scans accumulated.

V.3.5 PFL structure analysis

The PFL crystal structure in the protein data bank (1H16) was used to analyze which parts of PFL might change in conformation to move Gly-734 out from and back to the core of PFL. Residues 710-759 comprise a domain of PFL containing the Gly loop as well as 2 helixes before and after the loop; the sequence of this domain is highly homologous to YfiD, a 14 kDa enzyme in *E. coli* that is able to resecue PFL activity after PFL is damaged by O_2. [23] Pymol and ViewerLite software were used to generate the structural images for analysis (Fig V.8). There are several interesting H-bonds in the domain. The H-bonds I751-R712 (6.9 Å between α-carbons) and N740-P722 (7.4 Å between α-carbons) hold the helices before and after the glycine loop nearly parallel. Ile-751 also communicates with Pro-722 through H-bonds I751-Q747-F739-N740-P722, which connects the two helixes and one end of the glycine loop (F739). Another route for helix communication with the loop is via H-bonds R753-V732-Y735, in which the distance between Arg-753 and Val-732 α-carbons is 9.9 Å. The structure of the glycine loop is maintained by four H-bonds, V732-Y735, I730=V737, and F739-L728, which put Gly-734 at the tip of the loop pointing to Cys-418 and Cys-419. All these residues are conserved in PFL from different organisms as well as in *E. coli* YfiD (Fig V.9). [23, 24] We propose that this C-terminal region might be the "switch" to turn on the activation process. The movement might transfer the signal to the two helixes, which are then straighter, and flip over to expose the glycine loop. Meanwhile, the change of the helixes could be passed to the glycine loop by the H-bond chains starting from Arg-753 and Ile-751. The loop might be pulled out by the two H-bond chains, and lose its structure if the

4 H-bonds, holding the loop structure, are broken in the interaction between PFL and PFL-AE.

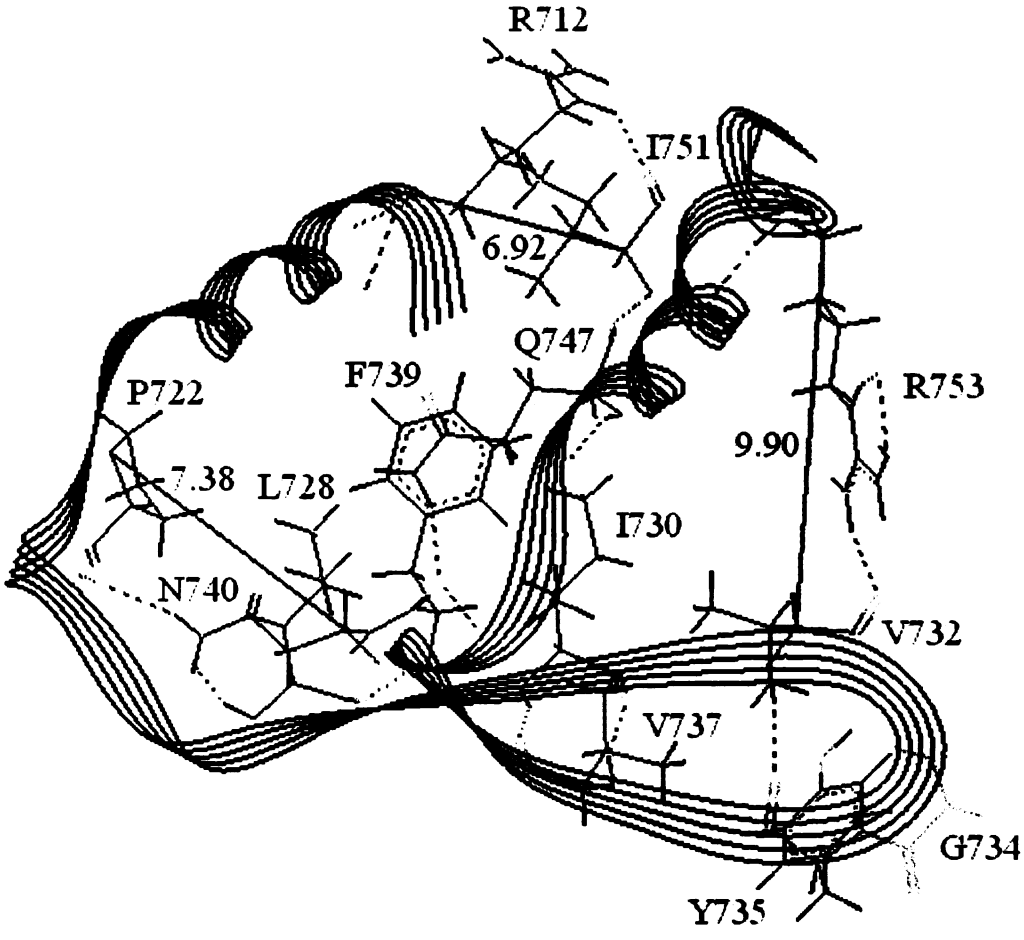

Figure V.8: Structure of PFL active site taken from PFL crystal structure (PDB 1H16). Dashed lines are hydrogen bonds. Solid lines are distances between α–carbons.

	R712	P722	L728	V732	F739	Q747	I751
EcPFL	NREMLLDAMENPEKYPQLTIRVSGYAVRFNSLTKQQQDVITRTFTQSM						
CPFL	R----------P---------L----RV----Y------F---------Q---------I--R						
AfPFL2	R----------P---------L---RV----5------5----------Q---------I--R						
CCPFL	R----------P---------6---R6-----Y-----F----------Q---------I--R						
EcYfiD	R----------P---------L---RV-----Y-----F----------Q---------I--R						

Figure V.9: Sequence conservations of the C-terminal region in PFL from different organisms and *E. coli* YfiD. The residues are numbered according to the *E. coli* PFL sequence.

The position of the C-terminus appears to be fixed tightly in the absence of PFL-AE. The C-terminus is inserted between two helixes from Gly-630 to Asp-690 (Fig V.10), which hold the C-terminal region by five H-bonds, M759-V645, S758-A644, T756-V670, T756-S668, and T754-D640. Binding of PFL-AE might break these H-bonds to release the C-terminus and trigger the conformational change.

The two helixes before and after the glycine loop are on top of Gly-734 in the PFL structure. To move the loop out of the protein, these two helices have to undergo a significant structure change, as proposed previously. The sequence 700 – 709 (before the helixes) and the sequence 750 – 759 (after the helixes) do not have real structure, but their positions are tightly held by other two helixes (4 H-bonds E700-A657, E700-F656, N706-Y665, and N706-F667 to fix the residues 700 – 710). The lack of secondary structure in these two sequences could make the conformational change of the glycine loop region easier. The hydrogen bonds between the sequences and other parts of the protein might help to lock the correct position of the glycine loop after activation.

Our proposal is that the PFL activation process might be triggered by PFL-AE binding, which could cause structural change in the C-terminal region, thus signaling the conformational change of the helixes. The structural change could pull the glycine loop out from PFL and render it accessible to the PFL-AE active site to generate the glycyl radical. After activation, Gly-734 is re-buried in the PFL core, and the hydrogen bonds between the two sequences (700 – 710 and 754 – 759) and other parts of the protein might help PFL return to its activated structure.

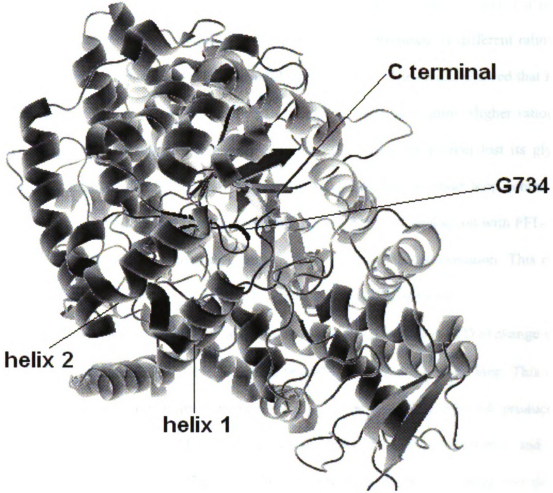

Figure V.10: Crystal structure of PFL (PDB 1H16). Gly-734 is black and at the center of PFL. Helix 1 is the structure after the glycine loop, and helix 2 is the structure before the loop. The C-terminal is inserted into two other helixes.

V.4 Conclusions

The investigation reported in this chapter grew from the unexpected observation that 100 μM PFL had 100 μM glycyl radical (from EPR spin quanitificaiton) when it was activated with 1 equivalent of PFL-AE for 30 min, and activated with 0.1 or 0.01 equivalents of PFL-AE for 2 h, whereas 100 μM PFL only had 30 μM glycyl radical if it

was activated with 1 equivalent of PFL-AE for 2 h. This unexpected result led us to examine in determine the quantification of glycyl radical produced by different ratios of PFL-AE to PFL when activated for varying lengths of time.. The results showed that PFL could be fully activated low ratios of PFL-AE during a 2 h activation. Higher ratios of PFL-AE to PFL resulted in more rapid activation, however the protein lost its glycyl radical during extended incubation. These results implied that the short loop containing Gly-734 might be pulled out from the core of PFL as a result of interaction with PFL-AE, and more PFL-AE would mean that more PFL is in this open conformation. This open conformation would lead glycyl radical being quenched by the solution.

The α-hydrogen on glycyl radical in activated PFL undergoes H/D exchange with solvent D_2O via Cys-419, [16] which is on an opposing loop to the glycine loop. This H/D exchange was used to examine the hypothesis that interaction with PFL-AE produces a more open conformation of PFL in which the Gly-734 is not in the core of PFL, and thus not in contact with Cys-419. The results demonstrated that the H/D exchange was slower in PFL with 1 equivalent of PFL-AE than that in PFL with 0.1 and 0.01 equivalents. PFL catalysis also requires interaction between Gly-734 and two cysteines Cys-418 and Cys-419; [6, 16, 19] we thus used PFL activity assays to further probe the position of the glycine loop during the interaction between PFL and PFL-AE. The activity of 100 μM PFL completely activated with 100 μM PFL-AE was only 1/3 of 100 μM PFL fully activated with 10 μM and 1 μM PFL-AE. These results support the hypothesis that Gly-734 in PFL is in an alternate more open position during interaction with PFL-AE, but less interaction with the cysteines, and thus less activity.

In order for the glycine loop to move out of the core of PFL, PFL has to undergo a conformational change; CD spectroscopy has provided evidence for such a change. The CD spectra demonstrated that more helical structure is lost in PFL upon interaction with more PFL-AE. Inspection of the PFL crystal structure provides support for the idea that the two α–helixes before and after the glycine loop might change in structure to pull Gly-734 out for activation. These two helixes could also be the site for binding to PFL-AE, and the movement of the PFL C-terminus might trigger a PFL conformational change through several H-bonds.

References:

1. Knappe, J.; Neugebauer, F. A.; Blaschkowski, H. P.; Gaenzler, M., *Proceedings of the National Academy of Sciences of the United States of America* **1984,** 81, (5), 1332-5.

2. Unkrig, V.; Neugebauer, F. A.; Knappe, J., *European Journal of Biochemistry* **1989,** 184, (3), 723-8.

3. Wagner, A. F. V.; Frey, M.; Neugebauer, F. A.; Schaefer, W.; Knappe, J., *Proceedings of the National Academy of Sciences of the United States of America* **1992,** 89, (3), 996-1000.

4. Roedel, W.; Plaga, W.; Frank, R.; Knappe, J., *European Journal of Biochemistry* **1988,** 177, (1), 153-8.

5. Wagner, A. F. V.; Demand, J.; Schilling, G.; Pils, T.; Knappe, J., *Biochemical and Biophysical Research Communications* **1999,** 254, (2), 306-310.

6. Henshaw, T. F.; Cheek, J.; Broderick, J. B., *Journal of the American Chemical Society* **2000,** 122, (34), 8331-8332.

7. Magnusson, O. T., Reed, G. H., Frey, P. A., *J Am Chem Soc* **1999,** 121, 9764-9765.

8. Becker, A.; Fritz-Wolf, K.; Kabsch, W.; Knappe, J.; Schultz, S.; Wagner, A. F. V., *Nature Structural Biology* **1999,** 6, (10), 969-975.

9. Becker, A.; Kabsch, W., *Journal of Biological Chemistry* **2002,** 277, (42), 40036-40042.

10. Lehtioe, L.; Leppaenen, V. M.; Kozarich, J. W.; Goldman, A., *Acta Crystallographica, Section D: Biological Crystallography* **2002,** D58, (12), 2209-2212.

11. Uhlin, U.; Eklund, H., *Nature* **1994,** 370, (6490), 533-9.

12. Eklund, H.; Uhlin, U.; Farnegardh, M.; Logan, D. T.; Nordlund, P., *Prog Biophys Mol Biol* **2001,** 77, (3), 177-268.

13. Stubbe, J.; Nocera, D. G.; Yee, C. S.; Chang, M. C., *Chem Rev* **2003,** 103, (6), 2167-201.

14. Frey, M.; Rothe, M.; Wagner, A. F. V.; Knappe, J., *Journal of Biological Chemistry* **1994,** 269, (17), 12432-7.

15. Aasa, R.; Vanngard, T., *J Magn. Reson* **1969,** 19, (3), 308-15.

16. Knappe, J.; Blaschkowski, H. P.; Groebner, P.; Schmitt, T., *European Journal of Biochemistry* **1974,** 50, (1), 253-63.

17. Knappe, J.; Elbert, S.; Frey, M.; Wagner, A. F. V., *Biochemical Society Transactions* **1993,** 21, (3), 731-4.

18. Parast, C. V.; Wong, K. K.; Lewisch, S. A.; Kozarich, J. W.; Peisach, J.; Magliozzo, R. S., *Biochemistry* **1995,** 34, (8), 2393-9.

19. Parast, C. V. Mechanistic studies of pyruvate formate-lyase: evidence for a catalytic radical interchange between Gly 734, Cys 419 and Cys 418. 1996.

20. Plaga, W.; Frank, R.; Knappe, J., *European Journal of Biochemistry* **1988,** 178, (2), 445-50.

21. Plaga, W.; Vielhaber, G.; Wallach, J.; Knappe, J., *FEBS Letters* **2000,** 466, (1), 45-48.

22. Greenfield, N. J., *Methods Mol Biol* **2004,** 261, 55-78.

23. Wagner, A. F. V.; Schultz, S.; Bomke, J.; Pils, T.; Lehmann, W. D.; Knappe, J., *Biochemical and Biophysical Research Communications* **2001,** 285, (2), 456-462.

24. Lehtioe, L.; Goldman, A., *Protein Engineering, Design & Selection* **2004,** 17, (6), 545-552.

CHAPTER VI

INVESTIGATIONS OF THE PYRUVATE FORMATE-LYASE CATALYTIC MECHANISM

VI.1 Introduction

PFL catalyzes the reversible conversion of pyruvate and CoA into formate and acetyl-CoA. [1] The mechanism proceeds via a radical route, in which a glycyl radical on Gly-734 initiates the reaction. [2, 3] Several lines of evidence combine to implicate two cysteines, Cys-418 and Cys-419, as catalytic residues. Inactivation of PFL by hypophosphite, an analogue of pyruvate, results in a 1-hydroxyethyl phosphate covalently bound to Cys-418. [4] Two PFL mutants, C418S-PFL and C419S-PFL, exhibit normal glycyl radical signals, but no activity. [5] Cys-419 is also essential for the glycyl radical H/D exchange in D_2O. [6] Therefore, Cys-418 and Cys-419 were suggested to be involved in PFL catalysis.

Based on the crystal structure and other studies of PFL, two mechanisms have been proposed by different research groups (scheme VI.1). [7-10] Both mechanisms involve an initial glycyl radical that abstracts a hydrogen from Cys-419 to generate a thiyl radical. The Kozarich mechanism proposes that this thiyl radical attacks the carbonyl carbon in pyruvate, causing the C-C bond to be broken. The acetyl group thereafter attaches to Cys-419, and the formate radical abstracts a hydrogen atom from Gly-734. The acetyl group is then transferred to Cys-418. After formate leaves the active site, the thiol end of CoA comes in and takes the acetyl group from Cys-418. Acetyl-CoA, the second product,

leaves the protein and PFL remains in the active form. In the Knappe mechanism, the thiyl radical on Cys-419 is transferred to Cys-418 to yield another thiyl radical, which then attacks pyruvate. The substrate is cleaved and the protein is acetylated directly on Cys-418. After that, the reaction follows the same route as the Kozarich mechanism. The difference between the two proposals is the role Cys-419 that plays in the mechanism, whether it is a residue to initiate pyruvate cleavage (Kozarich mechanism) or just a radical shuttle (Knappe mechanism).

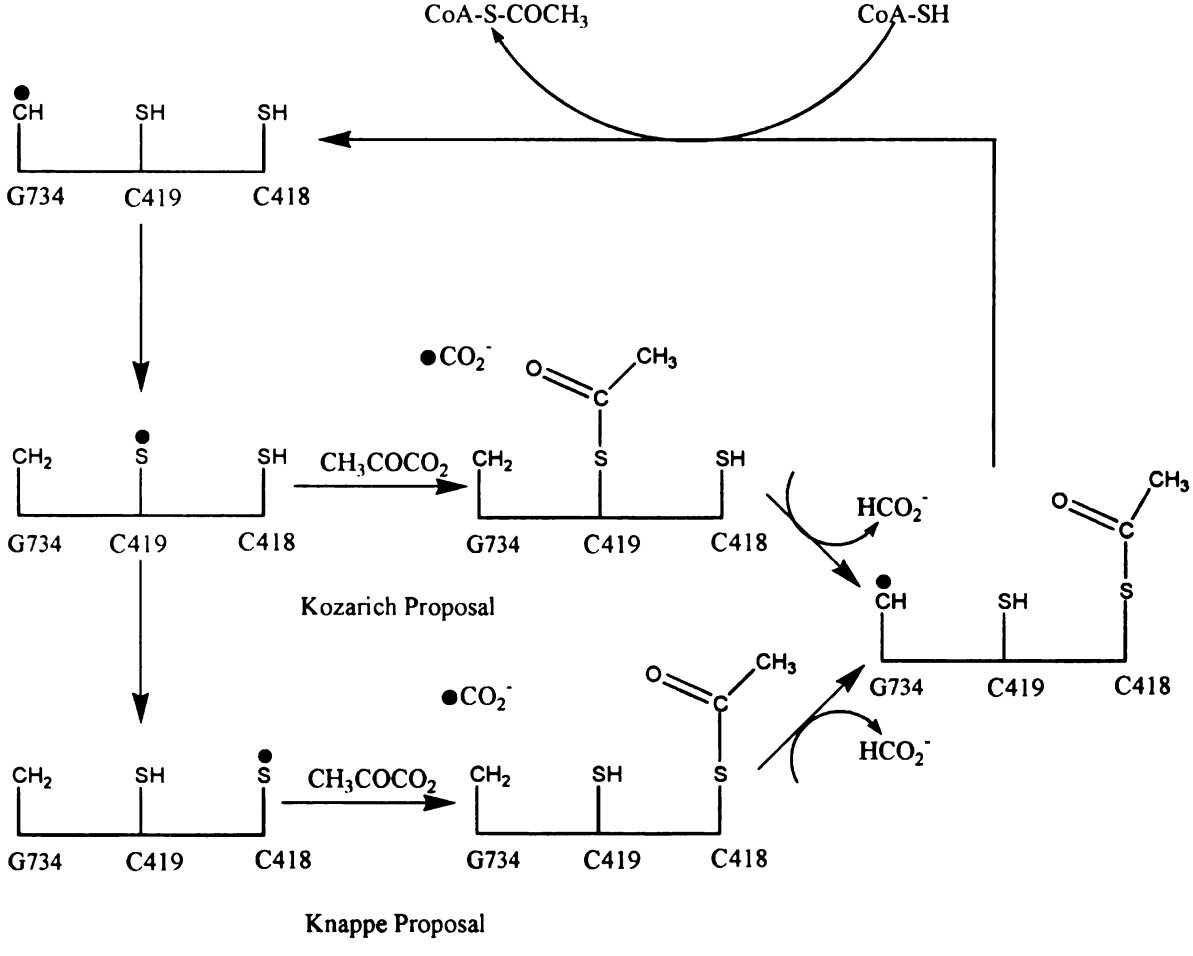

Scheme VI.1: Schematic representation of the PFL catalytic mechanism. Kozarich proposed that Cys 419 attacks the substrate, while Knappe proposed that Cys 418 initiated the first step.

The structure of PFL is similar to the subunit 1 of class I ribonucleotide reductase (RNR), which also uses a thiyl radical to initiate the reaction. [11] However, the first step in class I RNR is that the thiyl radical abstracts a 3'-hydrogen from the nucleotide. [12] This led us to question whether PFL catalysis might also involve a hydrogen abstraction from the methyl group in pyruvate, rather than a nucleophilic attack by a thiyl radical (scheme VI.2).

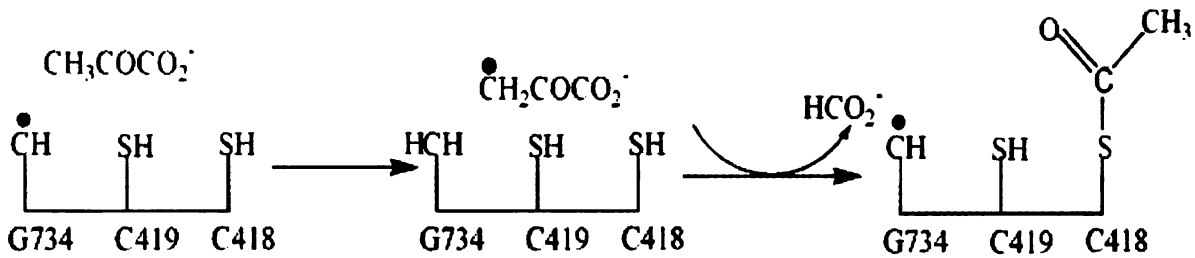

Scheme VI.2: Schematic representation of proposed PFL mechanism initiating with one hydrogen abstraction.

We have used a deuterium labeled substrate, 3,3,3-d_3-pyruvate to investigate the possibility of H atom abstraction PFL catalysis. The reaction rate of PFL with this substrate was compared with the rate of natural abundance pyruvate. The molecular weight of the acetyl-CoA produced from the labeled pyruvate during the PFL enzymatic reaction was determined by using mass spectrometry. To inspect which cysteine triggers the reaction, the radical signals of two activated PFL mutants C418A-PFL and C419A-PFL in H_2O and D_2O were measured by EPR.

VI.2 Materials and methods

VI.2.1 Chemicals and materials

All chemicals were of the highest quality commercially available except as noted otherwise. Overexpression and purification of PFL and PFL-AE were carried out following the procedures in chapter II. Protein and iron assays were conducted as described in chapter II.

VI.2.2 Synthesis of sodium 3,3,3-d_3-pyruvate

Ethyl pyruvate-3,3,3-d_3 was purchased from C/D/N isotopes INC. Sodium 3,3,3-$d_3$pyruvate was made from ethyl pyruvate-3,3,3-d_3 according to a Japanese patent. [13] Ethyl pyruvate-3,3,3-d_3 (0.3006 g) was dissolved in 100 mL H_2O to make a 25 mM solution. The solution was vigorously stirred in a 500 mL flask. NaOH (100 mL, 25 mM) was added drop wise into the solution to maintain the pH at 6 to 8, at room temperature. After the NaOH addition was complete, the reaction was further stirred for another 1 h. The solvent was removed under reduced pressure. The sodium 3,3,3-d_3-pyruvate was crystallized by addition of excess isopropanol. The solid was flitered and washed with isopropanol (3 x 50 mL). The yield was 0.2482 g (87.1%). When dissolved in D_2O (10 mg per 800 μL D_2O), no hydrogen peak was detected in ^{1}H-NMR. The solid was stored at 4 °C.

VI.2.3 PFL activity assay

All procedures were carried out under strictly anaerobic condition in the glove box (Mbraun). PFL activation mix (500 μL) contained 100 mM Tris-HCl pH 7.6, 100

mM KCl, 8 mM DTT, 10 mM oxamate, 0.2 mM AdoMet, 50 μM 5-deazariboflavin, 1.5 μM PFL, and 0.015 μM PFL-AE. 5-Deazariboflavin was added last in the dark, and the reaction was initiated via ambient light illumination, for 10 to 70 minutes. The mixture was then wrapped with aluminum foil after each illumination time and 10μL of solution was taken out for the PFL activity assay, and added to 790 μL of coupling enzyme mix described in Chapter V. The PFL activity was tested following the procedure described previously in Chapter V. The activity assay of activated PFL with 3,3,3-d_3-pyruvate was carried out following the same procedure except that the coupling enzyme mix contained 10 mM 3,3,3-d_3-pyruvate instead of natural abundance pyruvate.

VI.2.4 PFL reaction with 3,3,3-d_3-pyruvate

All procedures were carried out under strictly anaerobic conditions in the glove box (Mbraun). The enzyme reaction mix (500 μL) was prepared, containing 100 mM Tris-HCl pH 7.6, 100 mM KCl, 8 mM DTT, 10 mM sodium 3,3,3-d_3-pyruvate, 0.5 mM CoA tri-lithium salt, 2 mM AdoMet, 50 μM 5-Deazariboflavin, 6 μM PFL, and 0.06 μM PFL-AE. The solution was illuminated by ambient light for 2 hours and then moved out of the anaerobic chamber. It was exposed to air for 5 minutes on ice bath, shocked at 87°C for 30 seconds, and centrifuged at 12,000 rpm for 1 min, in order to cleave activated PFL, denature the fragments and release the product. The clear solution was stored at –80 °C for mass spectrometry

VI.2.5 Mass spectrometry measurement of acetyl-CoA from PFL enzyme reaction

The mass spectra were recorded on a linear quadrupole ion trap mass spectrometer (model LTQ, Thermo, San Jose, CA), equipped with a nanospray ionization (nanoESI) source. Samples were introduced to the mass spectrometer at an infusion flow rate of 0.2 μL/min. The nanoESI conditions were optimized to maximize the intensity of the ion of interest and to minimize the extent of in-source fragmentation. Spectra were acquired in a negative ionization mode. MS conditions were: spray voltage 1.5 kV, heated capillary temperature 200°C, capillary voltage –20 V, and tube lens voltage –75 V. MS/MS spectra of singly and doubly deprotonated precursor ions were acquired on monoisotopically isolated ions using standard isolation and excitation procedures.

VI.2.6 H/D exchange in mutants after reaction with pyruvate

All procedures were carried out under strictly anaerobic conditions in a glove box (Mbraun). C418A-PFL and C419A-PFL were provided by Jian Yang. The activation mix (200 μL), containing 100 mM Tris-HCl pH 7.6, 100 mM KCl, 200 μM PFL, 200 μM PFL-AE, 200 μM 5-deazariboflavin, 500 μM AdoMet, 10 mM DTT and 10 mM oxamate, was illuminated by a 500 W halogen light for 30 min in EPR tubes inserted in an ice/water bath (4 °C). After illumination, 200 μM pyruvate (final concentration) was added into each sample, which was then incubated for 10 min at room temperature. The samples were split in half, and 300 μL of H_2O or D_2O (75% D_2O final concentration) was added into the samples, followed by incubation for 2 min at room temperature. The samples were flash frozen in liquid N_2 in the glove box for EPR.

VI.2.7 EPR spectroscopy

EPR spectra were recorded in a Bruker ER-200D-SRC spectrometer at 60 K. X-band microwave frequency 9.37 GHz was used. The microwave power was 19 μW. The external magnetic field was scanned from 3000 to 4000 G. The static field was 1000 G. The modulation frequency was 100 kHz, and modulation amplitude was 5 G. The resolution was 1024.

VI.3 Results and discussion

VI.3.1 PFL activity assay of sodium pyruvate and sodium 3,3,3-d_3-pyruvate

In order to investigate the possibility of hydrogen atom abstraction as a key step of PFL catalysis, the H/D isotope effect of 3,3,3-d_3-pyruvate in PFL activity was determined. The turnover rates of sodium pyruvate and sodium 3,3,3-d_3-pyruvate in PFL catalysis are provided in Table VI.1. The average H/D isotope effect on the turnover rate was 1.1. The primary isotope effect (k_H/k_D) of a hydrogen abstraction reaction, which involves carbon-hydrogen bond breaking, usually has a value of 6 or even higher. [14] For example, the H/D isotope effect was found to be 7.4 in ethanolamine deaminase, an enzyme that utilizes a 5'-deoxyadenosyl radical generated from cobalamine coenzyme to abstract a hydrogen atom from ethanolamine. [15, 16] The small isotope effect observed for 3,3,3-d_3-pyruvate tells us that C-H bond cleavage does not contribute to the rate-determine step of the reaction. It is therefore most likely that hydrogen abstraction is not a step in pyruvate cleavage by PFL. The small isotope effect observed is in fact consistent

with a secondary H/D isotope effect, suggesting that the C-H bond cleavage is not involved in the mechanism.

Illumination Time (min)	μmol PYR[a]/min	μmol d_3-PYR[b]/min	PYR/d_3-PYR
10	0. 0019	0. 0016	1. 2
15	0. 052	0. 046	1. 1
20	0. 083	0. 080	1. 1
25	0. 11	0. 097	1. 1
35	0. 13	0. 10	1. 2
40	0. 14	0. 13	1. 1
50	0. 18	0. 15	1. 2
60	0. 19	0. 18	1. 1
70	0. 21	0. 18	1. 2
Average			1. 1

Table VI.1: Turnover rates of sodium pyruvate and 3,3,3-d_3-pyruvate in PFL enzymatic reaction for various illumination times. [a] Sodium pyruvate. [b] Sodium 3,3,3-d_3-pyruvate.

VI.3.2 Mass spectra of reaction products

To further investigate whether hydrogen abstraction from pyruvate is a step in PFL catalysis, mass spectra of the products from the PFL reaction with 3,3,3-d_3-pyruvate and CoA as substrates were acquired. If the radical form of PFL abstracts a deuteron from 3,3,3-d_3-pyruvate, the pyruvate radical might subsequently abstract a hydrogen from Gly-734, Cys-418 or Cys-419, or even from the solvent. Therefore, the product would have 1 dalton less than the d_3-acetyl-CoA. The MS study indicated that one of the products after a 2 h reaction PFL enzymatic reaction was 2',2',2'-d_3-acetyl-CoA, with a molecular mass of 811 ($[M-H]^-$, Fig VI.1.A). Fragmentations of the deprotonated molecule are shown in Fig VI.2.A. The mass of the fragments match the predicted degradation of 2',2',2'-d_3-acetyl-CoA (Fig VI.2.B). The results show that 2',2',2'-d_3-acetyl-CoA was produced from 3,3,3-d_3-pyruvate and CoA, with all three deuterium labels remaining in the product. No peak with one mass unit smaller than the molecule ion was detected (Fig VI.1.B),

providing no evidence for replacement of D by H of the final product. The results corroborate the isotope effect studies and further support the proposal that hydrogen atom abstraction is not a step in the PFL-catalyzed reaction.

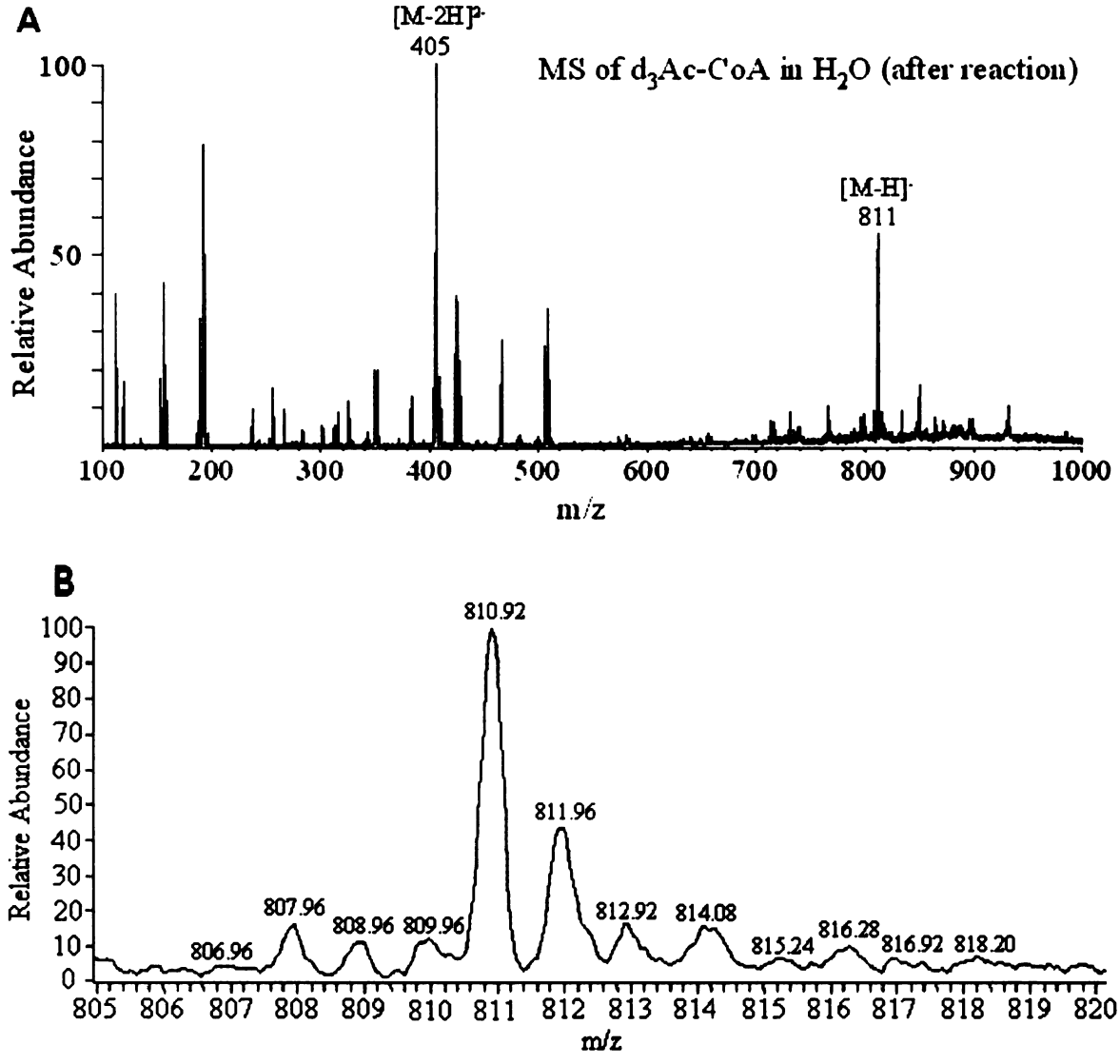

Figure VI.1: Electrospray mass spectra of 2',2',2'-d_3-acetyl-CoA after 2 hour reaction. A: Negative mode mass spectrum of 2',2',2'-d_3-acetyl-CoA itself, $[M-H]^-$ at m/z 811 and $[M-2H]^{2-}$ at m/z 405. B: Expanded m/z scale around $[M-H]^-$ peak. The intensity of the peak at m/z 809.96, 1 mass unit less than the $[M-H]^-$, was no more than intensity expected from the natural isotope distribution.

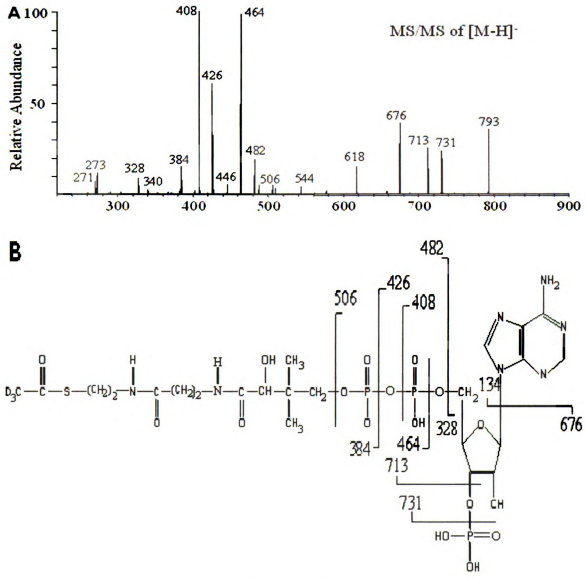

Figure VI.2: Fragmentations of 2',2',2'-d_3-acetyl-CoA. A: MS/MS fragmentations of the deprotonated molecule $[M-H]^-$. B: Structure of 2',2',2'-d_3-acetyl-CoA. How bond cleavage leading to observed fragments during CAD-MS/MS.

VI.3.3 Activity assay of C418A-PFL and C419A-PFL

To examine which cysteine residue, Cys-419 or Cys-418, initiates the reaction, two PFL mutants, C418A-PFL and C419A-PFL, were prepared, and their activities were tested to confirm the requirement of these two residues in PFL catalysis. Wild-type PFL, C418A-PFL and C419A-PFL were activated for the same amount of time as described in

Materials and Methods. The resulting activities of the enzymes are provided in Table VI.2. The activities of the two mutants are only approximately 1 – 2% of the wild type PFL. The radical on Gly-734 has been proposed to transfer to Cys-419 to generate a thiyl radical. [6] A mutation from cysteine to alanine would stop this radical transport, so the mutant would not be expected to have activity. Cys-418 has been proposed as the position for acetylation in the acetylated PFL intermediate, with CoA picking up the acetyl group from this residue. [6, 9, 10] An alanine instead of a cysteine at this position would prevent the acetylation of the enzyme and thereby prevent turnover. The small amount of activity remaining in the two mutants likely comes from wild type PFL contamination. The PFL gene in the host cells was not knocked out, so a small amount of wild-type PFL from *E. coli* cells would still be produced during the growth of the two mutants. The purification is not able to separate the wild type PFL from C418A-PFL and C419A-PFL.

Illumination Time (min)	**Wild PFL (μmol PYR/min)**	**C418A-PFL (μmol PYR/min)**	**C419A-PFL (μmol PYR/min)**
30	0. 16	0. 0010	0. 0024
40	0. 15	0. 0012	0. 0027
50	0. 17	0. 0013	0. 0033

Table VI.2: Activity assay of wild type PFL, C418A-PFL and C419A-PFL. The enzyme was activated by photoreducing PFL-AE for 30, 40, 50 minutes. The activity of the enzyme was represented by the turnover rate of pyruvate (μmol/min).

VI.3.4 H/D exchange of PFL and PFL mutants after reaction with pyruvate

A free Cys-419 has been shown to be required for H/D exchange. [6] A mechanism has been proposed in which the α-hydrogen on the glycyl radical is exchanged with the solvent deuterium via the labile thiol hydrogen on Cys-419. [6] We have used H/D exchange in C419A-PFL and C418A-PFL to investigate which cysteine residue initiates

the reaction. If Cys-419 performs the initial attack on pyruvate, as proposed in the Kozarich mechanism (Scheme VI.1), then Cys-419 would be acetylated upon reaction with pyruvate. In the case of the C418A-PFL mutant, this initial reaction should still occur, and the acetyl moiety should occupy Cys-419 since it could not be transferred to Cys-418. In this mutant, therefore, Cys-419 would not undergo H/D exchange once it had reacted with pyruvate. On the other hand, if the thiyl radical on Cys-418 performs the initial attack on pyruvate, as proposed in the Knappe mechanism, then neither Cys-418 nor Cys-419 should be acetylated and the C418A-PFL should exhibit a singlet EPR signal in D_2O. Our results support the mechanism put forward by Knappe. Activated wild-type PFL exhibits a doublet EPR signal in H_2O and a singlet in D_2O (Fig VI.3.A) as reported previously. [3, 6] C419A-PFL exhibits a doublet glycyl radical EPR signal in both H_2O and D_2O (Fig VI.3.B) as expected, since the cysteine was mutated to an alanine, and thus no labile hydrogen was available for H/D exchange. Fig VI.3.C shows that after reaction with, C418A-PFL has a doublet EPR signal in H_2O and has a singlet EPR signal in D_2O, indicating that Cys-419 is not acetylated and thus is able to transfer deuterium to the glycyl radical. The result suggests that the function of Cys-419 is not to attack pyruvate, but to transfer the radical to Cys-418, implying Cys-418 is likely the residue that initiates the cleavage of pyruvate.

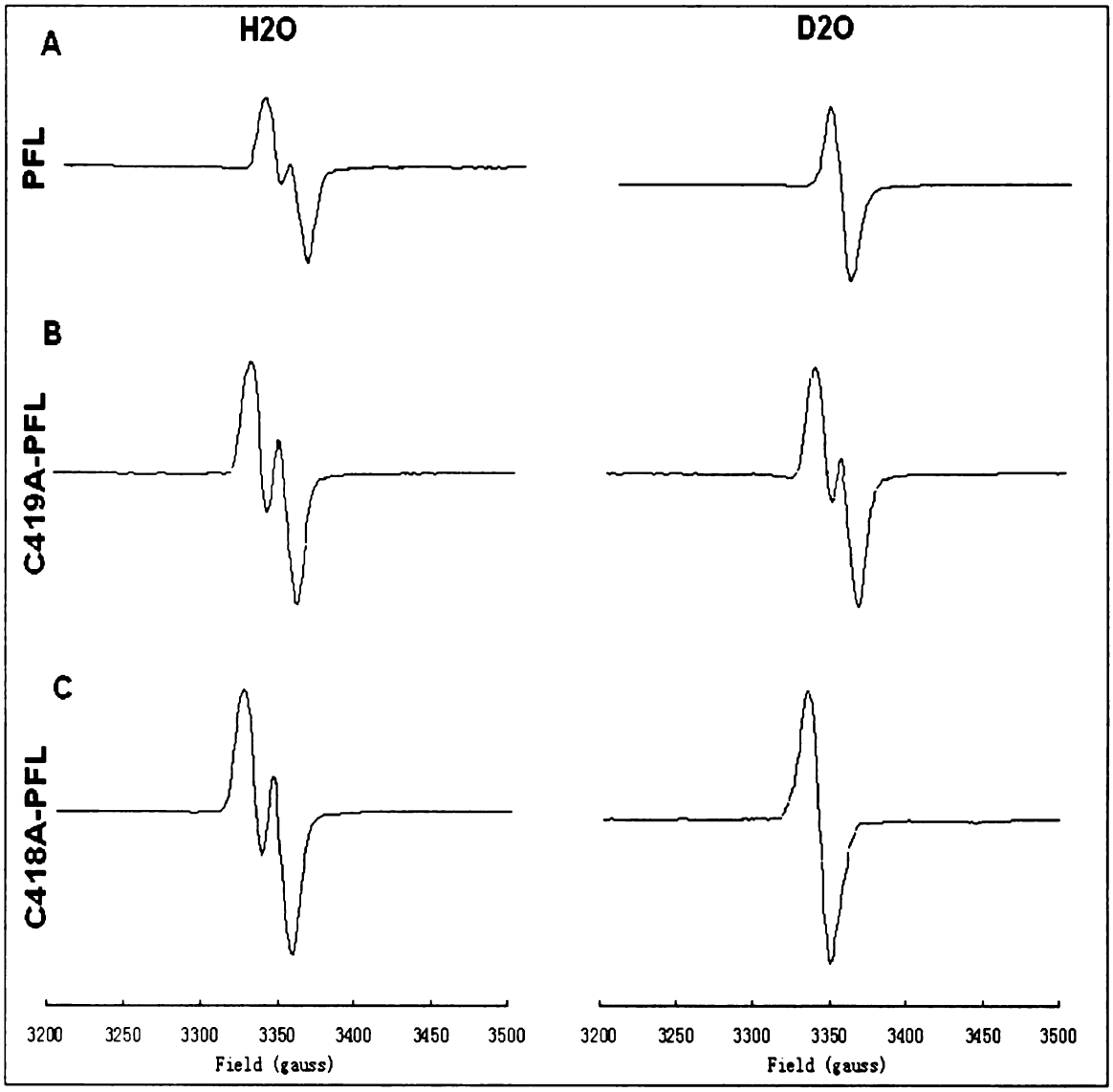

Figure VI.3: EPR spectra of PFL and PFL after reaction with pyruvate and addition of D_2O. EPR condition: T = 60 K, microwave frequency 9.37 GHz, power 19 μW, modulation amplitude 5 G, resolution 1024, scan twice. Left panel: protein in H_2O; right panel: protein in D_2O. A: activated PFL. B: activated C419A-PFL. C: activated C418A-PFL.

VI.4 Conclusions

PFL is the first enzyme that was shown to require a backbone glycyl radical to initiate catalysis. [3, 17] The radical mechanism led us to propose that the reaction might be

triggered by hydrogen abstraction from pyruvate. To investigate this possibility, a deuterium labeled substrate, 3,3,3-d_3-pyruvate was ued. The reaction rates of activated PFL with natural abundance pyruvate and deuterium labeled pyruvate as the substrates were measured, allowing us to determine an isotope effect of 1.1. This value is much smaller than a normal primary H/D isotope effect, which tells us that hydrogen atom abstraction does not contribute to the rate limiting step of the reaction. The small isotope effect is, however, consistent with a secondary isotope effect, suggesting the C-H bond broken is not involved in PFL reaction.

The product of PFL enzymatic reaction with 3,3,3-d_3-pyruvate and CoA as the substrates was examined by using mass spectrometry. The production of 2',2',2'-d_3-acetyl-CoA was confirmed by its molecular weight ($[M-H]^-$) at m/z 811, and the CAD-MS/MS fragmentations of the deprotonated molecule. If the reaction was initiated by hydrogen abstraction, there might be expected to be a D/H exchange on the final product, which would have one mass unit less than the d_3-labeled product. This was not observed in the mass spectrum of the product. This study again provided support for the idea that the reaction was not initiated via hydrogen abstraction.

Two published mechanistic proposals suggest a thiyl radical at either Cys-418 or Cys-419 attacks the carbonyl carbon in pyruvate to cleave the C-C bond. [6, 8-10] Two PFL mutants, C418A-PFL and C419A-PFL, were used to investigate these possibilities. As previously reported, [5, 7, 18] due to the essential roles of these two cysteines in catalysis, these mutants had very little enzymatic activity. [5, 7, 18] The small amount of activity is likely due to wild-type PFL contamination, which is expressed in the host *E. coli* cells and could not be separated from the mutants during purification. The small amount of

wild-type PFL would be activated in the activity assay, leading to observed activity in the mutants.

A glycyl radical could be generated on both of the mutants in the presence of reduced PFL-AE and AdoMet, and the activated mutants showed doublet EPR signals in H_2O after reacting with pyruvate as the substrate. The doublet EPR signal in wild-type PFL changes to a singlet signal in D_2O, to the solvent H/D exchange on glycyl radical mediated by Cys-419. [6] This result was re-produced in our lab, and H/D exchange in pyruvate-reacted C418A-PFL and C419A-PFL was used to investigate which cysteine residue initiates the attack on pyruvate. The activated and pyruvate-reacted C419A-PFL remained a doublet signal in D_2O, which was expected because the Cys-419 mediates the H/D exchange at Gly-734. The doublet EPR signal for activated C418A-PFL reacted with pyruvate changed to a singlet signal in D_2O, indicating that Cys-419 in this mutant was free to exchange the glycyl α-hydorgen with solvent deuterium. The results show that Cys-419 is not occupied by the acetyl group as the product from the pyruvate cleavage. These results suggest that Cys-419 in C418A-PFL does not attack pyruvate, although the mutant could be activated to generate glycyl radical. Since a thiyl radical has been proposed to initiate the pyruvate cleavage, the results imply that Cys-418 is likely the residue that initiates the first step of the reaction.

References

1. Knappe, J.; Blaschkowski, H. P.; Groebner, P.; Schmitt, T., *European Journal of Biochemistry* **1974,** 50, (1), 253-63.

2. Unkrig, V.; Neugebauer, F. A.; Knappe, J., *European Journal of Biochemistry* **1989,** 184, (3), 723-8.

3. Wagner, A. F. V.; Frey, M.; Neugebauer, F. A.; Schaefer, W.; Knappe, J., *Proceedings of the National Academy of Sciences of the United States of America* **1992,** 89, (3), 996-1000.

4. Plaga, W.; Frank, R.; Knappe, J., *European Journal of Biochemistry* **1988,** 178, (2), 445-50.

5. Knappe, J.; Elbert, S.; Frey, M.; Wagner, A. F. V., *Biochemical Society Transactions* **1993,** 21, (3), 731-4.

6. Parast, C. V.; Wong, K. K.; Lewisch, S. A.; Kozarich, J. W.; Peisach, J.; Magliozzo, R. S., *Biochemistry* **1995,** 34, (8), 2393-9.

7. Brush, E. J.; Kozarich, J. W., *Enzymes (3rd Ed.)* **1992,** 20, 317-403.

8. Lehtioe, L.; Leppaenen, V. M.; Kozarich, J. W.; Goldman, A., *Acta Crystallographica, Section D: Biological Crystallography* **2002,** D58, (12), 2209-2212.

9. Becker, A.; Fritz-Wolf, K.; Kabsch, W.; Knappe, J.; Schultz, S.; Wagner, A. F. V., *Nature Structural Biology* **1999,** 6, (10), 969-975.

10. Becker, A.; Kabsch, W., *Journal of Biological Chemistry* **2002,** 277, (42), 40036-40042.

11. Uhlin, U.; Eklund, H., *Nature* **1994,** 370, (6490), 533-9.

12. Stubbe, J.; van der Donk, W. A., *Chemical Reviews (Washington, D. C.)* **1998,** 98, (2), 705-762.

13. Synthesis of sodium pyruvate. JP 63-132856, 6/4/1988, 1988.

14. Westheimer, F. H., *Chem Rev* **1961,** 61, (3), 265-273.

15. Babior, B. M., *J Biol Chem* **1969,** 244, (2), 449-56.

16. Weisblat, D. A.; Babior, B. M., *J Biol Chem* **1971,** 246, (19), 6064-71.

17. Knappe, J.; Neugebauer, F. A.; Blaschkowski, H. P.; Gaenzler, M., *Proceedings of the National Academy of Sciences of the United States of America* **1984,** 81, (5), 1332-5.

18. Brush, E. J.; Lipsett, K. A.; Kozarich, J. W., *Biochemistry* **1988,** 27, (6), 2217-22.

CHAPTER VII

GENERAL CONCLUSIONS AND FUTURE DIRECTIONS

VII.1 The interaction between AdoMet and the iron-sulfur cluster in PFL-AE

Iron-sulfur cluster proteins have been identified in almost all types of organisms. [1] The chemical versatility of iron and sulfur makes iron-sulfur proteins great candidates for electron transfer. [2] The enzymes also play catalytic roles, both redox (e.g. nitrogenase, hydrogenase), [3, 4] and non-redox (e.g. aconitase). [5] *E. coli* Endonuclease III is an iron-sulfur cluster protein, in which the cluster appears to have neither an electron transfer nor a catalytic role. [6] Other functions of iron-sulfur cluster proteins include serving as sensors of iron, dioxygen, superoxide and possibly nitric oxide. [7-10] One of the intriguing roles for iron-sulfur cluster proteins is the reductive cleavage of AdoMet to generate the putative deoxyadenosyl radical. [11-13] AdoMet is cleaved at the C_5'-S bond (~ 60 kcal mol^{-1}) [11]; how the reduced enzyme injects one electron into AdoMet to yield the putative radical is an interesting question.

Sulfur pre-K-edge XAS can provide information on the Fe-S bond electronic structure. We expect that the presence of AdoMet might change the covalency of the Fe-S bonds of the cluster, due largely to the proximity of the sulfonium-sulfur. We use sulfur K-edge XAS of purified PFL-AE to examine this possibility. The PFL-AE used in these studies was purified in the presence of ascorbic acid (to provide a reducing environment without exogenous thiols), so we first used UV-Vis and EPR spectroscopy to determine

whether this protein had similar properties to PFL-AE purified in the presence of DTT (our standard purification conditions). The UV-Vis spectrum of the protein purified in the presence of ascorbic acid shows a broad band from 360 nm, with a shoulder from 410 nm, a distinctive feature for $[4Fe\text{-}4S]^{2+}$ cluster. The spectrum is very similar to that of PFL-AE purified in 1 mM DTT, which has been extensively characterized by chemical and spectroscopic methods. The reduced $[4Fe\text{-}4S]^{1+}$ cluster shows (g = 2.01, 1.92 and 1.87), which is also similar to the results (g = 2.02, 1.94, 1.88) for PFL-AE purified in 1 mM DTT. [14] In the presence of 3 equivalents of AdoMet, the EPR signal undergoes a significant change, with the g factors shifted to 2.00, 1.92 and 1.89. The change is similar to that observed for the PFL-AE purified in DTT and suggests that AdoMet directly coordinates the iron-sulfur cluster in a manner consistent with our previous reports

The effect of external thiolate on the cluster was examined by photoreducing the enzyme in the presence of 10 mM DTT or 10 mM cysteine. The reduction results in an axial signal with g-factors of g = 2.03 and 1.93 for DTT, and g = 2.00 and 1.93 for cysteine. The results suggest a more symmetric structure of the cluster in the presence of these thiols, implying that the exogenous thiolate might coordinate to the cluster to generate a cluster with four thiolate ligands. Addition of AdoMet to these samples results in a change in g-factors to g = 2.00, 1.92 and 1.89, suggesting that AdoMet binds to the unique iron in the cluster, replacing the putative thiolate ligand. Together, the EPR and UV-Vis data indicate that PFL-AE purified with ascorbic acid as reductant should be the same as the PFL-AE on which we have previously published.

The sulfur K-edge XAS spectra of PFL-AE and PFL-AE with AdoMet show a sharp rising feature at 2473.5 eV which is the sulfur K-edge absorption due to S 1s to C-S

σ* transition, and a broad pre-edge feature at 2470.3 eV due to 1s (μ_3-Ssulfide and terminal-$S_{thiolate}$) to Fe_{3d} unoccupied antibonding orbital transition. The intensity of the pre-edge increases upon AdoMet binding, indicating an increase in covalency of the Fe-S bonds. The corresponding DFT calculations demonstrate that the total covalency of the bonds increases 37%, in which 12% is from the bridging sulfide and 25% is from the terminal thiolate. A DFT optimized model shows that the AdoMet 5'C-$S_{sulfonium}^{+}$ σ* bond has a backbonding interaction with the filled Fe-S bond in the cluster, which shifts the charge density from the cluster to the 5'C-S^{+} bond. This effect makes the sulfides poorer donors to the Fe-S bond, and the terminal thiolates increase donation to compensate the change. Therefore, the pre-edge feature has the characteristies of a S 1s electron to Fe_{3d} antibonding orbital transition and the bridging sulfide to AdoMet 5'C-S^{+} σ* bond transition. The charge density shifts from the cluster to AdoMet might be thought of as a precursor to electron transfer from the cluster to the substrate.

VII.2 The vibrations of the iron-sulfur cluster in PFL-AE

Vibrational spectroscopy is an important tool to investigate the structures of iron-sulfur clusters. There are many resonance Raman studies of Fe_4S_4 cluster model compounds and proteins. [15] The resonance Raman spectra of PFL-AE in this thesis showed a typical $[4Fe\text{-}4S]^{2+}$ signal, with Fe-S^b stretching modes at 290 cm^{-1} and 320 cm^{-1}, a Fe_4S_4 cluster cubane symmetric breathing mode at 338 cm^{-1}, a Fe-S^t stretching mode at 370 cm^{-1}, and a Fe-S^t symmetric stretching mode at 396 cm^{-1}. [16-19] Upon AdoMet binding, the band at 396 cm^{-1} split into two bands at 391 and 401 cm^{-1}, and the relative intensity of

the bands at 338 cm^{-1} and 370 cm^{-1} was also changed. These changes indicate that the coordination of AdoMet to the unique Fe causes some changes in the bonding between the irons and terminal sulfurs.

We have proposed an oxygen from either H_2O or OH^- coordinates to the unique Fe in the absence of AdoMet, however no clear evidence for this was obtained from resonance Raman spectra. To investigate the proposal, nuclear resonance vibrational spectroscopy (NRVS), was used. ^{57}Fe was reconstituted into the unique site of PFL-AE after the cluster was oxidized to $[3Fe\text{-}4S]^{1+}$ state, however Mössbauer spectroscopy showed that 68% of the ^{57}Fe was scrambled into other sites of the cluster and/or at the unique site with no AdoMet bound. Due to this scrambling, we were not able to obtain good NRVS data on unique-site-labeled PFL-AE.

The vibrational modes of the ^{57}Fe labeled $[4Fe\text{-}4S]^{2+}$ cluster were obtained by NRVS from 0 – 660 cm^{-1}. A broad band comprising the cubane twist modes was observed below 100 cm^{-1}, and a strong band of the S-Fe-S' bending mode was observed at around 160 cm^{-1}. [20] The Fe-S stretching modes were detected as a doublet between 250 and 300 cm^{-1}, and a triplet between 340 and 390 cm^{-1}. [20] The Fe-O stretching mode night be one of the bands above 400 cm^{-1}. In the presence of AdoMet, the intensity of the Fe-ligand + Fe-S^t stretching mode at 432 cm^{-1} increased. The coordination of the amino N and carboxylate O from AdoMet to the unique Fe enhanced the Fe-ligand vibration. The intensity of the bands at 388 cm^{-1} (Fe-S^t stretching), 158 cm^{-1} (S-Fe-S' bending) increased, and the Fe-S^t stretching mode at 278 cm^{-1} was split in the presence of AdoMet. Both the NRVS and resonance Raman results provide evidence for AdoMet binding changing the Fe-S^t bonds, which coordinates the cluster to the protein. Neither techniques,

however, has allowed the identification of the exogenous ligand in the absence of AdoMet.

VII.3 PFL structure change during activation

Our results in Chapter V demonstrate that the presence of PFL-AE results in a lowered stability of the PFL glycyl radical. Several lines of evidence point to a change in PFL conformation to a more open structure in the presence of PFL-AE, in which the gylcyl radical is more solvent exposed, as the reason for the decreased stability. First, with stoichiometric quantities of PFL-AE present, the H/D exchange at Gly-734 is diminished, suggesting that there is less direct interaction between Gly-734 and Cys-419 at the active site. Second, fully activated PFL (as measured by glycyl radical content) has lower activity in the presence of stoichiometric PFL-AE than in the presence of catalytic amounts of PFL-AE, again suggesting that PFL-AE draws the Gly-734 loop out of the active site. Finally, CD spectra changes of PFL in the presence of PFL-AE are consistent with movement of the glycyl loop upon interaction with PFL-AE.

VII.4 The first step in PFL catalysis

It was proposed in our lab that PFL might initiate catalysis by hydrogen atom abstraction from the methyl group in pyruvate. The H/D isotope effect on pyruvate turnover (using 3,3,3-d_3-pyruvate) was much smaller (1:1) than a primary H/D isotope effect in hydrogen abstraction reaction, which should be 6 or even larger. [21] The small

isotope effect might be due to a secondary H/D isotope effect on the C-C bond broken in pyruvate.

The product of the PFL enzymatic reaction with 3,3,3-d_3-pyruvate and CoA as the substrates was confirmed as 2',2',2'-d_3-acetyl-CoA by mass spectrometry. It had a molecular weight at 811 ($[M-H]^-$), with fragmentations in CAD-MS/MS that could be interpreted as the degradation of the deprotonated molecule. If PFL catalysis involved hydrogen abstraction, a hydrogen could be taken from the solvent or the protein into the pyruvate radical. There was no deuterium to hydrogen exchange detected by mass spectrometry, which should have the molecular weight at 810. Combined with the KIE study of the deuterium labeled substrate, hydrogen abstraction could be ruled out as the first step in the PFL mechanism.

PFL catalysis has been proposed to involve a thiyl radical, either on Cys-418 or Cys-419, attacking the carbonyl carbon in pyruvate. [22, 23] The two mutants C418A-PFL and C419A-PFL, exihibit no catalytic activity, although a glycyl radical could be generated in both of the proteins. In the presence of pyruvate, the activated C419A-PFL had no H/D exchange at the glycyl radical, whereas the activated C418A-PFL did exchange. The results show that the Cys-419 is not acetylated by pyruvate in activated C418A-PFL, as a free thiyl group on Cys-419 is required for the exchange. The results imply that Cys-419 does not attack the substrate. Our results support the proposal that a key step in the PFL mechanism is a Cys-418 thiyl radical attacking pyruvate.

VII.5 Overview of PFL-AE and PFL catalytic mechanisms

A Fe_4S_4 cluster with three irons coordinated by three cysteines is the catalytic center of PFL-AE. A hydroxide ion might bind to the unique Fe of the cluster in the absence of AdoMet. Upon AdoMet binding, the cluster shifts some charge density to AdoMet 5'C-S^+ σ^* bond, the position where AdoMet is reductively cleaved. This might be the initial step for the cluster to transfer one electron to AdoMet. The produced putative deoxyadenosyl radical abstracts one hydrogen from Gly-734 which we believe is pulled out from PFL to bind the PFL-AE active site for activation. The radical would be passed to Cys-418, using Cys-419 as the radical shuttle. The thiyl radical then attacks pyruvate to initiate PFL catalysis.

VII.6 Future work on sulfur XAS of reduced PFL-AE

The current sulfur XAS spectra are from $[4Fe\text{-}4S]^{2+}$, which is not the active state of PFL-AE. It will be interesting to see the XAS data from the reduced $[4Fe\text{-}4S]^{1+}$ cluster. The spectral change of the protein with and without AdoMet can provide more information about how the electron is transferred from the cluster to the substrate. One problem might be the slow cleavage of AdoMet by PFL-AE.

VII.7 Future work on NRVS studies of PFL-AE in $H_2{}^{18}O$

The Fe-^{18}O stretching mode should have a down-shift in wavenumbers compared to the Fe-^{16}O stretching if the exogenous ligand to the unique iron is from the solvent.

The comparison between the experimental data and calculated vibrational frequency might provide the clue of which one, the OH^- or the H_2O, is the actual ligand.

VII.8 Future work on the PFL and PFL-AE interaction

The current evidence of the PFL conformational change during activation is indirect. The structures of PFL for PFL-AE binding and the hydrogen bond chains to transfer the activation signal are both proposals. The best way to examine the idea might be co-crystallize PFL, PFL-AE and AdoMet together. A successful experiment can tell exactly how PFL and PFL-AE contact with each other. Site-directed mutagenesis of the key residues, supposed to be involved in the conformational change transfer, can be used to test the proposal.

VII.9 Future work on the investigation of the first step in PFL catalysis

The evidence of the thiyl radical on Cys-418 attacking pyruvate is also indirect. More convincing evidence will be a direct observation of a thiyl radical on the residue, which is not transferred from Cys-419, and a confirmation that this radical is able to attack pyruvate and get acetylated.

References:

1. Beinert, H.; Holm, R. H.; Munck, E., *Science (Washington, D. C.)* **1997,** 277, (5326), 653-659.

2. Lovenberg, W., *Iron-Sulfur Proteins*. Academic Press: New York, 1973; Vol. I and II.

3. Burgess, B. K.; Lowe, D. J., *Chem Rev* **1996,** 96, (7), 2983-3012.

4. Vignais, P. M.; Colbeau, A., *Curr Issues Mol Biol* **2004,** 6, (2), 159-88.

5. Beinert, H.; Kennedy, M. C.; Stout, C. D., *Chemical Reviews (Washington, D. C.)* **1996,** 96, (7), 2335-2373.

6. Thayer, M. M.; Ahern, H.; Xing, D.; Cunningham, R. P.; Tainer, J. A., *Embo J* **1995,** 14, (16), 4108-20.

7. Hentze, M. W.; Kuhn, L. C., *Proc Natl Acad Sci U S A* **1996,** 93, (16), 8175-82.

8. Beinert, H.; Kiley, P., *FEBS Letters* **1996,** 390, (2), 239.

9. Gaudu, P.; Weiss, B., *Proc Natl Acad Sci U S A* **1996,** 93, (19), 10094-8.

10. Hidalgo, E.; Bollinger, J. M., Jr.; Bradley, T. M.; Walsh, C. T.; Demple, B., *J Biol Chem* **1995,** 270, (36), 20908-14.

11. Frey, P. A.; Magnusson, O. T., *Chemical Reviews (Washington, DC, United States)* **2003,** 103, (6), 2129-2148.

12. Sofia, H. J.; Chen, G.; Hetzler, B. G.; Reyes-Spindola, J. F.; Miller, N. E., *Nucleic Acids Research* **2001,** 29, (5), 1097-1106.

13. Cheek, J.; Broderick, J. B., *Journal of biological inorganic chemistry : JBIC : a publication of the Society of Biological Inorganic Chemistry* **2001,** 6, (3), 209-26.

14. Walsby, C. J.; Ortillo, D.; Yang, J.; Nnyepi, M. R.; Broderick, W. E.; Hoffman, B. M.; Broderick, J. B., *Inorganic Chemistry* **2005,** 44, (4), 727-741.

15. Spiro, T. G. C., Roman S., *Resonance Raman spectroscopy. Physical Methods in Bioinorganic Chemistry*. University Science Books: Sausalito, CA, 2000; p pp 97 - 112.

16. Broderick, J. B.; Duderstadt, R. E.; Fernandez, D. C.; Wojtuszewski, K.; Henshaw, T. F.; Johnson, M. K., *Journal of the American Chemical Society* **1997,** 119, (31), 7396-7397.

17. Duin, E. C.; Lafferty, M. E.; Crouse, B. R.; Allen, R. M.; Sanyal, I.; Flint, D. H.; Johnson, M. K., *Biochemistry* **1997,** 36, (39), 11811-11820.

18. Roman S. Czernuszewicz, K. A. M., Michael K. Johnson, Andrew Gewirth, Thomas G. Spiro, *Journal of American Chemical Society* **1987,** 109, (23), 7178-87.

19. Johnson, M. K.; Czernuszewicz, R. S.; Spiro, T. G.; Ramsay, R. R.; Singer, T. P., *J Biol Chem* **1983,** 258, (21), 12771-4.

20. Xiao, Y.; Koutmos, M.; Case, D. A.; Coucouvanis, D.; Wang, H.; Cramer, S. P., *Dalton Trans* **2006,** (18), 2192-201.

21. Westheimer, F. H., *Chem Rev* **1961,** 61, (3), 265-273.

22. Becker, A.; Fritz-Wolf, K.; Kabsch, W.; Knappe, J.; Schultz, S.; Wagner, A. F. V., *Nature Structural Biology* **1999,** 6, (10), 969-975.

23. Parast, C. V.; Wong, K. K.; Lewisch, S. A.; Kozarich, J. W.; Peisach, J.; Magliozzo, R. S., *Biochemistry* **1995,** 34, (8), 2393-9.